Technical Report TR-216227
N00014-82-C-0121

(12)

A PHYSICAL SEDIMENT MODEL FOR THE PREDICTION OF SEAFLOOR GEOACOUSTIC PROPERTIES

Burlie A. Brunson
Eugene J. Molinelli
Planning Systems Incorporated
7900 Westpark Drive, Suite 600
McLean, Virginia 22102

July 1982

Final Report

Distribution in Accordance with List
Provided in Contract N00014-82-C-0121

Prepared for

OFFICE OF NAVAL RESEARCH
Department of the Navy
800 North Quincy Street
Arlington, Virginia 22217

NAVAL OCEAN RESEARCH AND DEVELOPMENT ACTIVITY
Code N68462
NSTL Station, Mississippi 39529

UNCLASSIFIED

SECURITY CLASSIFICATION OF THIS PAGE (When Data Entered)

REPORT DOCUMENTATION PAGE		READ INSTRUCTIONS BEFORE COMPLETING FORM
1. REPORT NUMBER TR-216227	2. GOVT ACCESSION NO. AD-A119445	3. RECIPIENT'S CATALOG NUMBER
4. TITLE (and Subtitle) A PHYSICAL SEDIMENT MODEL FOR THE PREDICTION OF SEAFLOOR GEOACOUSTIC PROPERTIES		5. TYPE OF REPORT & PERIOD COVERED Final Report 1 Jan 82-30 Jul 82 6. PERFORMING ORG. REPORT NUMBER TR-216227
7. AUTHOR(s) Burlie A. Brunson Eugene J. Molinelli		8. CONTRACT OR GRANT NUMBER(s) N00014-82-C-0121
9. PERFORMING ORGANIZATION NAME AND ADDRESS Planning Systems Incorporated 7900 Westpark Drive, Suite 600 McLean, Virginia 22102		10. PROGRAM ELEMENT, PROJECT, TASK AREA & WORK UNIT NUMBERS PE 62759N RF59-701
11. CONTROLLING OFFICE NAME AND ADDRESS Office of Naval Research Dept. of the Navy 800 N. Quincy Street, Arlington, VA 22217		12. REPORT DATE July 1982 13. NUMBER OF PAGES 141
14. MONITORING AGENCY NAME & ADDRESS (if different from Controlling Office) Naval Ocean Research and Development Activity Code N68462 NSTL Station, MS 39529		15. SECURITY CLASS. (of this report) Unclassified 15a. DECLASSIFICATION/DOWNGRADING SCHEDULE

16. DISTRIBUTION STATEMENT (of this Report)

Distribution in accordance with list provided in contract:
NORDA, Bay St. Louis, MS 39529 (2 cys)
ONR, Arlington, VA 22217 (1 cy); Boston, MA 02210 (1 cy)
NRL, Washington, D.C. 20375 (6 cys)
DTIC, Alexandria, VA 22314 (12 cys)

17. DISTRIBUTION STATEMENT (of the abstract entered in Block 20, if different from Report)

Same as Block 16

18. SUPPLEMENTARY NOTES

19. KEY WORDS (Continue on reverse side if necessary and identify by block number)

sediment acoustics, bottom loss, physical sediment model

20. ABSTRACT (Continue on reverse side if necessary and identify by block number)

A study was performed to adapt, implement, and test a version of the Biot/Stoll physical sediment model in a form which allows the prediction of those geoacoustic properties needed by current Navy acoustic or bottom loss calculation models. Particular attention was paid to the depth and frequency dependence of compressional wave speed and attenuation; two properties considered to be most important to acoustic modeling. —> and

DD FORM 1 JAN 73 1473 EDITION OF 1 NOV 65 IS OBSOLETE

UNCLASSIFIED

SECURITY CLASSIFICATION OF THIS PAGE (When Data Entered)

Abstract (cont.)

Additionally, input sensitivity studies yielded insight into certain "critical factors" important to accurate geoacoustic property predictions. Model predictions of seafloor geoacoustic properties were compared with speed and attenuation values measured directly or inferred from acoustic measurements for a deep water site near DSDP site 135, and a shallow water site near Panama City, Florida. The acoustic significance of observed differences in geoacoustic properties was assessed by comparing the outputs of a complex reflection coefficient model using inputs derived from physical sediment properties using the Biot/Stoll approach and inputs derived from acoustical measurements using the inversion technique developed for the Bottom Loss Upgrade (BLUG). The study yielded positive evidence that the physical sediment approach is useful. The Biot/Stoll model is a potentially powerful tool for estimating or extrapolating geoacoustic parameters, particularly when a priori estimates are needed in geographic areas or frequency regimes which have not been acoustically surveyed.

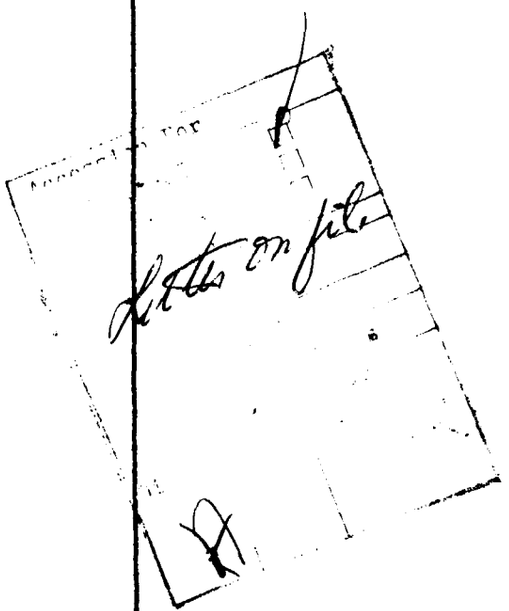

EXECUTIVE SUMMARY

A study was performed to adapt, implement, and test a version of the Biot/Stoll physical sediment model in a form which allows the prediction of those geoacoustic properties needed by current Navy acoustic or bottom loss calculation models. Particular attention was paid to the depth and frequency dependence of compressional wave speed and attenuation; two properties considered to be most important to acoustic modeling.

Model inputs were obtained from published measurements of sediment physical properties, or from generally accepted empirical or physical relationships between sediment physical properties. The sensitivity of the model outputs to variations in the model inputs was assessed. This resulted in the identification of several "critical factors" whose accurate specification is essential to the prediction of geoacoustic properties of the seafloor. For deep sea cases, the "critical factors" include: grain bulk modulus (K_r), frame bulk modulus (K_b), shear and compressional frame logarithmic decrements, and porosity. In low porosity sands, one must add permeability to the list because of its effect on fluid mobility and hence viscous losses.

To assess the performance of the Biot/Stoll model, two test cases were selected. Model predictions were compared with speed and attenuation values measured directly or inferred from acoustic measurements for a deep water site near Deep Sea Drilling Project (DSDP) site 135, and a shallow water site near Panama City, Florida. The acoustic significance of the differences observed in each of these comparisons was tested. The outputs of a bottom loss model using inputs derived from sediment physical properties using the Biot/Stoll approach were compared with bottom loss outputs from the same model using inputs derived from acoustical measurements

using the inversion technique developed for the Bottom Loss Upgrade (BLUG). These comparisons provided an indirect measure of the capability of the Biot/Stoll model to provide suitable acoustic model inputs.

The study yielded positive evidence that the physical sediment model approach is useful. The Biot/Stoll model is a potentially powerful tool for estimating or extrapolating geoacoustic parameters which are in turn controlling factors in propagation for many deep-water tactical applications and nearly all shallow-water applications. The approach may prove to be particularly valuable for a priori estimates of bottom interaction effects in geographic areas or frequency regimes which have not been acoustically surveyed.

TABLE OF CONTENTS

TABLE OF CONTENTS

LIST OF FIGURES

LIST OF FIGURES

LIST OF TABLES

I. INTRODUCTION

Background

The operation of Navy sonar and weapons systems depends critically upon the exploitation of acoustic signals and the discrimination against unwanted noises and reverberant echoes. These acoustic signals and noises must, of course, propagate through the complex ocean medium from source to receiver, and in many areas of the world, be perturbed by interaction with the seafloor. For effective sonar system design and deployment, it is essential for the Navy to gain a detailed understanding of the nature and effect of these perturbations caused by the acoustic response of the ocean bottom, and to integrate the additional knowledge into its acoustic prediction capabilities.

The Navy is continuously involved in efforts to improve the manner in which bottom interaction is treated in acoustic models and analysis procedures. In line with these efforts the Navy is currently implementing a new low-frequency bottom loss calculation technique designed to replace the bottom loss curves commonly used in propagation loss predictions at the Fleet Numerical Oceanographic Center (FNOC), by on-board prediction systems, and by the environmental-acoustics and system R&D community. This bottom loss upgrade (BLUG) will replace the current bottom loss provinces which are keyed to a small set of "typical" bottom loss curves, with a new set of provinces which are keyed to the geographic distribution of geophysical and geoacoustic properties of the seafloor.

For the purpose of this study the geophysical properties of the seafloor re er to the physical properties of the sediment and basement. These include, for example, density, porosity, permeability, compressibility, and shear modulus. Geoacoustic properties are restricted to those properties which directly describe the nature of acoustic propagation in the

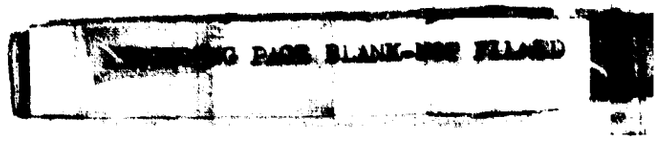

seafloor. They include the propagation speeds and absorption of acoustic energy as well as certain parameters derived from them, such as velocity and attenuation gradients and acoustic impedance.

BLUG assumes that the sediment can be described by the three geophysical properties: sediment thickness, sediment density, and surface layering; and the six geoacoustic properties: compressional wave speed ratio at the seafloor interface, compressional wave speed gradient at the top of the sediment, curvature of the speed profile in the sediment, compressional wave attenuation in the sediment, compressional wave attenuation gradient in the sediment, and basement reflectivity. However, these properties are not readily available to the bottom loss modeler because of the scarcity of direct measurements of the geoacoustic properties of marine sediments. An alternative, indirect, source for this information is needed.

The initial BLUG implementation calls for the construction of a limited set of these nine parameters derived by "inversion" of existing bottom loss data. This inversion technique with its inherent limit in descriptive parameters can lead to physically unrealistic bottom properties which, although consistent with the bottom loss data, may not be easily extrapolated to a new area or frequency. Some difficulty in geographic extrapolation results from the complex interplay among the sediment properties when they are used to calculate bottom loss curves. If one or more of the properties changes, then the newly calculated bottom loss may not be valid even though the originally calculated bottom loss agreed with the data from which it was derived. At the present time, geographic extrapolation is by assignment of bottom loss provinces based primarily on sediment type and thickness or, is possible, by comparison between geoacoustic properties from the areas of interest. This acoustic data is not readily available on a wide geographic scale, making accurate extrapolation difficult.

A further problem arises when one wishes to extrapolate bottom loss data at a known frequency to obtain estimates at a new frequency. Some of the key geoacoustic bottom properties are frequency dependent. Recent work by Stoll[1] and Brunson and Johnson[2] has indicated that the attenuation and velocity may have dependencies which are not linear in frequency, as BLUG assumes. This is particularly noticeable in certain sediments found in shallow water areas. The impact is pronounced at the higher frequencies at which tactical sonars and weapons sysetms operate. The non-linear nature of these geoacoustic parameters is not included in the current bottom loss extrapolation methods.

All of this suggests that some attention should be paid to identifying a method of determining important geoacoustic properties of the sediment (those needed for bottom-loss calculations) more easily than through direct measurement or inversion of bottom loss data. As a promising candidate, we have considered a method employing a sediment model which uses measured or empirically derived sediment physical properties (e.g., grain size, porosity, density, and permeability) as inputs. Such inputs are more widely available geographically and may be used to determine the profiles of compressional speed and attenuation needed for bottom loss calculations. The sediment model which we feel offers the best chance of success is generally attributed to Biot; it has been described in the literature by Stoll and Bryan[3] and Stoll[4,5] (1977), and has

---

[1]Stoll, R.D., 1979, "Experimental Studies of Attenuation in Sediments," J. Acoust. Soc. Amer., 66, pp. 1552-1160.

[2]Brunson, B.A. and R.K. Johnson, 1980, "Laboratory Measurements of Shear Wave Attenuation in Saturated Sand," J. Acoust. Soc. Amer., 68.

[3]Stoll, R.D. and G.M. Bryan, 1970, "Wave Attenuation in Saturated Sediments," J. Acoust. Soc. Amer., pp. 1440-1447.

[4]Stoll, R.D., 1974, "Acoustic Waves in Saturated Sediments," In L. Hampton (Ed.), Physics of Sound in Marine Sediments, New York, Plenum Press, pp. 19-39.

been recently applied in experimental studies by Plona,[6] Beebe,[7] Brunson and Johnson,[2] and Brunson and Matthews.[8] Proper implementation and application of such a model could lead to significant improvements in the Navy's ability to accurately extrapolate bottom loss data in both space and frequency, for numerous Fleet and R&D applications. In addition, this model could supply geoacoustic inputs to those acoustic models requiring this form of seafloor description.

---

[5]Stoll, R.D., 1977, "Acoustic Waves in Ocean Sediments," Geophysics, 42, pp. 715-725.

[6]Plona, T.J., 1980, "Observations of a Second Bulk Compressional Wave in a Porous Medium at Ultrasonic Frequencies," Appl. Phys. Lett., 36, pp. 259-261.

[7]Beebe, J.H., 1980, "An Experimental Investigation of Ocean Sediment Effects Upon Long-Range Transmission Loss in Shallow Water," Technical Memorandum TM 80-247, Pennsylvania State University.

[8]Brunson, B.A. and J.E. Matthews, 1981, "Grain Shape and Sorting Effects on the Frequency Dependence of Shear Wave Attenuation in Water Saturated Sediments," Unpublished paper presented at 101st meeting, Session QQ, Acoustical Society of America.

Technical Objectives

The objectives of the study were to adapt, implement, and test a version of the Biot/Stoll sediment model in a form which would allow the prediction of those geoacoustic properties needed by current Navy acoustic propagation or bottom loss calculation models. Particular interest was to be paid to the depth and frequency dependence of compressional wave speed and attenuation. These have been shown to be the geoacoustic properties most important to the acoustic propagation, or bottom loss, modeler.

An appropriate version of the Biot/Stoll model was implemented and tested. The model inputs were obtained from published measurements of sediment physical properties, or from generally accepted empirical or physical relationships between sediment physical properties. Care was taken to select physical properties which were consistent with the known limits of values for such properties. The model outputs included predictions of acoustic wave speed and attenuation. These were provided as functions of frequency and depth in the sediment column.

For selected cases the model predictions were compared with speed and attenuation values measured directly or inferred from acoustic measurements. Such comparisons served to indicate the validity of the physical sediment model approach to sediment geoacoustic property prediction. These comparisons also served to indicate whether the physical properties selected as model inputs were appropriate representations of the physical properties of the sediment being modeled. Further checks on model input and output adequacy were provided by comparison with published values of sediment geophysical and geoacoustic properties.

An assessment was made of the suitability of this type of model, given the availability and variability of required inputs, for applications in support of bottom loss modeling

and for generation of geoacoustic inputs to acoustic propagation models.

The technical objectives of Phase I of this study have thus been met, and recommendations for further research are presented in Section VI of this report.

II. PHYSICAL SEDIMENT MODEL

Background

The area of physical sediment modeling has been a subject of research for some time. Generally, the sediment is treated as an elastic or viscoelastic solid. This treatment accounts for observed wave speeds quite well, but is unable to provide satisfactory estimates of acoustic attenuation.

Recently, geoacoustic modeling of the seafloor has become an important component of acoustic propagation analysis and modeling in the ocean. Many ocean areas in the world and in particular many strategically important areas are bottom limited at least some portion of the time. Moreover, a number of modern tactical and surveillance sonar systems are designed to operate in source/receiver geometries where only bottom-interacting paths are available. This situation complicates the exploitation of acoustic energy transmitted through the ocean since the performance of sonar, weapons, and commnications systems become dependent upon the transmission properties of the seafloor. As propagation models become more sophisticated, their ability to correctly handle the interaction of acoustic energy with the seafloor becomes more critical. The result is that a large amount of effort on the part of geologists, geophysicists, and acousticians is being expended in attempts to better understand the geoacoustic properties of the seafloor. An understanding of the physical processes that occur when acoustic energy interacts with the seafloor is essential to the development of better treatments of bottom interaction.

A leading proponent of geoacoustic modeling is Ed Hamilton. In a series of papers[9-12] dating back more than a

[9]Hamilton, E.L., 1971, "Prediction of in-situ Acoustic and Elastic Properties of Marine Sediments," Geophysics, 36, pp. 266-284.

decade, he sought to provide the underwater acoustician with descriptions and empirical relationships of seafloor sediments. His approach to sediment modeling is principally empirical in nature but includes elements of linear viscoelastic theory as presented by Ferry.[13] This theory assumes that a complex ratio exists between stress and strain and the damping or absorption is then represented by the phase angle of the ratio. The absorption is predicted to vary as the first power of frequency. The empirical work of Hamilton derives from many measurements on cores, artificial sediments, and in-situ acoustic measurements. His reported results cover a frequency range from 4 Hz to 1 MHz, although the bulk of the data are taken above 1 kHz.

Another approach to sediment modeling has been pursued by Stoll and described in a series of papers[4,5,14] spanning a slightly shorter time frame than Hamilton's. Stoll builds upon a theory of propagation of elastic waves in a fluid-saturated porous solid described by Biot.[15-17] This theory allows for

[10]Hamilton, E.L., 1974, "Prediction of Deep-Sea Sediment Properties: State-of-the-Art," In A.L. Inderbitzen (ed.) Deep-Sea Sediments, Physical and Mechanical Properties, New York, Plenum Press, pp. 1-43.

[11]Hamilton, E.L., 1974, "Geoacoustic Models of the Sea Floor," In L. Hampton (ed.), Physics of Sound in Marine Sediment, New York, Plenum Press, pp. 181-221.

[12]Hamilton, E.L., 1980, "Geoacoustic Modeling of the Sea Floor," J. Acoust. Soc. Amer., 68, pp. 1313-1340.

[13]Ferry, J.D., 1961, "Viscoelastic Properties in Polymers," New York, John Wiley and Sons.

[14]Stoll, R.D., 1980, "Theoretical Aspects of Sound Transmission in Sediments," J. Acoust. Soc. Amer., 68, pp. 1341-1350.

[15]Biot, M.A., 1956, "Theory of Elastic Wave Propagation in a Fluid-Saturated Porous Solid," I. Low Frequency Range, J. Acoust. Soc. Amer., 28, pp. 168-178.

[16]Biot, M.A., 1956, "Theory of Elastic Wave Propagation in a Fluid-Saturated Porous Solid," II. Higher Frequency Range, J. Acoust. Soc. Amer., 28, pp. 179-191.

relative motion to occur between the fluid which fills the pores of a saturated sediment and the skeletal frame of the sediment. The result is a viscous loss which is highly dependent upon the ability of the fluid to move through the sediment, an ability which is related to the sediment permeability. This model predicts a slight dispersion in the propagation speed and a non-linear relationship between attenuation and frequency. A formulation of the Stoll/Biot model is presented in Stoll's 1977 paper[5], and formed the core of the model implemented by this study.

[17]Biot, M.A., 1962, "Generalized Theory of Acoustic Propagation in Porous Dissipative Media," J. Acoust. Soc. Amer., 34, pp. 1254-1264.

Biot/Stoll Theory

The theory developed by Biot[15-17] is a comprehensive description of the acoustic response of linear, porous materials containing compressible fluid.

Biot's theory predicts that in the absence of boundaries, three kinds of body waves may exist in a fluid saturated porous medium. One of the compressional waves, which is called the first kind, and a shear wave are akin to those body waves found in ordinary elastic media. The second kind of compressional wave is highly attenuated in a manner similar to a diffusion process. These compressional waves of the second kind may be important in acoustical problems involving very compressible fluids like air or perhaps in very gassy sediments where the effective compressibility of the pore fluid has been greatly reduced due to the presence of dissolved or free gas. For most geophysical applications, compressional waves of the second kind are not important, and are not considered in this study.

When relative motion between the sediment frame and the pore fluid is allowed, the predicted values of speed and attenuation depend upon frequency. At low frequencies, the flow in the pores is laminar, the speed is essentially constant, and the attenuation varies as the square of the frequency. At high frequencies, the flow pattern is complex, the speed is again approximately constant, although higher than at low frequencies, and the attenuation varies as the square root of the frequency. At intermediate frequencies, a transition zone exists. The details of the frequency dependence in the transition zone depend upon the compressibility and viscosity of the fluid and the moduli and permeability of the sediment frame. The frequency dependence of compressional wave speeds is more pronounced than shear wave speeds for the same sediment. The solution on which the frequency dependence of fluid flow resistance is based is valid for frequencies where the

wavelength is large compared to the intergranular pore size. For sands, this puts the upper limit on frequencies at about 10^6 Hz, which is high enough to cover the frequency range of interest in geophysical applications.

The Biot formulation assumes a perfectly elastic sediment frame. To accommodate the observed loss due to frictional forces at the grain-to-grain contacts between particles, Stoll[3,4] has regarded the bulk and shear moduli of the sediment assemblage as slightly nonlinear or complex constants with small imaginary parts. The bulk moduli of the individual grains and the fluid remain as elastic constants. This leads to a physically realistic model of a saturated sediment capable of accounting for both frictional and viscous losses in sediments of differing properties across a broad frequency range.

Formulation of the Model

A mathematical formulation of the Biot sediment model incorporating the modification and notation presented by Stoll[5] follows below.

Assuming that the response of the framework of sediment particles in a fluid environment can be described by a set of constitutive relationships of the form (using tensor notation for brevity in presentation).

$$\tau_{ij} = 2\mu e_{ij} + \delta_{ij} \cdot [(H-2\mu)e - C\zeta] \qquad (1)$$

$$P = M \cdot \delta - C \cdot e \qquad (2)$$

where τ_{ij} and e_{ij} are the stress and strain components, respectively, of an element of volume attached to the sediment frame; P is the pore fluid pressure; H, C, M and μ are linear or "slightly non-linear" operators that characterize the elastic and inelastic response of the frame; and δ_{ij} is the Kronecker delta. The volumetric strain of an element attached to the frame is represented by e, and ζ is the volume of fluid which has flowed out of the element.

Combining these constitutive relationships with the equation describing the motion of the fluid relative to the frame and the stress-equation of motion for the volume attached to the frame, Stoll derived the equations of motion governing the propagation of dilatational and shear waves in the sediment. For the dilatational motion of the frame,

$$\nabla^2(He-C\zeta) = \frac{\partial^2}{\partial t^2}(\rho e-\rho_f\zeta) \qquad (3)$$

For the motion of fluid relative to the frame,

$$\nabla^2(Ce-M\zeta) = \left[\frac{\partial^2}{\partial t^2}(\rho_f e-m\zeta)\right] - \frac{\eta F}{k}\frac{\delta\zeta}{\delta t} \qquad (4)$$

Similarly for shear waves the motion of the frame is described by,

$$\mu\nabla^2\tilde{w} = \frac{\partial^2}{\partial t^2}(\rho\tilde{w}-\rho_f\tilde{\theta}) \tag{5}$$

and for shear motion of fluid relative to the frame,

$$\frac{\eta F}{k}\frac{\partial\tilde{w}}{\partial t} = \frac{\partial^2}{\partial t^2}(\rho_f\tilde{w}-m\tilde{\theta}) \tag{6}$$

where $\tilde{w}$ is the curl of the frame displacement vector $\tilde{u}$, and $\tilde{\theta}$ is a function of the porosity β and the displacement vectors of the frame $\tilde{u}$ and the fluid $\tilde{v}$.

Solutions for e and ζ are assumed to be of the form

$$e = A_1 e^{i(\omega t-\ell x)} \tag{7}$$

and

$$\zeta = A_2 e^{i(\omega t-\ell x)} \tag{8}$$

while $\tilde{w}$ and $\tilde{\theta}$ take the form

$$\tilde{w} = A_3 e^{i(\omega t-\ell x)} \tag{9}$$

and

$$\tilde{\Theta} = A_4 e^{i(\omega t-\ell x)} \tag{10}$$

where ℓ is the wave number and ω is the circular frequency. Substituting Equations (7) and (8) into Equations (3) and (4) results in two equations in A_1 and A_2. If solutions exist for A_1 and A_2, it must hold that the determinant of the coefficients for A_1 and A_2 equals zero.

Stoll presents the determinant relation:

$$\begin{vmatrix} H\ell^2 - \rho\omega^2 & \rho_f\omega^2 - C\ell^2 \\ C\ell^2 - \rho_f\omega^2 & m\omega^2 - M\ell^2 - i\frac{\omega F\eta}{k} \end{vmatrix} = 0 \qquad (11)$$

a solution for the complex wave number ℓ will yield the phase velocity (from the real part) and the absorption (from the imaginary part) for the two kinds of compressional waves.

A similar substitution of Equations (9) and (10) into Equations (5) and (6) leads to a determinant for the coefficients of A_3 and A_4 equal to:

$$\begin{vmatrix} \rho\omega^2 - \mu\ell^2 & \rho_f\omega^2 \\ \rho_f\omega^2 & m\omega^2 - \frac{i\omega F\eta}{k} \end{vmatrix} = 0 \qquad (12)$$

The solution for the complex wave number ℓ in this case yields the phase velocity (from the real part) and absorption (from the imaginary part) for the shear wave.

If the determinant in Equation (11) is reduced, we obtain the following fourth order complex equation

$$a_1\ell^4 + a_2\ell^2 + a_3 = 0 \qquad (13)$$

Similarly, the reduction of the determinant in Equation (12) yields the second order complex equation

$$b_1\ell^2 + b_2 = 0 \qquad (14)$$

The constants a_1, a_2, a_3, b_1, and b_2 are complex and defined as follows:

$$a_1 = C^2 - HM \ , \tag{15}$$

$$a_2 = (Hm + \rho M - 2C\rho_f)\omega^2 - i\frac{\omega F\eta}{k}H \ , \tag{16}$$

$$a_3 = (\rho_f{}^2 - \rho m)\omega^4 + i\frac{\omega^3 F\eta}{k}\rho \ , \tag{17}$$

$$b_1 = -\mu m\omega^2 + i\frac{\omega\mu F\eta}{k} \ , \tag{18}$$

$$b_2 = (\rho m - \rho_f{}^2)\omega^4 - i\frac{\omega^3 F\eta}{k}\rho \ , \tag{19}$$

We see from Equations (17) and (19) that

$$b_2 = -a_3 \tag{20}$$

in Equations (15), (16), (17), (18), and (19), ρ is the saturated sediment density; ρ_f is the density of the pore fluid; k is the sediment permeability; η is the fluid viscosity; and ω is the circular frequency $2\pi f$. The complex contants C, H, and M are functions of the fluid, frame, and grain bulk moduli (K_f, K_c, and K_r, respectively), frame shear modulus μ, porosity β, and the parameter m which accounts for the tortuosity of the interstitial pore spaces. They have been made complex to account for the frame inelasticity. This has been done by assuming the frame bulk modulus K_c and frame shear modulus μ to be complex with small imaginary parts. These constants are defined by Stoll[4] as follows:

$$C = \frac{K_r(K_r - K_c)}{D - K_c} \tag{21}$$

$$H = \frac{(K_r - K_c)^2}{D - K_c} + K_c + \frac{4\mu}{3} \tag{22}$$

$$M = \frac{K_r^2}{D - K_c} \tag{23}$$

where

$$D = K_r \left[1 + \beta \left(\frac{K_r}{K_f} - 1 \right) \right] . \tag{24}$$

The term $\frac{F\eta}{k}$ is used to account for frequency dependent viscous effects by applying the complex correction F to the fluid viscosity. This factor was derived by Biot[17] by considering the actual micro-velocity field that exists within the pore channels and considering the ratio of the friction force exerted by the fluid on the frame to the average relative velocity for oscillatory motion to be $\beta^2 F\eta/k$. The correction factor is a function of κ, where

$$F = F(\kappa) = \frac{1}{4} \frac{\kappa T(\kappa)}{1 - \frac{2T(\kappa)}{i\kappa}} \tag{25}$$

$$\kappa = a(\omega \rho_f / \eta)^{1/2} \tag{26}$$

and

$$T(\kappa) = \frac{\text{ber}'(\kappa) + i\ \text{bei}'(\kappa)}{\text{ber}(\kappa) + i\ \text{bei}\ (\kappa)} \tag{27}$$

The functions ber(κ) and bei(κ) are real and imaginary parts of the Kelvin function. The functions ber'(κ) and bei'(κ) are the derivatives of the Kelvin functions.

To account for the unknown nature of the pore size and shape, the parameters a [in Equation (26)] and m [in Equations (16)-(19)] are introduced. The parameter a has the dimension of length and depends upon both the size and shape of the pores and can be related to grain size, permeability, and porosity. The parameter m is defined as:

$$m = \alpha \rho_f / \beta \quad \alpha \geq 1 \tag{28}$$

This parameter, always greater than ρ_f/β, has been substituted for ρ_f/β in Equations (4) and (6) to account for the fact that not all of the pore fluid moves in the direction of the macroscopic pressure gradient because of the tortuous, multi-directional nature of the pores. As a result, less fluid flows in or out of an element for a given acceleration than if all the pores were uniform and parallel to the gradient. This appears as an increase in the fluid inertia. Stoll[4] states that for uniform pores with axes parallel to the pressure gradient, α would equal one, while for a random system of uniform pores with all possible orientations the theoretical value of α is three. In practice, α is treated as an empirical parameter. The essential difference between a and m is in their usage; m has an inertial effect on the fluid flow, reducing this flow for the more random pore orientation; a affects the viscous resistance to fluid flow and results in an increased attenuation for high frequencies.

Physical Parameters

To evaluate the solutions of the compressional wave and shear wave determinants, Equations (13) and (14), one must specify values for thirteen physical parameters. The parameters are listed in Table 1.

The solutions result in predictions of the phase speeds and absorption for the two types of compressional waves and the shear wave which propagates through a fluid saturated porous medium. Accommodations have been made to allow for frame inelasticity, thus predictions may be made for unconsolidated sediments. The predictions may be made at frequencies of interest as long as the basic assumption that the acoustic wavelength remains large compared to the intergranular pore size is valid. This allows predictions for frequencies up to approximately 10^6 Hz for sands with higher frequencies for smaller grained sediments typical of deep sea silts and clays.

As stated in Section I, one of the technical objectives of this study is to predict the depth dependence of body wave speed and attenuation in addition to their frequency dependence. This cannot be accomplished using the Biot/Stoll sediment model except by providing the physical parameters at depths of interest in the sediment column being modeled. This is the method which has been used to accomplish the objective.

The procedures and techniques used to specify the physical parameter required to evaluate the solutions to Equations (13) and (14) will be discussed in detail in Section III.

TABLE 1. BIOT/STOLL PHYSICAL PARAMETERS

Symbol	Physical Property	Units
ρ_r	Density of sediment grains	$kg \cdot m^{-3}$
K_r	Bulk modulus of sediment grains	$N \cdot m^{-2}$
ρ_f	Density of pore fluid	$kg \cdot m^{-3}$
K_f	Bulk modulus of pore fluid	$N \cdot m^{-2}$
η	Viscosity of pore fluid	$kg \cdot m^{-1} \cdot s^{-1}$
β	Porosity	--
K	Permeability	m^2
a	Pore size parameter	m
α	Structure factor	--
μ_b	Shear modulus of frame (real part)	$N \cdot m^{-2}$
μ_b^*	Shear modulus of frame (imaginary part)	$N \cdot m^{-2}$
K_b	Bulk modulus of frame (real part)	$N \cdot m^{-2}$
K_b^*	Bulk modulus of frame (imaginary part)	$N \cdot m^{-2}$

III. APPROACH

Case Selection Criteria

In order to determine the degree to which we have succeeded in meeting the technical objectives stated in Section I, it was necessary to select a few realistic test cases for our sediment model to simulate.

The case selections were made with four basic requirements in mind.

Input Data Availability--The Biot Stoll model requires several physical input parameters identified in Table 1. The ability to accurately simulate the geoacoustic properties of the seafloor is dependent upon the availability of several of these at the location of interest to the sediment modeler. The sources of these required inputs include directly measured physical properties such as those obtained by analysis of cores, sediment grab samples, or Deep Sea Drilling Project (DSDP) drill holes. Additionally, certain other physical properties may be obtained through empirical relationships established between the measured properties and those required for model inputs. The cases selected did have some directly measured physical properties available which allowed us to obtain the others required.

Representativity--The cases selected must include one representative of a deep water site and one of a shallow water site. They must span the range from low porosity sands to high porosity clays. The sediment columns must be simple with minimal layering. Simplicity of the column is important in this initial phase to allow the evaluation of the basic mechanisms employed in the model without the complications of sediment type changes.

Geoacoustic Data Availability--The model predicts the geoacoustic properties of the sediment. Cases must supply some test of the accuracy of those predictions. This requires that the test sites be characterized geoacoustically through direct measurement (velocity measurements, attenuation measurements) or indirectly by acoustic sampling techniques (seismic profiling, mode attenuation inversion, acoustic bottom loss inversion, transmission loss inversion).

Acoustic Data Availability--Since the ultimate use of the geoacoustic predictions is to provide the basis for acoustic prediction, it is desirable to have some acoustic data available to allow one to assess, in some form, the acoustic significance of any disagreements observed in the geoacoustic data/prediction comparisons. This data may be bottom loss, transmission loss, or model predictions of these quantities based upon the geoacoustic properties observed or predicted at the site of interest.

Sources for Model Parameters

For a given case, values for the thirteen parameters listed in Section II must be provided; yet, measurements of all thirteen are rarely, if ever available. Parameters not directly measured can be assigned values in two ways. The unavailable parameters can be derived using their physical (i.e., theoretical) relationships to some or all of the measured parameters. The unavailable parameters can also be obtained empirically, either from the measured parameters or from other information about the case such as location, depth, and sediment type. In this section, we discuss methods for obtaining each of the thirteen parameters required by the Biot/Stoll model. Special emphasis is placed on the depth dependence of the model parameters. Though we do not intend that the list be exhaustive, we do believe it includes all the important relationships presently in use by the geophysics comunity. Many of these relationships are compiled in the work of Ogushwitz.[18]

Density of Sediment Grains--A fundamental parameter, density of grains (ρ_r), can be inferred from measurements of water content and density of wet sediment,[19] or it can be looked up in handbooks of laboratory measurements according to mineral content. It does not vary significantly over the range of pressures associated with burial depths up to 1,000 m.

Bulk Modulus of Grains--Like the density of the grains, bulk modulus can be obtained from handbooks according to mineral type, and is taken to be constant for depth of burial up to 1,000 m. For grains composed of several minerals, an

[18]Ogushwitz, P.R., 1982, "Applicability of the Biot Theory. I. Low Porosity Materials" (manuscript to be submitted to Journal of the Acoustical Society of America).

[19]Keller, G.H., 1974, "Marine Geotechnical Properties: Interrelationships and Relationships to Depth of Burial," Deep Sea Sediments, ed. by A.L. Inderbitzen, Plenum Pub. Corp., New York.

average bulk modulus based on the volume fraction and modulus of each can be calculated as described by Hamilton.[20] For two components

$$K_r = \frac{K_1K_2(1+V_1^2+V_2^2)+V_1V_2(K_1^2+K_2^2)}{2K_2V_1+2K_1V_2} \qquad (29)$$

K_1 = bulk modulus of first component

K_2 = bulk modulus of second component

V_1 = volume fraction of first component

V_2 = volume fraction of second component

Density of Pore Fluid--In all applications, the pore fluid is seawater. To first order, the specific gravity of seawater (ρ_f) is constant and equal to 1000 kg m^3 (1 gm cm^3). Increases in specific gravity up to 5% are caused by the effects of oceanic ranges for temperature, salinity, and pressure, with pressure having the greatest effect. High precision formulas appear in the oceanographic literature,[21] but they tend to provide much more detail than is needed here to describe the properties of marine sediments. For the depth dependence of density in deep water where the temperature is approximately 1°C, and the salinity 35 parts per thousand, a table (Table 2) can be constructed of the depth dependence, and values of density can be obtained by interpolation.

Bulk Modulus of Pore Fluid--To first order, the bulk modulus of sea water is constant and equal to 2.3×10^9 N m^{-2}

[20] Hamilton, E.L., 1969, "Sound Velocity, Elasticity, and Related Properties of Marine Sediments, North Pacific," II, Elasticity and Elastic Constants, NUC TP 144, Naval Undersea Research and Development Center, San Diego, California.

[21] Chen, C.T. and F.J. Millers, 1977, "Precise Equation of State of Seawater for Oceanic Ranges of Salinity, Temperature, and Pressure," Deep Sea Research, 24, pp. 365-369.

TABLE 2

SEAWATER DENSITY

Pressure (10^5 N m^{-2})	Density (10^3 kg m^{-3})
0	1.028
100	1.033
200	1.037
300	1.042
400	1.046
500	1.051
600	1.055
700	1.059
800	1.063
900	1.067
1000	1.071

Seawater density table for deep water from Ogushwitz.[18]
NOTE: 100×10^5 N m^{-2} corresponds to the hydrostatic pressure of approximately 1000 meters of water.

(2.3×10^{10} dynes cm^{-2}). Variations up to 10% are due to changes in hydrostatic pressure. Table 3 relates hydrostatic pressure to the bulk modulus of seawater.

Viscosity of Pore Fluid--As with the other fluid parameters, viscosity is constant to first order (equal to 19×10^{-4} kg m^{-1} sec^{-1}, or 19×10^{-3} poise), with variations of less than 5% associated with hydrostatic pressure changes. Table 4 gives the relationship to pressure for deep seawater.

Porosity--Porosity (β) is usually derived from measurements of water content.

There are also empirical methods for inferring porosity. Porosity ranges can be associated with sediment size classes. For example, Figure 1, modified from Hamilton,[22] shows porosity ranges associated with clays, silts, and sands (.7 to .9; .5 to .8; and .4 to .5, respectively). Porosity can be associated with wet bulk density, as in Figure 2, also given by Hamilton.[22]

Porosity values as a function of depth in the sediment can be obtained either from measurements of water content in cores, or from empirical relationships provided by Hamilton.[23]

$$\beta = 0.720 - 0.987 \cdot z + 0.830 \cdot z^2 \qquad (30)$$

for calcareous sediments

$$\beta = 0.720 - 0.816 \cdot z + 0.361 \cdot z^2 \qquad (31)$$

for terrigenous sediments

---

[22]Hamilton, E.L., 1970, "Sound Velocity and Related Properties of Marine Sediments, North Pacific," J. Geophys. Res., 75, pp. 4423-4446.

[23]Hamilton, E.L., 1975, "Acoustic and Related Properties of the Sea Floor: Density and Porosity Profiles and Gradients," NUC TP459, Naval Undersea Center, San Diego, California, p. 47.

TABLE 3

SEAWATER BULK MODULUS

Pressure (10^5 N m^{-2})	Density (10^9 N m^{-2})
0	2.15
100	2.22
200	2.29
300	2.36
400	2.44
500	2.51
600	2.58
700	2.66
800	2.73
900	2.80
1000	2.88

Seawater bulk modulus table for deep water from Ogushwitz[18]. NOTE: 100×10^5 N m^{-2} corresponds to the hydrostatic pressure of approximately 1000 meters of water.

TABLE 4

SEAWATER VISCOSITY

Pressure (10^5 N m^{-2})	Viscosity (10^{-4} kg m^{-1} sec^{-1})
0	19.40
203	18.99
340	18.84
523	18.76
791	18.76
1105	18.84
1758	19.03

Seawater viscosity table for deep water from Ogushwitz.[18] NOTE: 100×10^5 N m^{-2} corresponds to the hydrostatic pressure of approximately 1000 meters of water. 10^{-4} kg m^{-1} sec^{-1} = 10^{-3} poise.

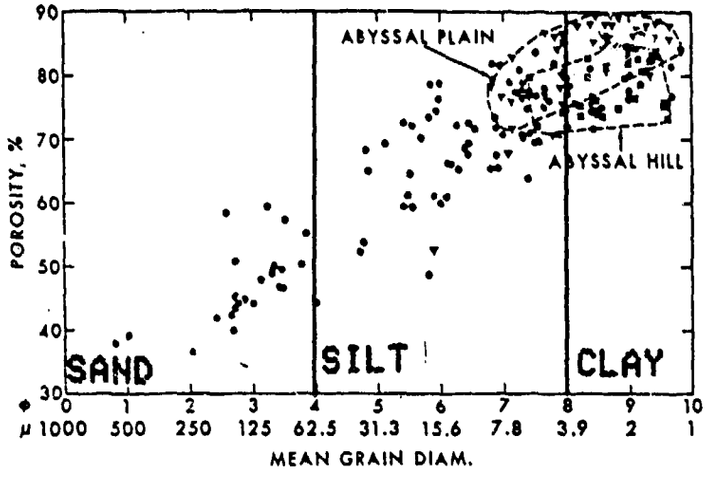

Figure 1. Porc ity versus Mean Diameter of Mineral Grains. Grain Diameter is Divided into Three Size Classes: Sand, Silt, and Clay (Modified from Hamilton[22]).

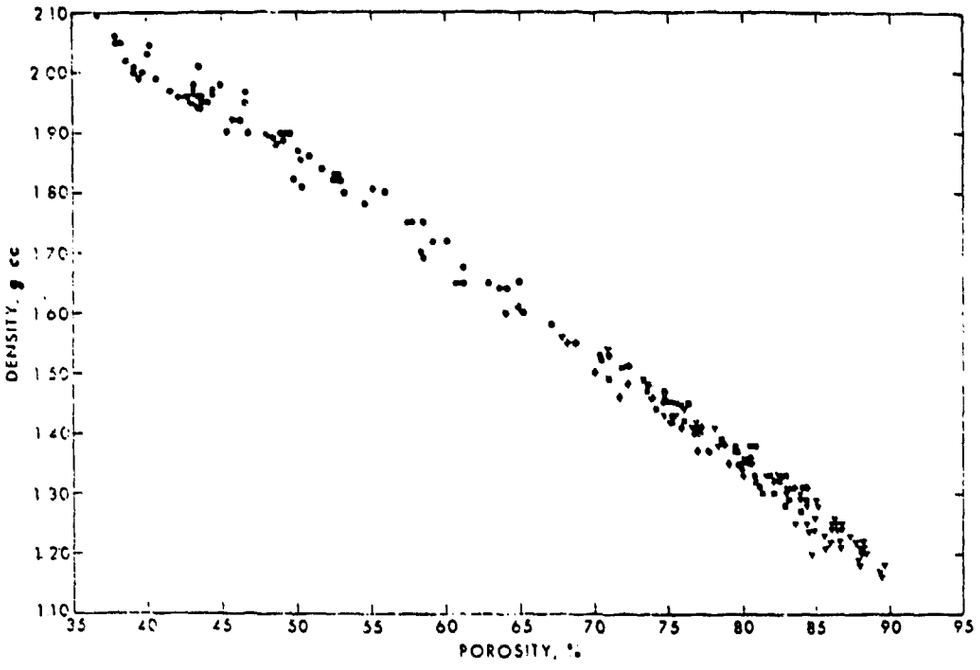

Figure 2. Saturated Bulk Density Versus Porosity (Hamilton[22]).

$$\beta = 0.814 - 0.813 \cdot Z - 0.164 \cdot Z^2 \quad (32)$$

for pelagic clay

$$\beta = 0.900 - 0.016 \cdot Z - 3.854 \cdot Z^2 \quad (33)$$

for radiolarian ooze

and

$$\beta = 0.861 - 0.549 \cdot Z + 0.492 \cdot Z^2 \quad (34)$$

for diatomaceous ooze

Here, β is porosity in decimal fraction and Z is sediment depth in kilometers (10^3 m).

Values for porosity with depth must be corrected for overburden pressure in order to obtain the relevant in situ values. Domenico[24] gives pressure corrections for Ottawa sands and glass beads. Van der Knaap[25] and Toksoz, et al,[26] give more general corrections. In all cases, these corrections are small in the upper 1,000 m of the sediment.

Permeability--Permeability (in m^2) is usually measured directly only in laboratory experiments. Permeability can also be related to porosity and sediment texture through the physical relationship of the Kozeny-Carman equation given by Carman[27] (in his equation 1.37) in the form

---

[24]Domenico, S.N., 1977, "Elastic Properties of Unconsolidated Porous Sand Reservoirs," Geophysics, 42, pp. 1339-1368.

[25]Van der Knapp, W., 1960, "Non-linear Behavior of Elastic Porous Media," Journ. Soc. Petroleum Engineers AIME TP 8072.

[26]Toksoz, M.N., C.H. Cheng, and A. Timur, "Velocities of Seismic Waves in Porous Rocks," Geophysics, 41, pp. 621-645.

[27]Carman, P.C., 1956, Flow of Gases Through Porous Media, Academic Press, New York.

$$k = \frac{1}{KS_0^2} \frac{\beta^3}{(1-\beta)^2} \tag{35}$$

where k = permeability in m^2,

S_0 = specific surface of the particles in sediment in m^{-1} (surface area per unit volume)

K = constant independent of particle shapes and sizes or sediment porosities, ≈5.0.

A sphere of diameter d has a specific surface area of

$$S_0 = 6/d \tag{36}$$

If d_m is the diameter of a sphere with the same specific surface area as the average specific surface area of the actual grains in the sediment, then Equation (35) can be rewritten as

$$k = \frac{d_m^2}{36K} \frac{\beta^3}{(1-\beta)^2} \tag{37}$$

Often, measurements of a mean grain size (d_{m_g}) are available so that Equation (37) seems applicable. However, the relation of d_{m_g} to d_m is not clear and may depend upon the technique used to measure d_{m_g}.

If, for a sediment, a value of permeability (k_0) is known at a known porosity (β_0), then the constant of proportionality in Equations (35) and (37) can be determined:

$$\frac{1}{KS_0^2} = \frac{d_m^2}{36K} = \frac{k_0(1-\beta_0)^2}{\beta_0^3} \tag{38}$$

and both equations become

$$k = \left[\frac{k_0(1-\beta_0)^2}{\beta_0^3}\right] \frac{\beta^3}{(1-\beta)^2} \tag{39}$$

There is a great deal of empirical evidence that supports the Kozeny-Carman relation in unconsolidated sediments for the porosity range .3 to .8, over a broad range of grain sizes and shapes. One of us (Brunson)[28] has shown that Kozeny-Carman compares well with observations even for sediments with a distribution of grain sizes, provided the distribution of S_0 values are averaged, not the distribution of grain sizes.

Purely empirical relationships between permeability and porosity have been developed by Bryant, et al,[29] based on sediments in the Gulf of Mexico. For sediments composed of 80% clay, Bryant and coworkers found

$$k_1 = \exp(15.05 \cdot \beta - 27.37) \qquad (40)$$

for 60-80% clay

$$k_1 = \exp(14.18 \cdot \beta - 26.50) \qquad (41)$$

for silty sands and sandy silts

$$k_1 = \exp(15.59 \cdot \beta - 26.65) \qquad (42)$$

for sandy clays and silts

$$k_1 = \exp(17.51 \cdot \beta - 26.93) \qquad (43)$$

and, for the combined data

$$k_1 = \exp(14.30 \cdot \beta - 26.30) \qquad (44)$$

In Equations (40) to (44), permeability, k_1, is in units of cm sec^{-1}. To convert to m^2, one must remove the character of the

---

[28]Brunson, B., 1982, Laboratory Measurements of Shear Wave Attenuation in Natural and Synthetic Sediments: The Importance of Grain Shape and Sorting, oral presentation given at the SEG/USN Shear Waves and Pattern Recognition Symposium, NSTL Station, Mississippi, March 1982.

[29]Bryant, W.R., W. Hottman, and P. Trabant, 1975, Permeability of Unconsolidated and Consolidated Marine Sediments," Gulf of Mexico, Mar. Geotech., 1, pp. 1-14.

fluid from the measurement. This is done by the multiplication of factor $\eta/\rho g$ where η = viscosity, ρ = density, and g = gravitational acceleration. For seawater, this factor has a value of about 1.9×10^{-7} m sec, so k (in m^2) = 1.9×10^{-9} k_1 (in cm sec^{-1}).

Another empirical fit was developed by Krumbein and Monk[30] to relate permeability in sands to the distribution of grain sizes

$$k = 7.6\ d_{m_g}{}^2\ e^{-1.31\sigma_\phi} \times 10^{-6} \qquad (45)$$

Here,

d_{m_g} = mean grain diameter in mm = $2^{-\phi_m}$

ϕ_m = mean value of ϕ

ϕ = $-\log_2 d$

d = grain diameter

σ_ϕ = standard deviation of ϕ values due to the distribution of d values.

Poresize Parameter--The poresize parameter, a, can be determined from experiments in which all the other parameters are known. For a particular type of sediment, it can be related to the mean grain size as done by Stoll,[4] who found the poresize to be between 1/6 and 1/7 of the mean grain size. However, the constancy of this ratio among sediments of different types has not been demonstrated and is not expected. Hovem and Ingram[31] identify the poresize with twice the hydraulic radius (r_h), i.e.,

---

[30] Krumbein, W.C. and G.D. Monk, 1942, "Permeability as a Function of the Size Parameters of Unconsolidated Sand," Petroleum Technology, Am. Inst. Mining and Metallurgical Engineers, Tech. Pub. No. 1942, pp. 1-9.

[31] Hovem, J.M. and G.D. Ingram, 1979, "Viscous Attenuation of Sound in Saturated Sand," J. Acoust. Soc. Amer., 66, pp. 1807-1812.

$$a = 2r_h \tag{46}$$

where

$$r_h = \frac{\text{volume filled with fluid}}{\text{wetted surface}} = \frac{\beta}{(1-\beta)S_0} \tag{47}$$

For the general sediment, however, S_0 is not known and we've just replaced one unknown parameter with another. Hovem and Ingram[31] further assume spherical grains so that

$$S_0 = \frac{d}{6}$$

then

$$a = 2r_h = \frac{\beta}{(1-\beta)} \frac{d}{3} \tag{48}$$

but, in general, a shape correction factor is needed to multiply d. For distributions of grain size, it is important to average S_0, not the individual d values.

If we do not make the assumption that the grains are spheres, we can still use Equations (46) and (47) to relate the poresize parameter to permeability and porosity. Substituting (46) and (47) into (35), we see that

$$k = \frac{a^2}{4K} \beta \tag{49}$$

and therefore that

$$a = 2\sqrt{K}\left(\frac{k}{\beta}\right)^{1/2} \tag{50}$$

As noted before for unconsolidated sediments in a large range of porosities, K is approximately constant and equal to 5.0. Therefore,

$$a = 4.47 \left(\frac{k}{\beta}\right)^{1/2} \tag{51}$$

Depth dependence of a can then be related to depth changes in k and β.

If β and K are unknown, but assumed constant, and pore size and permeability are known to be a_0 and k_0, respectively, then Equation (49) can be solved for the factor $\beta/4K$.

$$\frac{k_0}{a_0^2} = \frac{\beta}{4K} \tag{52}$$

Then changes in the value of a can be related to changes in permeability by the equation

$$a = \left(\frac{a_0^2}{k_0}\, k\right)^{1/2} \tag{53}$$

Structure Factor--Structure factor, α, is a measure of the tortuosity of the pore spaces and theoretically varies from a value of 1 for uniform pores with parallel axes to a value of 3 for random systems of pores with all possible orientataions. Stoll[4] uses a value of 1.25 for sands and 3.0 for clays. Domenico[24] shows empirically that in sands for depths of burial up to 1,000 m, α is essentially constant and close to, but greater than 1.0. Domenico[24] and Brunson[28] also show that as grains deviate from ideal beads, the value of α drops rapidly from 3.0 to 1.0.

A physical relationship advanced by Berryman[32] is that

$$\alpha = 1 - r \cdot \left[1-\frac{1}{\beta}\right] \tag{54}$$

where r is a measure of the induced mass of a fluid due to the oscillation of solid particles in the fluid. According to Berryman, r can be modeled, and for spheres, r=1/2; but for

[32]Berryman, J.G., 1980, "Confirmation of Biot's Theory," Appl. Phys. Lett., 37, pp. 382-384.

other geometries, no values of r are given. There is consequently little advantage gained by the use of Equation (54).

Shear Modulus of Frame, Real Part--Values of the frame's shear modulus (μ_b) are rarely obtained by direct measurement. It can be related physically to values of the frame bulk modulus (K_b, which will be discussed later in this report) if a Poisson's ratio, R_p, is known.

$$\mu_b = \frac{3K_b(1-2R_p)}{2(1+R_p)} \tag{55}$$

Stoll[5] and Domenico[24] show that R_p for a dry sand lies in the range .1 to .25. While values for R_p in clay frames have not been presented in the literature, they must be less than the theoretical upper bound of 0.5.

Frame shear modulus can also be derived physically from measurements of the shear velocity V_s using

$$\mu_b = \rho V_s^2 \tag{56}$$

where ρ = the density of the frame = $(1-\beta)\rho_r$.

The depth dependence of the frame shear modulus can be related empirically to stress, according to sediment type using equations developed by Richart, et al.[33] For clays ($.33 \leq \beta \leq .60$)

$$\mu_b = \frac{1630(2.97-\varepsilon)^2}{(1+\varepsilon)} \cdot \tau_0^{1/2} \tag{57}$$

and for sands ($.24 \leq \beta \leq .59$)

$$\mu_b = \frac{1230(2.97-\varepsilon)^2}{(1+\varepsilon)} \cdot \tau_0^{1/2} \tag{58}$$

[33]Richart, F.E., J.R. Hall, and R.D. Woods, 1970, Vibrations of Soils and Foundations, Prentice Hall, Englewood Cliffs, pp. 111-118.

where

$$\varepsilon = \text{void ratio} = \beta/(1-\beta) \tag{59}$$

and τ_0 = average stress in frame.

The vertical stress, τ_1, at a depth, Z, in the sediment is computed by integrating the buoyancy-reduced weight of the overlying material, i.e.,

$$\tau_1 = \int_0^Z (1-\beta)(\rho_r-\rho_f)g\,dZ \tag{60}$$

where β and ρ_f are both allowed to vary with depth. Given τ_1, the average stress, τ_0, is by definition

$$\tau_0 = \frac{1}{3}(\tau_1+\tau_2+\tau_3) \tag{61}$$

where τ_2 and τ_3 are the horizontal components of stress. A value for τ_0 is obtained by assuming that $\tau_2=\tau_3=\tau_1$ for clays, and that $\tau_2=\tau_3=0.5\tau_1$ for sands. This derivation of the average stress is attributed to Stoll.[5]

Another approach to determining the shear modulus of the frame is introduced by Ogushwitz[18] based upon work by Berryman.[34,35] The approach, called the self consistent method (SCM), applies the mathematical constraint on the frame modulus that, for a traveling acoustic plane wave, the waves scattered by the voids (or vacuum inclusions) must vanish identically everywhere in the material. This condition is reached by

---

[34]Berryman, J.G., 1980, "Long Wavelength Propagation in Composite Elastic Media. I. Spherical Inclusions," J. Acoust. Soc. Amer., 68, pp. 1809-1819.

[35]Berryman, J.G., 1980, "Long Wavelength Propagation in Composite Elastic Media. II. Ellipsoidal Inclusions," J. Acoust. Soc. Amer., 68, pp. 1820-1831.

fixing the elastic properties of the grain and inclusions, and by fixing the inclusion shapes. Then, the elastic properties of the frame are varied until the scattering vanishes. In this condition, the inclusions are transparent to the incident plane wave. The procedures and advantages of the SCM are provided in complete detail by Berryman,[34,35] and are not repeated here, except to note that the procedure is iterative and requires (in our application) K_r, μ_r, inclusion shape and initial guesses for K_b and μ_b. Values for K_r have already been discussed. Values for μ_r can similarly be obtained from the literature or handbooks. Inclusion shapes are spheres, discs, needles, and prolate spheroids and oblate spheroids with a continuum of aspect ratios. By selecting one of the first three inclusion geometries, one avoids the necessity of specifying still another free parameter--the aspect ratio.

Shear Modulus of Frame, Imaginary Part--The imaginary part of the shear modulus (μ_b^*) is related to dissipation of shear waves propagating through the frame. This can only be derived from measurements of the log decrement of shear waves (Δ_s) and the real part of the frame shear modulus. By definition,

$$\mu_b^* = \frac{\mu_b \Delta_s}{\pi} \tag{62}$$

Ogushwitz[18] claims that for sediment applications $\mu_b^* \sim 0.0$.

Bulk Modulus of Frame, Real Part--This parameter, denoted by the symbol K_b, can be obtained by direct measurement. It can also be related to measured values of the frame shear modulus (μ_b), if Poisson's ratio (R_p) is known, using Equation 55.

In lieu of R_p, a measured value of the velocity of propagation of longitudinal waves (V_E) and the log decrement of longitudinal waves (Δ_E) can be used to calculate a complex

Young's Modulus (E and E*) and thence K_b through the relations

$$E = \rho V_E^2 \tag{63}$$

where, again, $\rho = (1-\beta)\rho_r$,

$$E^* = \frac{E\Delta_E}{\pi} \tag{64}$$

and

$$K_b = \frac{(\mu_b E - \mu_b^* E^*)(9\mu_b - 3E) + (\mu_b^* E + E^* \mu_b)(9\mu_b^* - 3E^*)}{(9\mu_b - 3E)^2 + (9\mu_b^* - 3E^*)^2} \tag{65}$$

These same measurements will also yield the imaginary part of the frame bulk modulus (K_b^*) as shown in the discussion of the next parameter. Equations (55), (56), (63), (64), and (65) are used by Stoll and Bryan[3] and Beebe.[7] It should be noted here that the range of acceptable values for the Poisson's ratio, R_p, places strong constraints on the acceptable values of V_E and V_S, because R_p is a function of their ratio. For $0.1 \leq R_p \leq 0.25$, the velocity ratio must be $1.48 \leq V_E/V_S \leq 1.58$.

The self consistent method (SCM) can also be used to derive K_b from μ_r, κ_r, and inclusion geometry, as noted in the discussion of μ_b.

Empirical relations between K_b and porosity have been developed by Hamilton.[36] For natural marine sands

$$\log K_b = 2.70932 - 4.25391 \cdot \beta \tag{66}$$

For St. Peter's or Ottawa sand

$$\log K_b = 2.57664 - 4.27516 \cdot \beta \tag{67}$$

---

[36] Hamilton, E.L., 1971, "Elastic Properties of Marine Sediments," J. Geophys. Res., 76, pp. 579-604.

For natural silty clays

$$\log K_b = 2.73580 - 4.25075 \cdot \beta \qquad (68)$$

These equations give K_b in units of 10^9 dynes cm^{-2}, or 10^8 N m^{-2}.

Bulk Modulus of Frame, Imaginary Part--The imaginary part of the bulk modulus (K_b^*) can be derived from measurements of the log decrement of compressional waves (Δ_p) and the real part of the bulk modulus by the definition

$$K_b^* = \frac{K_b \Delta_p}{\pi} \qquad (69)$$

If Δ_p is not available, but Δ_E is, along with μ_b, μ_b^*, and E, then

$$K_b^* = \frac{(\mu_b^* E + E^* \mu_b)(9\mu_b - 3E) - (\mu_b E - \mu_b^* E^*)(9\mu_b^* - 3E)}{(9\mu_b - 3E)^2 + (9\mu_b^* - 3E^*)^2} \qquad (70)$$

Ogushwitz[18] claims that for sediment applications $K_b^* \approx \mu_b^* \approx 0.0$.

This concludes the discussion of the physical and empirical relationships that can be used to generate the thirteen parameters of the Biot/Stoll model. It is clear that many of the relationships cannot be used unless specialized measurements are available and that certain combinations of relationships are redundant while other combinations are impossible. Our choice of relationships in a particular case depends upon the measurements available, and our desire to minimize dependence on empirical relationships. Even under casual inspection, it should be apparent that porosity and grain size are parameters frequently related to the other model parameters, and therefore are of fundamental importance.

Implementation of the Model on a Computer

A FORTRAN code for the solution of the Biot/Stoll equations, with options for providing or deriving the thirteen model parameters using many of the relationships described in the preceding section (including the self consistent method), was obtained from P. Ogushwitz,[37] installed by Planning Systems Incorporated on a Control Data Corporation (CDC) model 6600 computer at the David W. Taylor Naval Ship Research and Development Center (DTNSRDC), and was modified. For listings of the original code, see Ogushwitz.[18] The modifications we made included adding more options for deriving the thirteen model parameters. The outputs included velocity and attenuation measures at specific depths and frequencies for all three types of waves and, if two or more depths were specific, gradients of velocity and attenuation. Selected output parameters were transferred to a separate file for plotting on a Tektronix graphics system.

[37] Ogushwitz, P.R., Bell Laboratories, Whippany, New Jersey. Personal communication.

Sensitivity of Model Results to Inputs

With such variety of sources and derivations for the model input parameters as described earlier, it is to be expected that for a particular application several candidate values for a single input can be obtained. In such circumstances, one's experience can be used to select a favored value; but, it is important to know what effect the range of acceptable inputs will have on the results.

Consequently, for the cases explored below, we ran the model several times. The first run was termed a base case and included favored values. For subsequent runs, each case differed from the base case in the value of a single input parameter. For each parameter for which we felt a range of acceptable values existed, we substituted an upper bound in one run and a lower bound in the next. Then we moved on to another parameter.

By this process we were able to identify parameters whose acceptable range had relatively large effects on the model results. Such parameters were called "critical factors"; identifying them was a major objective of this work.

Model Performance Assessment

In order to render an objective assessment of the predictive performance of the Biot/Stoll model, it is necessary to make some comparisons of the model outputs with geoacoustic observations at the sites of interest. Recognizing that there will be differences between the speeds and attenuations predicted by the model, and those observations to which they are compared, some measure of the acoustic significance of the observed difference should be provided. We addressed both of these issues in an approach designed to provide insight into the model's performance, and the acoustic significance of any observed differences.

Geoacoustic Data Comparisons--The primary measure of the performance of the physical sediment model is its ability to accurately reproduce the geoacoustic properties of the area in which it is being exercised, given the physical properties of the seafloor in that area.

Using the approach outlined above, the required model inputs are derived from measurements or appropriate empirical and physical relationships. It is hoped that these inputs are of sufficient accuracy to yield valid approximations to the geoacoustic properties.

Primary standards of geoacoustic properties are not easily obtained. Sediment cores on which acoustic analysis has been performed are sometimes available for the upper few meters of the sediment column. Grab samples of surficial sediments generally do not yield reliable acoustic speeds. Deep Sea Drilling Project (DSDP) drill hole cores seldom contain complete logs of sound speed, and often no values are reported whatsoever. Very little attenuation data is available for direct comparison.

Given the scarcity of primary standards, one must rely on secondary standards for the geoacoustic comparisons. Seismic

profiling yields estimates of sound speed in the sediment and usually serve as the main source for such information. Recently, techniques have been developed to produce attenuation estimates, but these data are scarce. Another source of sound speed and attenuation versus depth is the inversion of seismic, bottom loss, or transmission loss data. In one approach, initial estimates are made of the geoacoustic properties of the seafloor. These estimates are then used as inputs to a numerical simulation model, and comparisons are made between the model outputs and the acoustic observations. The geoacoustic parameter estimates are iteratively refined until an acceptable degree of model-to-data agreement is obtained. Though not unique, some confidence in the solution is obtained because the data is fitted both in angle and frequency. If the data are of high quality, then the resultant geoacoustic parameter estimates may provide excellent representations of actual sediment geoacoustic properties--provided the depth dependence of the actual sediment is as smooth as the model presumes.

The Navy's Bottom Loss Upgrade (BLUG) currently under way at FNOC relies upon bottom loss inversion techniques to produce estimates of seafloor geoacoustic properties. Measured bottom loss data from many locations have been inverted to yield compressional wave speed and absorption as a function of depth in the seafloor. As mentioned earlier, the functional forms of speed and attenuation are greatly simplified. The first is quadratic, the second linear in depth. The BLUG inversion process described by Spofford[38] is based directly upon bottom loss measurements, and takes into account both the measurement geometry and the sediment type in which the measurement is made. The resultant set of geoacoustic parameters (idealized as they are) serves as a good secondary standard for model

[38]Spofford, C.W., 1980, "Inference of Geo-Acoustic Parameters from Bottom Loss Data," in Bottom-Interacting Ocean Acoustics, edited by W.A. Kuperman and F.B. Jensen, Plenum Press, New York, pp. 154-173.

prediction comparisons. This is particularly likely when nearby DSDP cores and other supporting data are available to suggest homogeneous sediments and the appropriate geophysical properties to be used as model inputs. This is the approach taken to establish some measure of the performance of the Biot/Stoll model for locations where the combination of BLUG and DSDP data allow it to be pursued. These locations are generally restricted to deep water.

We would like to assess also the capability of the Biot/Stoll model to accurately predict the geoacoustic properties in shallow water. This is particularly important because of the presence of larger grain permeable sediments in shallow water regions. Such sediments exhibit non-linear frequency response best modeled by methods which account for viscous interaction between interstitial fluids and sediment grains. This is a property of the Biot/Stoll model. The non-linear frequency dependence is most apparent in the acoustic attenuation. For this reason, we sought to identify a data set which would allow the frequency dependence of attenuation to be modeled and tested by observations. Beebe[7] has reported such a geoacoustic data set and the needed physical property inputs have been included in his report. Additionally, BLUG has a shallow water geoacoustic model which may be used for comparison, albeit the geoacoustic data is not backed by acoustic observations in the area of interest. The Beebe and BLUG geoacoustic parameters will be used for model performance in the shallow water case.

Acoustical Significance Studies--Once the geoacoustic model-to-data comparisons are completed, one may ask if the observed differences are acoustically significant. That is, do the geoacoustic parameter differences manifest themselves as observable differences in acoustic bottom or transmission loss?

To assess the acoustical significance, one would like to compare bottom loss or transmission loss derived from the model geoacoustic outputs directly with measured bottom loss or transmission loss. The difficulty with direct comparisons between modeled and observed losses is that one must not only correctly model the seafloor properties, but also account for the accompanying measurement conditions such as geometry and processing. While this can be done, the resources to do so, i.e., measurement simulation software, were not readily available.

For this study, we have opted to compare the bottom loss predictions derived from a multi-layered, plane wave, complex reflection coefficient simulation model called REFLEC. This model has been developed by scientists at the Naval Ocean Research and Development Activity using an approach described by Brekhovskikh[39] and has been used in studies designed to test the sensitivity of the complex reflection coefficient to sediment layering.[40] The model is capable of using the geoacoustic properties provided by the Biot/Stoll model or derived from bottom loss measurements using BLUG inversion techniques. The sediment properties are used to generate a multi-layered approximation to the sound speed and attenuation profiles. The number and thickness of the layers are selected automatically by a preprocessor which takes into account the sound speed gradient and the frequency at which the reflection coefficient calculation is to be performed. The layers are not allowed to exceed 0.1 wavelengths in thickness, thus ensuring a smooth approximation of the sound-speed profile.

---

[39]Brekhovskikh, L.M., 1960, Waves in Layered Media, Academic Press, New York.

[40]Gilbert, K.E., 1980, "Reflection of Sound from a Randomly Layered Ocean Bottom, J. Acoust. Soc. Am., 68, pp. 1454-1458.

The output of REFLEC consists of either the complex reflection coefficient or a bottom loss derived from that coefficient. These are available at any grazing angle specified for any frequencies of interest. The model can produce estimates for any desired frequency bandwidth (e.g., one-third octave) by averaging the results for discrete frequencies within the desired band. This frequency averaging option was used in the bottom loss simulations provided for this study.

The acoustical significance is then assessed by comparing the bottom loss estimates from REFLEC using BLUG derived geoparameters, with those estimates obtained using Biot/Stoll derived geoparameters. This bottom loss simulation was done at high and low frequency to allow the importance of differences in both sound speed and attenuation to be addressed.

Such a bottom loss comparison is in effect a "snapshot" of the impact of geoacoustic differences as a function of frequency for a single bottom interaction for a discrete selection of grazing angles. A more rigorous assessment of acoustic significance of such geoacoustic differences could be obtained by using the bottom loss estimates or the geoacoustic properties themselves to describe the bottom interaction portion of an acoustic transmission simulation. This type of simulation would allow subtle differences in the two bottom descriptions to manifest themselves as differences in acoustic transmission as repeated bottom interactions accumulate along a simulated propagation track. Neither time nor resources allowed such an assessment to be made for this study.

It is felt that the approach taken is a valid attempt to demonstrate the acoustic significance of observed geoacoustic differences between BLUG derived geoacoustic parameters and Biot/Stoll predictions for the same case. Care was taken not to introduce the complications which would prevail if direct bottom loss measurements were used without appropriately accounting for the measurement conditions such as source and

receiver geometry, environmental conditions, processing techniques, source (shot) properties, and waterborne propagation complications.

IV. RESULTS

DSDP Site 135

This site, the first of the two cases studied, is an area of thick calcareous sediment in the deep ocean. Physical properties are available from Volume XIV of the Initial Reports of the Deep Sea Drilling Project.[41] Geoacoustic properties are supplied indirectly through the acoustic bottom loss inversion techniques of BLUG for several Naval Air Development Center (NADC) bottom loss measurement sites in the area. NADC site 910, described by Spofford,[38] was singled out for comparison.

According to the DSDP report,[41] site 135, at 35°20.8'N, 10°25.5'W, lies 40 km southeast of the southern edge of the Horseshoe Abyssal Plain in 4200 m of water on a topographic high 750 m above the abyssal plain. The site is south of the seismically active Azores-Gibraltar fracture zone. The top 325 m of the sediment is comprised of nannoplankton chalk ooze of Pleistocene, Pliocene, and Miocene age. Below this was sampled 364 m of mostly terrigenous sediments with some silicified intervals and marl or limestone. A prominent reflecting horizon at approximately 0.4 s can be traced from beneath the adjacent abyssal plain onto the topographic high. This reflector corresponds to the major unconformity beneath the chalk ooze. The depth of the basalt basement is estimated to be 1000 m.

Properties--Fluid density, bulk modulus, and viscosity were interpolated from the seawater tables in Section III for the appropriate hydrostatic pressure and are listed in Table 5.

[41] Pimm, A.C., editor, 1971, Initial Reports of the Deep Sea Drilling Project, Vol. XIV: Covering Leg 14 of the Cruises of the Drilling Vessel GLOMAR CHALLENGER, Lisbon, Portugal to San Juan, Puerto Rico, October-December 1970, Prepared for the National Science Foundation, Washington, D.C.

TABLE 5

DSDP SITE 135 PHYSICAL PROPERTIES

	Depth in Sediment 0 m	Depth in Sediment 300 m	Units	Source
ρ_r	2400	2400	kg m^{-3}	DSDP cores
κ_r	1.4×10^{10} to 7.9×10^{10}	1.4×10^{10} to 7.9×10^{10}	N m^{-2}	see text
ρ_f	1047	1049	kg m^{-3}	Seawater Tables
κ_f	2.458×10^{9}	2.480×10^{9}	N m^{-2}	Seawater Tables
η	18.80×10^{-4}	18.79×10^{-4}	kg $m^{-1} s^{-1}$	Seawater Tables
β	.59	.43	--	DSDP cores
k	6.75×10^{-14} to 17.77×10^{-18}	1.22×10^{-14} to 1.6×10^{-18}	m^2	approx. grain size, Eqs. (37) & (39)
a	1.5×10^{-6}	$.64 \times 10^{-6}$	m	approx. grain size, Eqs. (48) & (53)
α	1.25	1.25	--	Stoll[4]
μ_b	0	5.44×10^{8}	N m^{-2}	grain density porosity & Eqs. (57), (59), (60), (61)
μ_b*	0	$.17 \times 10^{8}$ to 1.04×10^{8}		real frame shear log decs. from Hamilton Eq. (62)
K_b	0	9.07×10^{8} to 52.6×10^{8}	N m^{-2}	real frame shear modulus, Poisson's ratio range, Eq. (55)
K_b*	0	$.26 \times 10^{8}$ to 3.12×10^{8}	N m^{-2}	real frame bulk modulus = 16.3×10^{8} and Eq. (69). Log decs from Hamilton.

At 4200 m, in this part of the Atlantic Ocean, the speed of sound in seawater is 1532 ms^{-1}. The bulk modulus and density of the pore fluid at the top of the sediment given in Table 5 return the proper value for sound speed; so by this check we have confidence in those values.

Water content measurements on cores extracted from various depths in the DSDP drill hole are reported[41] and yield the porosity values presented in Table 6. For purposes of modeling the upper 325 m of sediment, we further assigned a value of .43 for a depth of 325 m. These porosity values are within .05 of the values obtained from independent measurements on the DSDP cores using the GRAPE (Gamma Ray Attenuation Porosity Evaluator). These values also parallel the Hamilton relation (Equation 30) for calcareous sediments, but are between .10 and .15 lower.

Bulk density measurements on cores extracted from various depths in the DSDP drill hole were used with the porosity values to determine grain densities. Table 7 gives the values of grain density derived in this manner. Though the density decreases with depth in the table, the differences were deemed to be within the error of the measurement technique and the grain density was assumed constant with the average value of 2400 kg m^{-3}.

To derive the bulk modulus of the grains, there is only the information from Appendix III of the DSDP Report[41] that the sediment is between 95 and 99% calcium carbonate (C_aCO_3) tests, and between 1 and 5% undifferentiated clay. In the sea-floor literature, we were unable to identify a value for the bulk modulus of such tests. Beebe[7] implies a relatively high value of 7.9×10^{10} N m^{-2} for calcium carbonate sediments off Daytona Beach, Florida. For quartz, an appropriate value[42] is 3.3×10^{10} N m^{-2}. Considering that a ratio of sound speed in

[42]Kinsler, L.E. and A.R. Frey, 1962, Fundamentals of Acoustics, John Wiley and Sons, New York.

TABLE 6

POROSITY VS. DEPTH FROM DSDP SITE 135

Depth (m)	Average Porosity
0	.590
85	.530
175	.430
260	.430

TABLE 7

GRAIN DENSITY VS. DEPTH FROM DSDP SITE 135

Depth (m)	Porosity	Bulk Density (kg m^{-3})	Grain Density (kg m^{-3})
0	.59	1645	2570
85	.53	1695	2480
175	.43	1730	2280
260	.43	1680	2210
		average =	2385
		round =	2400

water to sound speed at the sediment surface should be about .996 in this area, we derived another value for the grain bulk modulus of 1.4×10^{10} N m^{-2}. This range, from 1.4×10^{10} to 7.9×10^{10} N m^{-2}, is large and has quite noticeable effects on the profiles of velocity in the sediment, as will be shown in the section on model sensitivity. For now, we report the range in Table 5.

The DSDP Report gives no direct measure of permeability or poresize; but it does provide grain size distribution in terms of the size classes--less than 5% sand, less than 20% silt, and approximately 80% clay. According to the Wentworth scale, clay particles have diameters less than 4×10^{-6} m, so we took a mean grain size to be 3×10^{-6} m (.0003 cm). Assuming the grains are nearly spherical, we associated a value of the permeability and the poresize parameter with this grain size at the top of the sediment using Equations (37) and (48), respectively. The resulting values, 6.75×10^{-14} m^2 and 1.5×10^{-6} m^2, are listed in Table 5. An alternate approach to the surface permeability was to use Equation (40) for Gulf of Mexico sediments, which gave 17.7×10^{-18} m^2.

The depth dependence of permeability was related to the depth dependence of porosity using the Kozeny-Carman relation in the form of Equation (39), setting k_0 and β_0 equal to their surface values. The permeability at 300 m thus obtained was 1.22×10^{-14} m^2. The Gulf of Mexico equation gave 1.6×10^{-18} m^2. This range of permeability values are given in Table 5.

The depth dependence of poresize was related to the depth dependence of the Kozeny-Carman permeability using Equation (53). The result, $.64 \times 10^{-6}$ m, is reported in Table 5.

For the structure factor, a value close to 1.0 is appropriate for angular clay sized particles. We used a value of 1.25 (Table 5).

The frame shear modulus, real part, was derived from the stress using Equations (59), (60), (61), and (57). These equations predict no frame at the surface of the sediment, then a rapid change with depth to a finite value of shear modulus. Table 5 shows the surface and 300 m values.

The imaginary part of the frame shear modulus was derived using Equation (62) with estimates of the frame log decrement that varied between .1 and .6, as described by Hamilton.[43] The imaginary parts thus varied between $.17 \times 10^8$ and 1.04×10^8 N m^{-2}, as shown in Table 5.

The frame bulk modulus, real part, was derived from the frame shear modulus, real part, using Equation (55). A range of values was obtained by substituting a range of Poisson's ratios from .25 to .45. The range of real frame bulk moduli is 9.07×10^8 to 52.6×10^8 N m^2, and is shown in Table 5. This large range points up the sensitivity of the calculation to the precise choice of Poisson's ratio. This large range in frame bulk modulus, real part, does have a noticeable effect on the profiles of speed, as will be shown.

The imaginary part of the frame bulk modulus was derived using Equation (69) with estimates of the frame log decrement that varied between .05 and .6. Hamilton[43] notes the log decrement of compressional waves should be less than the log decrement of the shear waves by as much as a factor of 10 in silts and clays. Applying this range of log decrements to a real part fixed at 16.3×10^8 N m^{-2} (the middle of the Poisson ratio range), we calculated a range of values for the imaginary part of $.26 \times 10^8$ to 3.12×10^8 N m^{-2} (Table 5).

Sensitivity Analysis--The outputs of the model, i.e., the profiles of speed and attenuation for compressional and shear

[43]Hamilton, E.L., 1976, "Attenuation of Shear Waves in Marine Sediments," J. Acoust. Soc. Am., 60, pp. 334-338.

waves, are dependent on the choices made for the model inputs. From Table 5, it is clear that the most uncertain input values in the case of DSDP site 135 are the parameters K_r, k, μ_b*, K_b, and K_b*. Of course, there are uncertainties associated with each input value in Table 5, though they are not all listed explicitly. Resources did not allow us to examine each one in detail. We did perform other preliminary comparisons and found no great uncertainties or sensitivities among the remaining parameters. For our model sensitivity analysis, we defined a base state rather arbitrarily (Table 8) within the ranges specified in Table 5 for the five parameters K_r, k, μ_b*, and K_b*. Each of the five parameters were then allowed to vary over the range and the model outputs were plotted in three forms: compressional speed vs. depth; compressional attenuation vs. depth; and compressional attenuation vs. frequency. The depth range was confined between 0 and 300 m and the frequency range between 0 and 1600 Hz. Plots are grouped at the end of this section in order to allow easier reading of the text.

Figures 3,4, and 5 show the effect of varying the grain bulk modulus over its range. Though the shapes of the speed profiles are similar, the values are not. At the surface, the difference is about 70 m s^{-1} (~4.4%) in sound speed, and at 300 m it is 200 m s^{-1} (~10%). Varying the grain bulk modulus makes almost no difference to the attenuation values (Figures 4 and 5). We conclude that for sound speed, properly fixing the value of K_r is critical.

Figures 6 to 8 show the effect of varying the permeability algorithm. Even though the permeability difference is four orders of magnitude, neither the speed nor the attenuation are affected. This is due to the relatively small role played by viscous losses between frame and fluid at these frequencies in clays. We conclude that at frequencies less than 1600 Hz for clays, permeability is not a critical factor.

TABLE 8. SENSITIVITY ANALYSIS
DSDP SITE 135

Model Parameter	Driving Parameter	Range Low	Range High	Base Value
K_r	K_r (N m^{-2})	1.4×10^{10}	7.9×10^{10}	7×10^{10}
k	functional dependence	Kozeny-Carman [Eq. (37)]	Bryant, et al [Eq. (39)]	Kozeny-Carman [Eq. (37)]
μ_b*	shear log decrement	.1	.6	.5
K_b	Poisson's ratio	.25	.45	.35
K_b*	Compressional log decrement	.05	.6	.5

The parameter μ_b^* is discussed jointly with κ_b^* in a later paragraph.

Figures 9 to 11 show the effect of varying the frame bulk modulus over its range, defined in terms of the Poisson's ratio as given in Table 8. Speed (Figure 9) is not much affected at the surface (in this figure the shallowest point is at 1 m depth) where the frame moduli go to zero. But at 300 m, where the frame bulk modulus derived from a Poisson's ratio of .45 is five times as large as that from a Poisson's ratio of .25, the difference is 500 m s^{-1} (25%). The base case, which has a Poisson's ratio halfway between the maximum and minimum, does not have sound speeds midway between the other two. This indicates that the speeds are more sensitive to changes in the Poisson's ratio as this parameter approaches its theoretical limit of 0.5. Since we expect that the Poisson's ratio is more likely to be lower than .35, rather than higher, the actual speed is probably within about 5% of the speed of the base case. The attenuation (Figures 10 and 11) is about four times as large for the large Poisson's ratio as for the small. This effect is due to the dependence of the imaginary part of the frame bulk modulus on the frame's real part, according to Equation (69), and the dependence on the frame imaginary part of the system imaginary part in the Biot disperson relation. Once again, the base case is probably a better representative of the actual value than the case of the large Poisson's ratio would indicate. The variation of Poisson's ratio has no effect on the shape of the attenuation curves against either depth or frequency. Still, we must conclude that for both sound speed and attenuation fixing either the frame bulk modulus or the Poisson's ratio is critical.

For fixed bulk and shear moduli of the frame, the effects of varying the compressional and shear log decrements are shown in Figures 12 to 14. Speeds (Figure 12) are unaffected.

Attenuation (Figures 13 and 14) varies by an order of magnitude, but its shape is not affected. Note that compressional attenuation is reduced even by reducing the shear log decrement. Both shear and compressional log decrements are critical.

We have seen in these sensitivity studies that K_r and K_b affect the magnitude more than the shape of the speed profiles, and that μ_b*, K_b*, and K_b affect the magnitude, but not the shape of the attenuation curves. Here, it is appropriate to talk about these shapes. The frequency dependence of attenuation, of course, comes from the complex viscosity correction term [F(K)] in the Biot theory itself. But, what of the depth dependence?

The Biot theory has no depth dependence, so that variations with depth must be due to variations of the input parameters. In our application, the depth dependent inputs were the fluid properties (ρ_f, K_f, and η), the porosity (β), and frame shear modulus (μ_b). The fluid properties change slowly; their changes are noticeable only over thousands of meters, and so they can not be driving the depth dependent structure we've seen. We can see the effect of the remaining two parameters by holding the porosity fixed and letting μ_b vary, through its dependence on the effective stress (Equations 57 and 60). Figure 15 shows the results for two values of fixed porosity, appropriate to the upper and lower values in the sediment column. We conclude that the porosity changes with depth are driving the vertical structure down to 175 m depth below which relatively small changes in speed are associated with increases in stress and therefore frame shear modulus. Figure 16 shows the same result for attenuation. Figure 17 shows that attenuation vs. frequency has its magnitude but not its shape affected by porosity.

The large range of sound speeds associated with a change of porosity of .2 indicates that even for an uncertainty of .05 in porosity (~10%), as is appropriate in this case, speed may

be noticeably affected (~100 m s^{-1}). All this seems to identify porosity as one of the critical parameters.

Geoacoustic Property Comparisons--The profiles of speed and attenuation output by the Biot/Stoll model were compared to profiles independently derived from bottom loss measurements through the inversion technique of BLUG. The base case from the sensitivity analyses is plotted with BLUG profiles designed to fit data from NADC site 910, in Figures 18 to 20. As can be seen, the speed profiles are roughly parallel. BLUG shows a great deal less structure and lies about 70 m s^{-1} below the Biot/Stoll base case. Also shown in Figure 18 is the constant sound speed assigned during the interpretation of the DSDP sesimic data. The attenuation curves are similarly shaped in frequency, but the BLUG values are lower. The attenuation vs. depth curves are quite distinct, with Biot/Stoll showing steeper attenuation gradients at the surface and higher attenuations.

The offset in speed values at the surface falls within the bounds caused by the uncertainty in our grain bulk modulus value. In fact, the BLUG surface value makes use of the observation that in this area the sediment surface sound speed is .996 of the water sound speed. Taking advantage of the same observation, we can fix the grain bulk modulus for our physical model. No other model parameter is capable of shifting the sediment surface sound speed value. At this point, we set the grain bulk modulus equal to 1.4×10^{10} N m^{-2}. In essence, we have treated the grain bulk modulus as an adjustable parameter; but in fact, it is not a free parameter. Because it is a physical quantity, the same value must hold true in other physically similar environments. An important test of the Biot/Stoll applicability is then to determine whether the same grain bulk modulus holds in other calcareous deposits. Such a test, however, was not performed in this study. It is our intention to do it in future work.

The offset in attenuation values at depth falls within the bounds caused by the uncertainty in frame log decrements. We used this to help us select values for the log decrements. We set the shear log decrement to 0.1 and the compressional log decrement to 0.05. These choices were consistent with Hamilton's[43] range and his observation that $\Delta_p/\Delta_s \approx .1$, and gave attenuations at depth that are close to the BLUG values. Once again, we adjusted our parameters; but once again, the price was dear--these values must hold true in all sediments of the type found here. In the case of attenuation, we did have the option of adjusting the Poisson's ratio, but this was not done because the effect is relatively small as the ratio is decreased below 0.35.

After these adjustments, the comparisons between the BLUG profiles and the Biot/Stoll profiles are as shown in Figures 21 to 23. Notable differences remain. Biot/Stoll shows more vertical structure in both speed and attenuation than does BLUG. The acoustic consequence of these differences are discussed in the next section. Figure 24 shows the values of bulk sediment density assumed by BLUG, given directly from DSDP measurements, and recalculated from the Biot input parameters porosity and grain and fluid densities. These differences also have acoustic consequences as will be discussed.

Acoustic Significance--As described in Section III, the profiles of speed, attenuation, and density were used to run a plane wave complex reflection coefficient model named REFLEC that calculates bottom loss vs. grazing angle. To compare the influence of the geoacoustic differences of the upper 300 m of sediment, we artificially located basalt basement at 300 m in the REFLEC runs. The consequences of this are mentioned during the following discussions. The comparisons were made at two frequencies: 100 Hz and 1600 Hz, and the results are shown in Figures 25 and 26.

At 100 Hz, both models show the same gross structure: increasing bottom loss to a relative maximum which occurs at the angle that grazes the basement; decreasing loss as waves reflecting off the basement traverse shorter paths through the sediment; and an abruptly increasing loss as waves penetrating the basement half space do not return.

The two models differ in the angle at which grazing of the basement (penetration to 300 m) occurs. Based on the velocity profiles and Snell's law we calculated that waves traveling in the Biot/Stoll sediment become horizontal at 300 m when their grazing angle is 33.7°, while BLUG requires a steeper wave with a 39.9° grazing angle. This is due to the lower speeds in the Biot/Stoll sediment. These angles are borne out by the locations of the peaks in Figure 25. The loss associated with angles between 17 and 40° is more for the Biot/Stoll sediment, because of the longer path lengths of waves traversing it than traverse the BLUG sediment. The difference is nearly 7 dB at 35°. Where deeply penetrating paths are nearly identical in length (beyond 40°), the loss in the Biot/Stoll sediment is slightly greater due to its greater attenuation. Between 18° and 25°, loss in the Biot/Stoll sediment does not increase, while in the BLUG sediment loss increases rapidly. This is due to the locally intense speed gradient in the Biot/Stoll sediment between 100 and 175 m depth. Beyond 31°, energy encounters the lower Biot/Stoll speed gradient below 175 m, resulting in greatly increased pathlengths and thus greater attenuation.

At the important small angles where loss is very low, the Biot/Stoll sediment is less lossy than the BLUG sediment. Though the difference is slight, it does mean that at low angles the Biot/Stoll sediment allows several times the number of bottom "bounces" as does the BLUG sediment, thus implying that signals can propagate substantially greater distances before reaching a given, say 6 dB, loss. This feature is due to the

rapid drop in Biot/Stoll attenuation in the vicinity of the sediment surface.

At 1600 Hz, there is no effect of basement at 300 m. For grazing angles greater than 15°, the refracting waves are so grossly attenuated that the curve resembles that for simple reflection from a homogeneous half-space. This is demonstrated in Figures 27a and 27b in which the bottom loss curves calculated via REFLEC for the Biot/Stoll and the BLUG sediments are each replotted with bottom loss derived from the square of the reflection coefficient for a homogeneous half space. This is calculated according to Equation 2.17 of Brekhovskikh[39] with the density and velocity in each half space set to the surface values in the Biot/Stoll and BLUG sediments, respectively. The singularity around the 7° angle of intromission is caused by the total transmission that occurs there. It can be seen that the Biot/Stoll sediment returns no refracted waves for grazing angles greater than 15°. The BLUG sediment continues to return refracted waves out to 21° because its higher gradient at depths less than 85 m leads to shorter refracted paths. Between 0 and 15°, loss is lower because sound waves entering the sediment return a significant amount of energy to the water columnn. Here, Biot/Stoll losses are less because attenuation values are lower (Figure 26).

Based on these observations, we conclude that, though there is agreement to first order, the acoustic implications of differences between BLUG and Biot/Stoll sediments, in some applications, are significant.

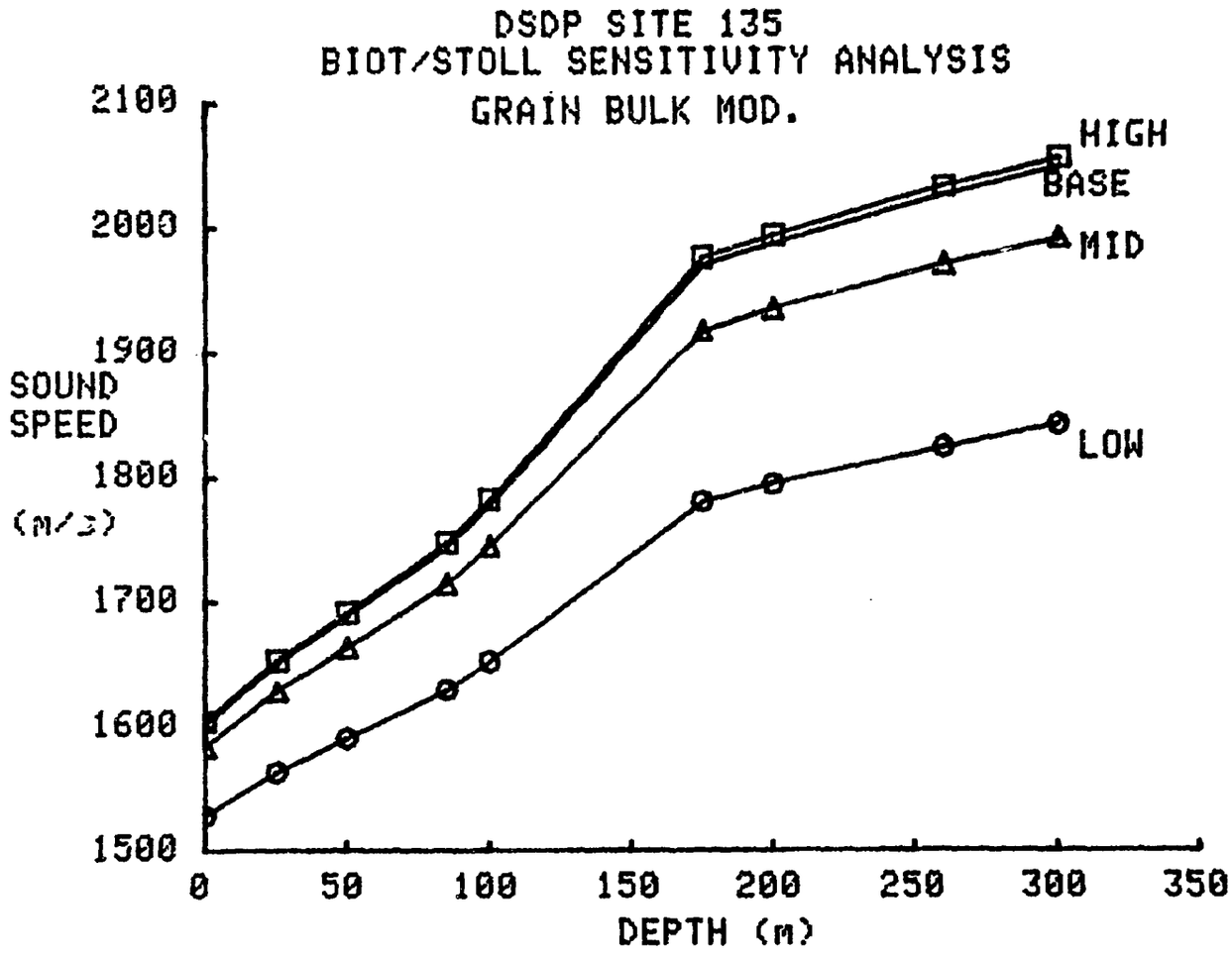

Figure 3. Sound Speed (at 200 Hz) versus Depth at DSDP Site 135 Showing the Effect that Varying the Grain Bulk Modulus has on the Output of the Biot/Stoll Model. Base, High, and Low Grain Bulk Moduli are Defined in Table 8.

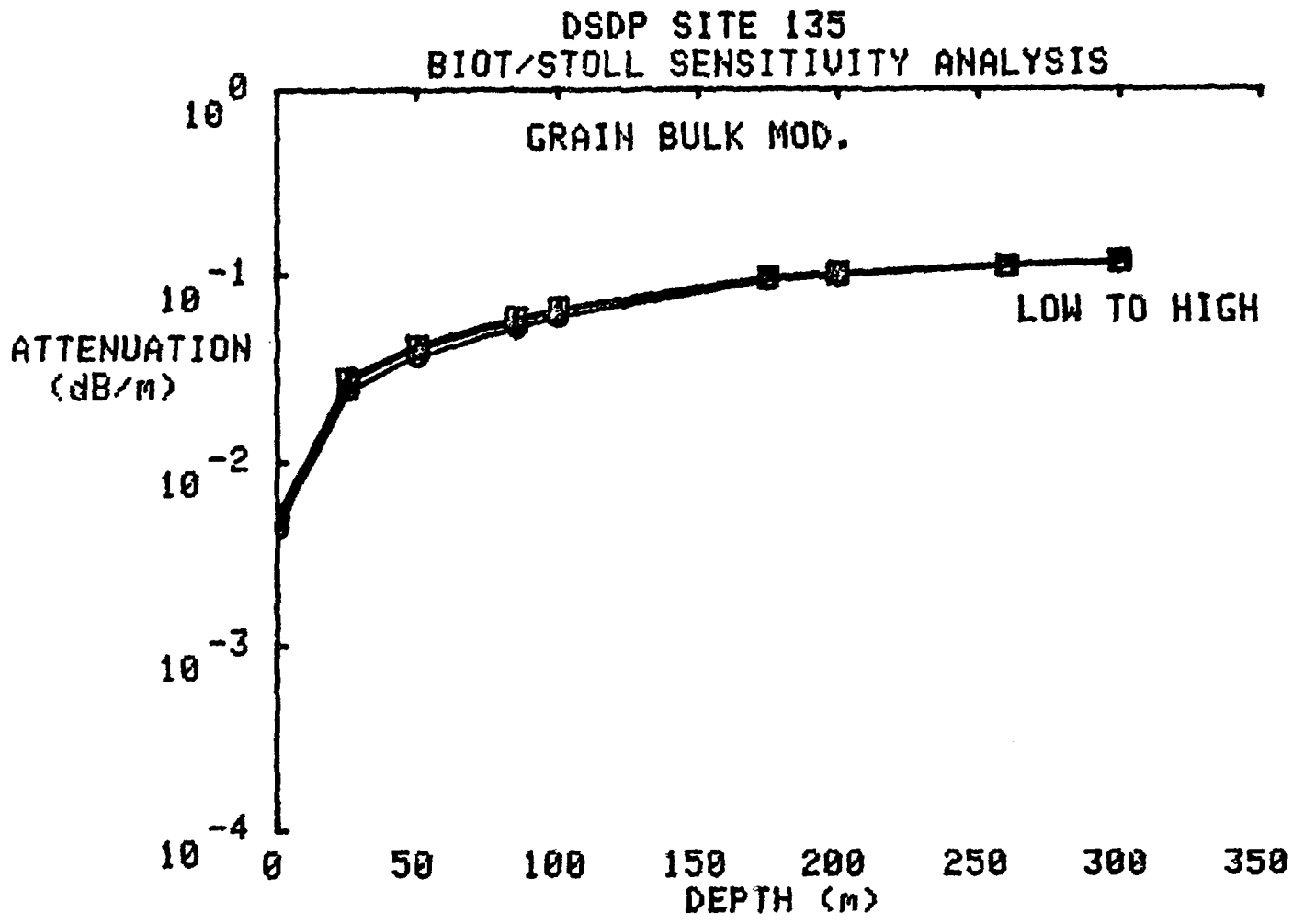

Figure 4. Same as Figure 3, but for Attenuation (at 200 Hz) versus Depth.

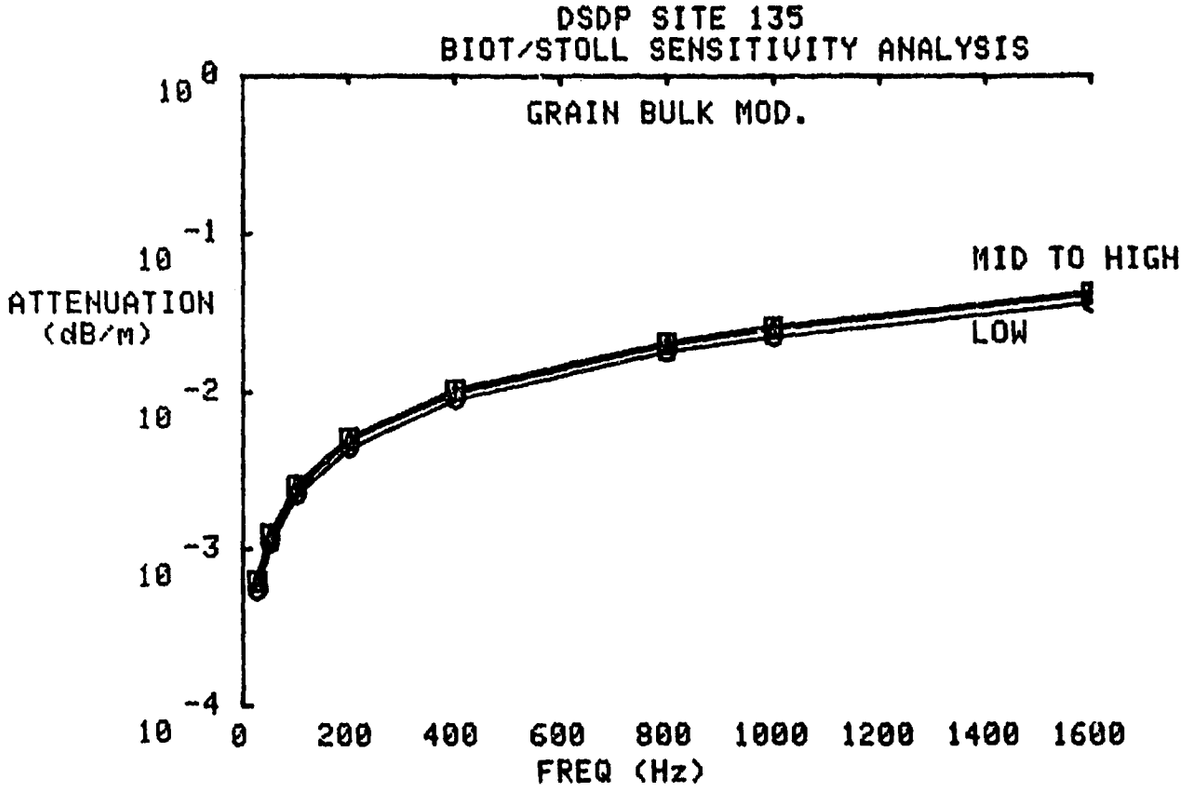

Figure 5. Same as Figure 3, but for Attenuation (at 0 m) versus Frequency.

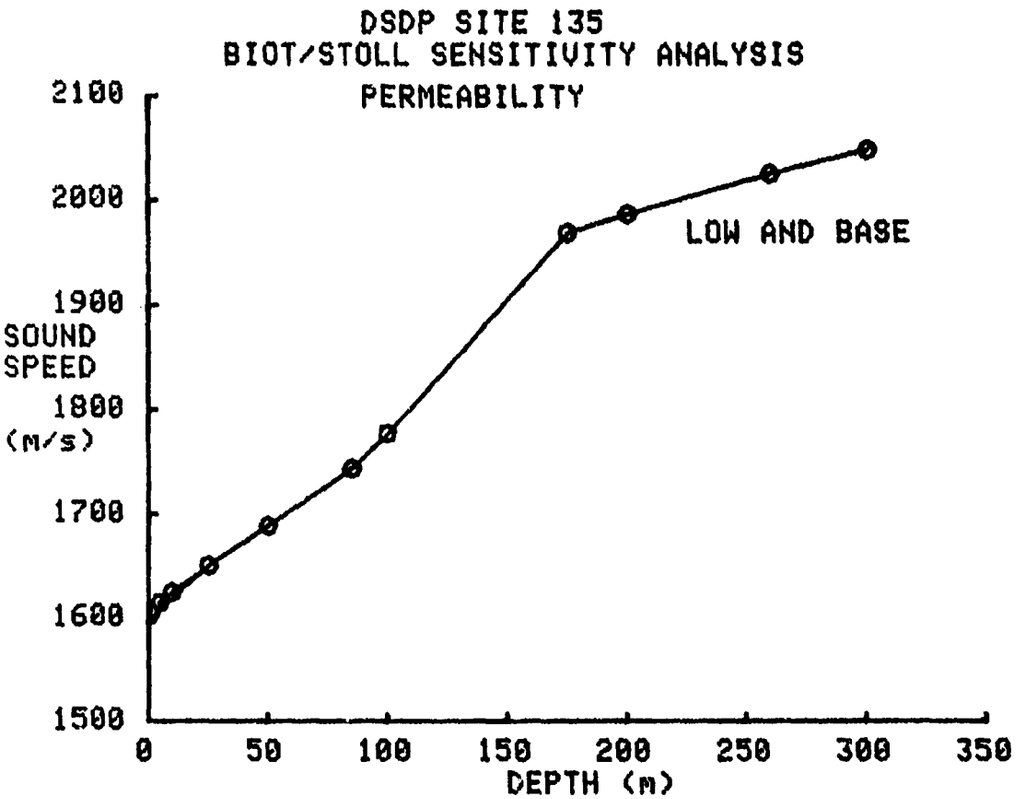

Figure 6. Sound Speed (at 200 Hz) versus Depth at DSDP Site 135 Showing the Effect that Varying the Permeability has on the Output of the Biot/Stoll Model. Base and Low Permeabilities are Defined in Table 8.

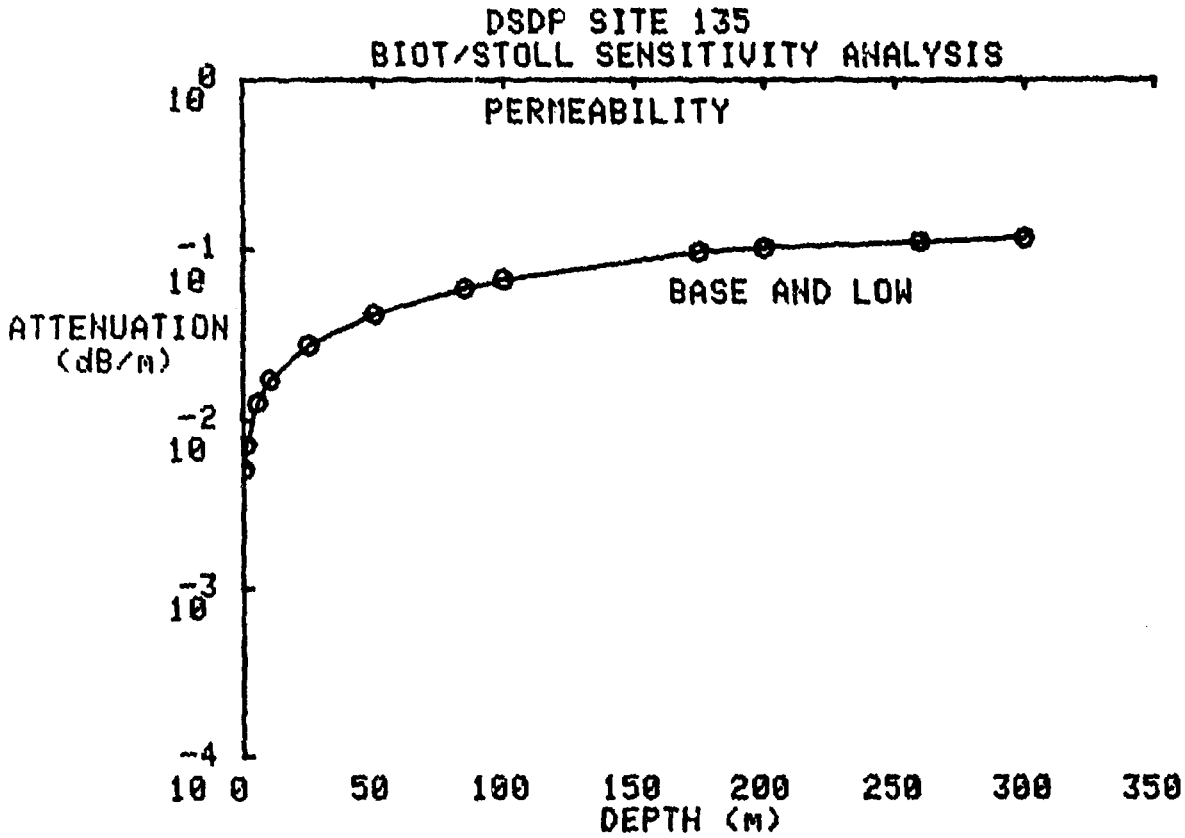

Figure 7. Same as Figure 6, but for Attenuation (at 200 Hz) versus Depth.

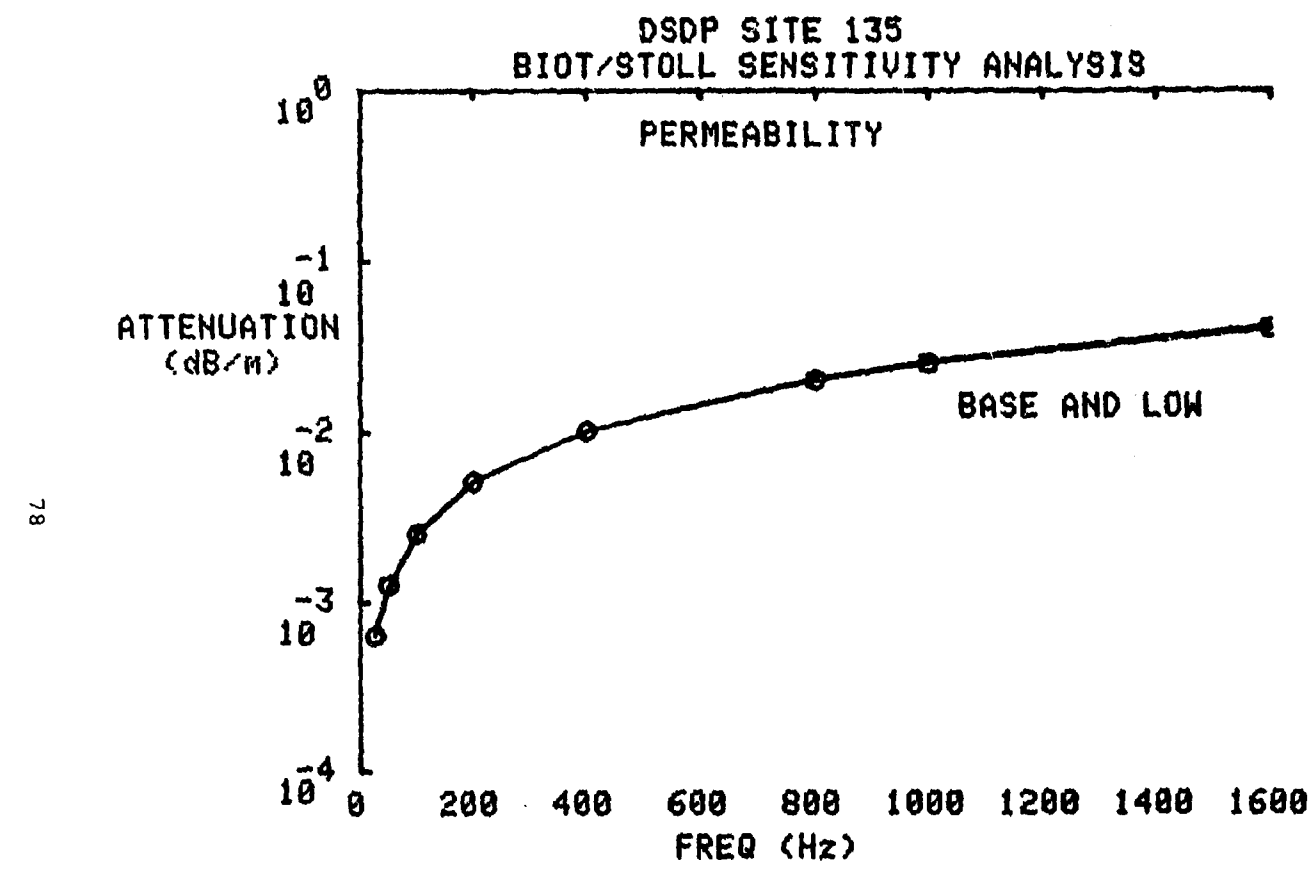

Figure 8. Same as Figure 6, but for Attenuation (at 0 m) versus Frequency.

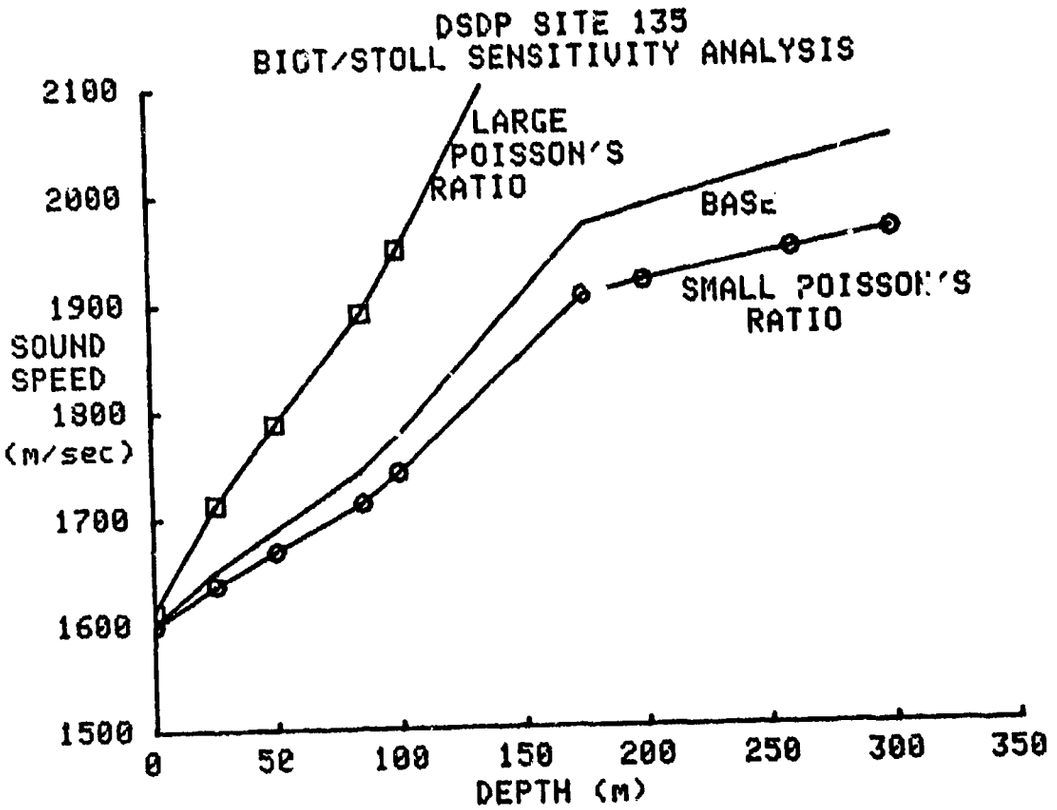

Figure 9a. Sound Speed (at 200 Hz) versus Depth at DSDP Site 135 Showing the Effect that Varying the Poisson's Ratio has on the Output of the Biot/Stoll Model. Base, Small, and Large Poisson's Ratios are Defined in Table 8. Note that the top curve goes off scale.

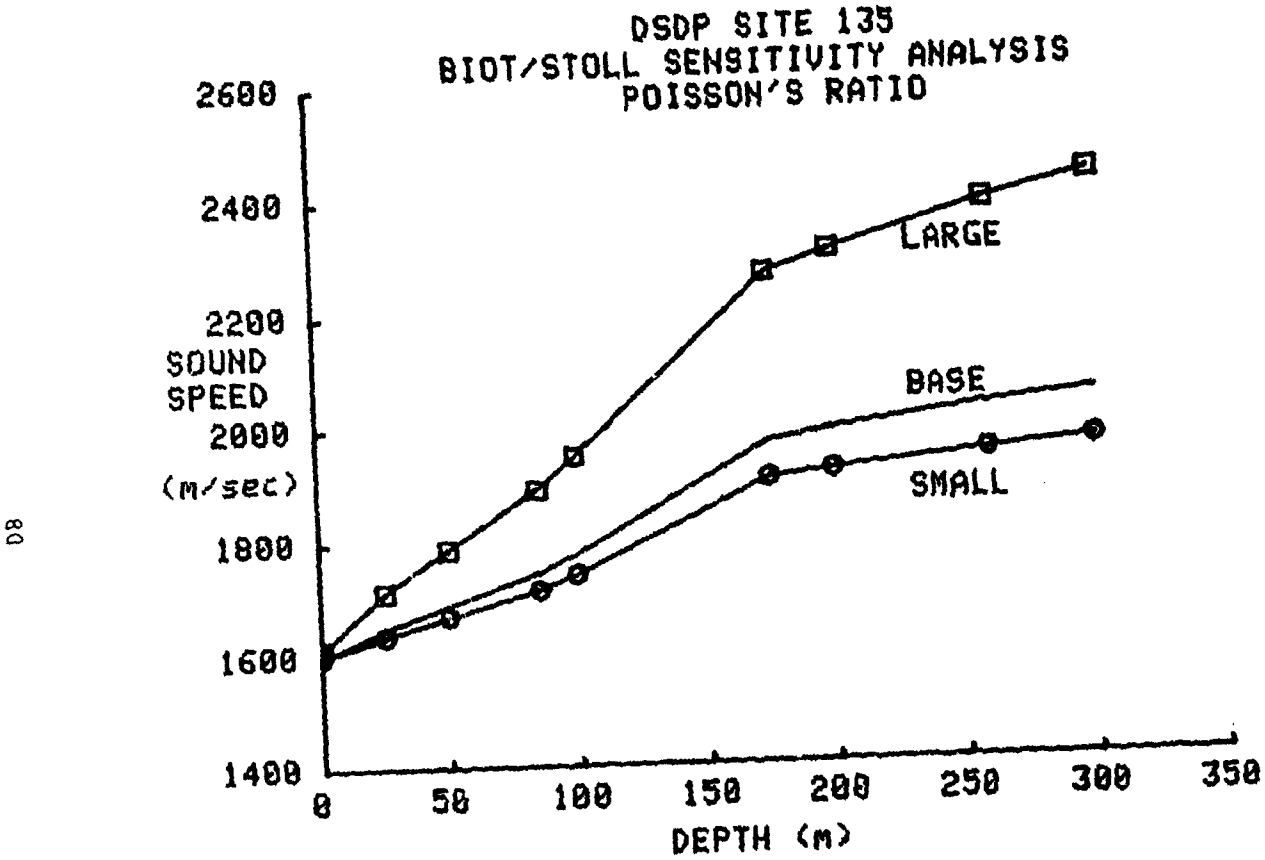

Figure 9b. Same as Figure 9a, but Replotted on a Condensed Scale to Show all of the Top Curve.

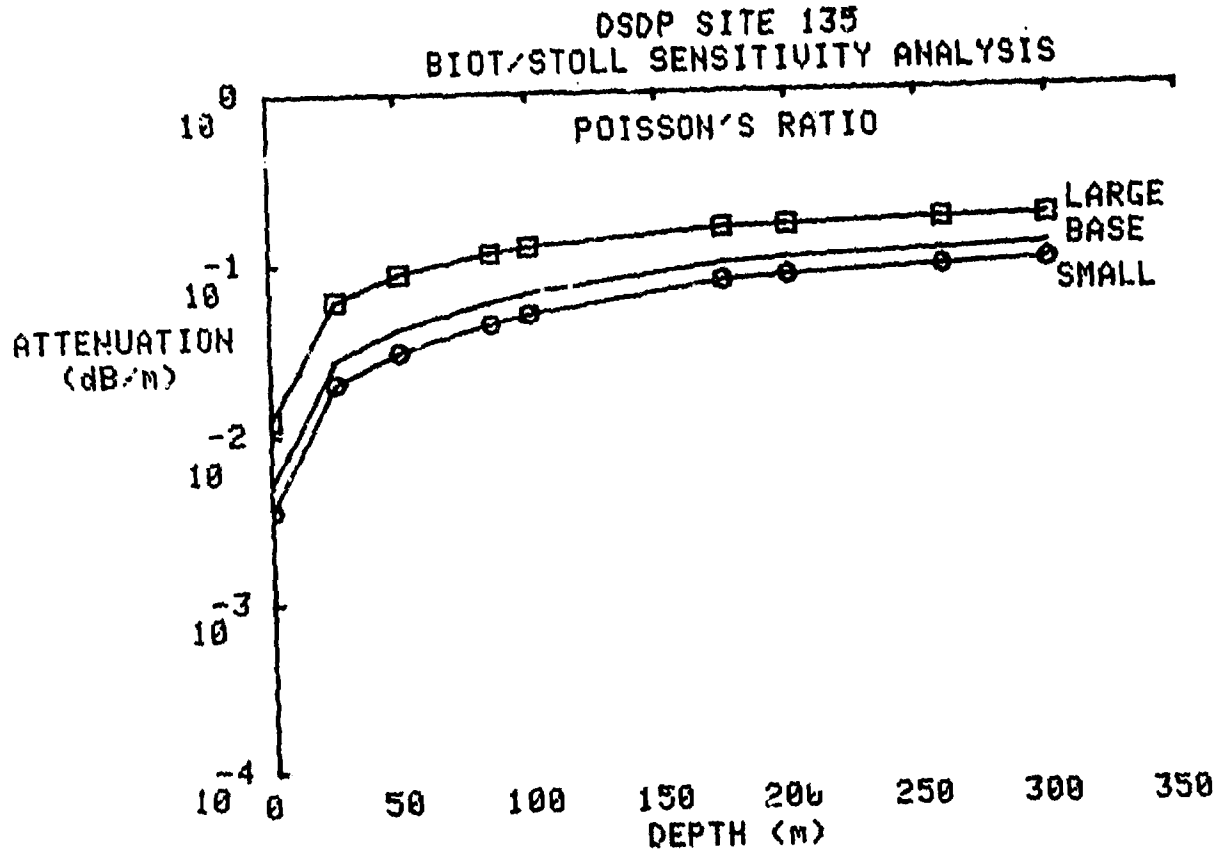

Figure 10. Same as Figure 9a, but for Attenuation (at 200 Hz) versus Depth.

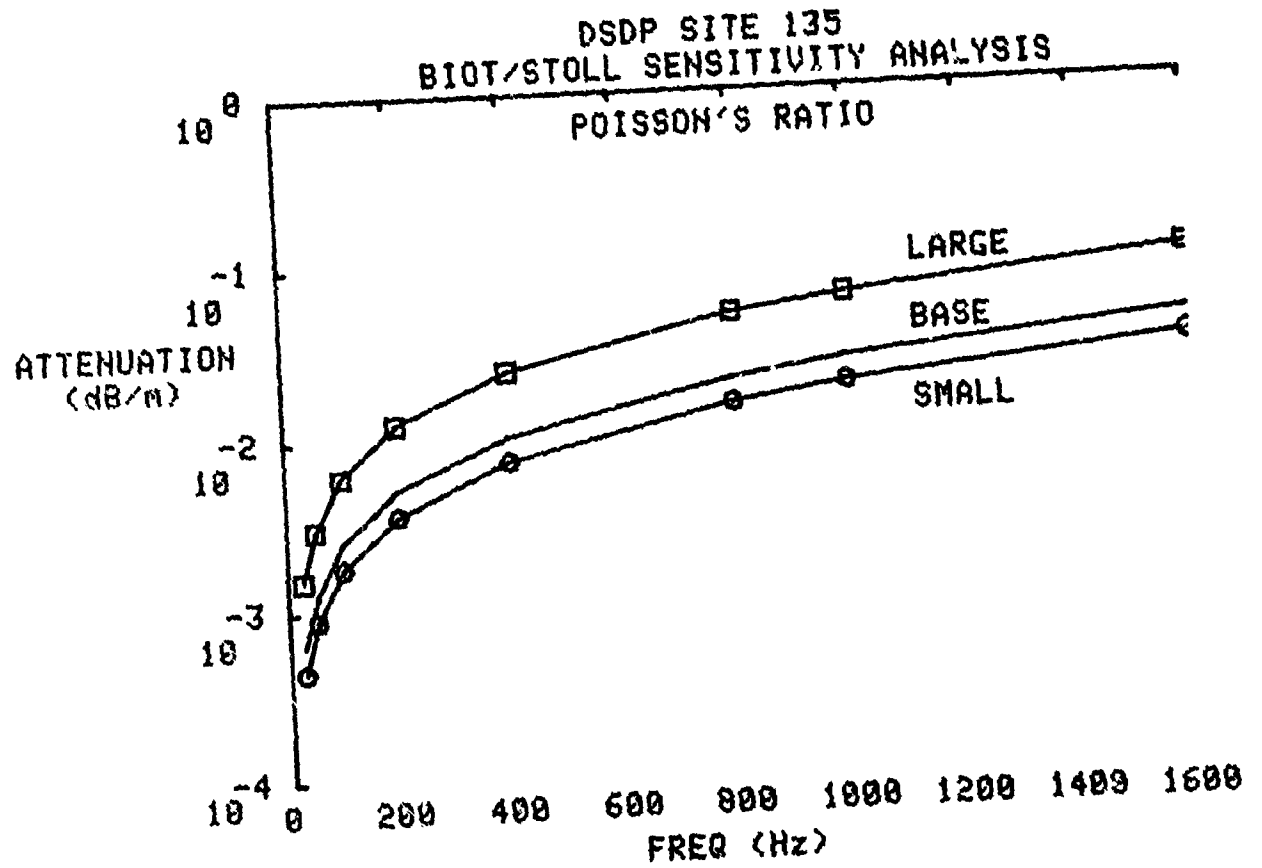

Figure 11. Same as Figure 9a, but for Attenuation (at 0 m) versus Frequency.

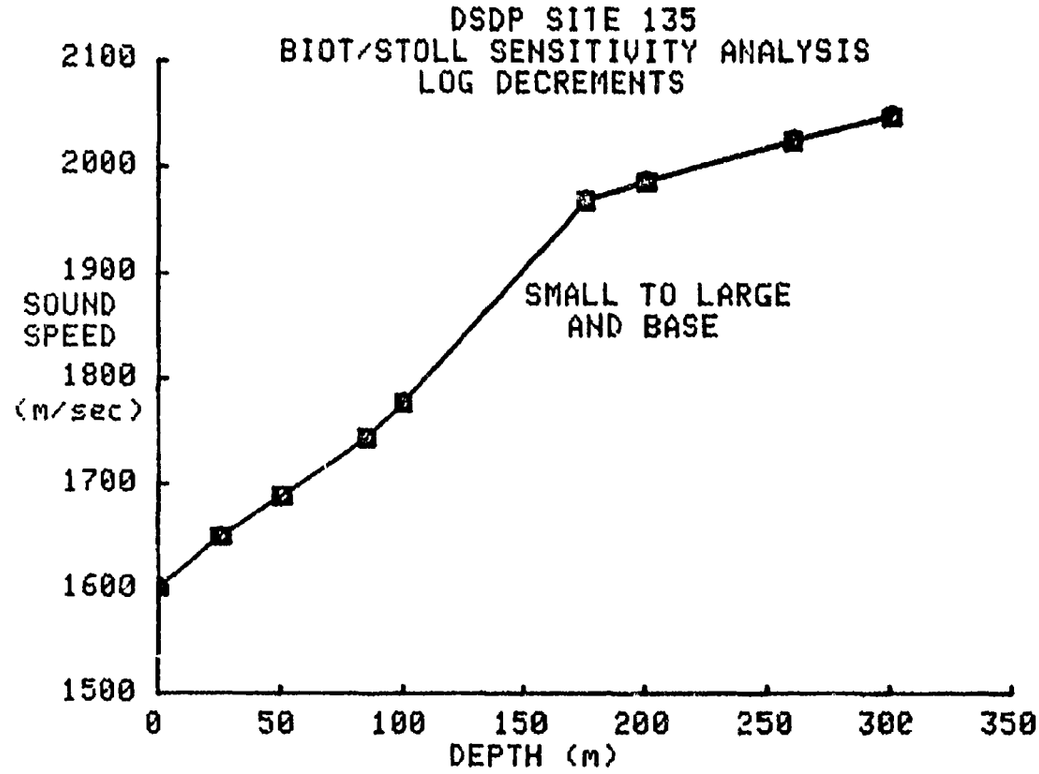

Figure 12. Sound Speed (at 200 Hz) versus Depth at DSDP Site 135 Showing the Effect that Varying the Logarithmic Decrements of Both Shear and Compressional Waves has on the Output of the Biot/Stoll Model. There is no Effect on Speed. Log Decrement Values are Given in the Caption to Figure 13.

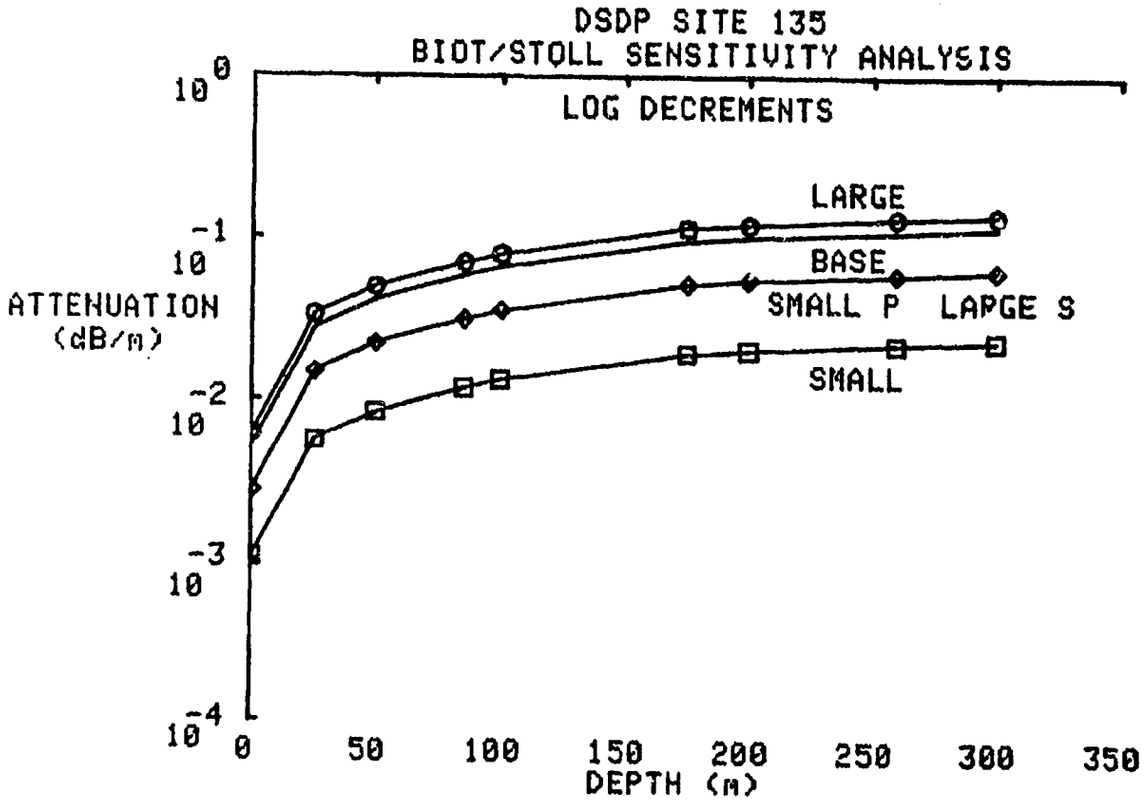

Figure 13. Same as Figure 12, but for Attenuation (at 200 Hz) versus Depth. The Large Logarithmic Decrement (Log Dec) Values are .6 for Both Shear (S) and Compressional (P) Waves. The Base Values are .5 for Both. The Small Log Decs are .1 for Shear Waves and .05 for Compressional Waves.

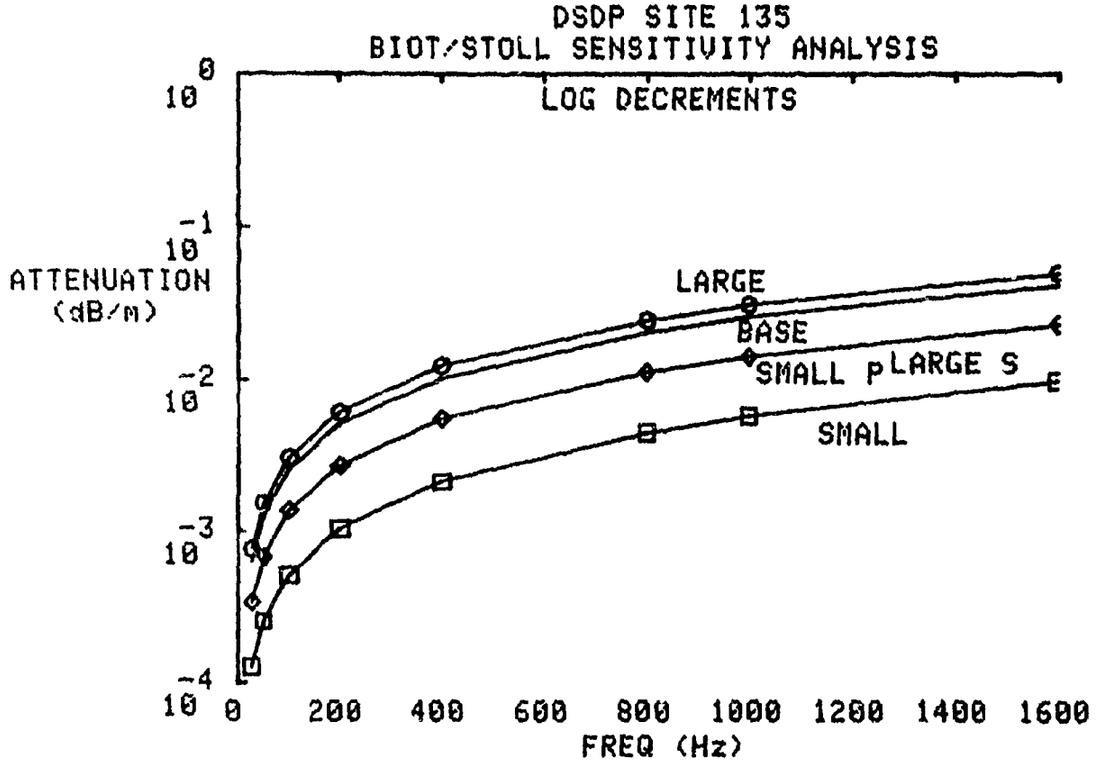

Figure 14. Same as Figure 13, but for Attenuation (at 0 m) versus Frequency.

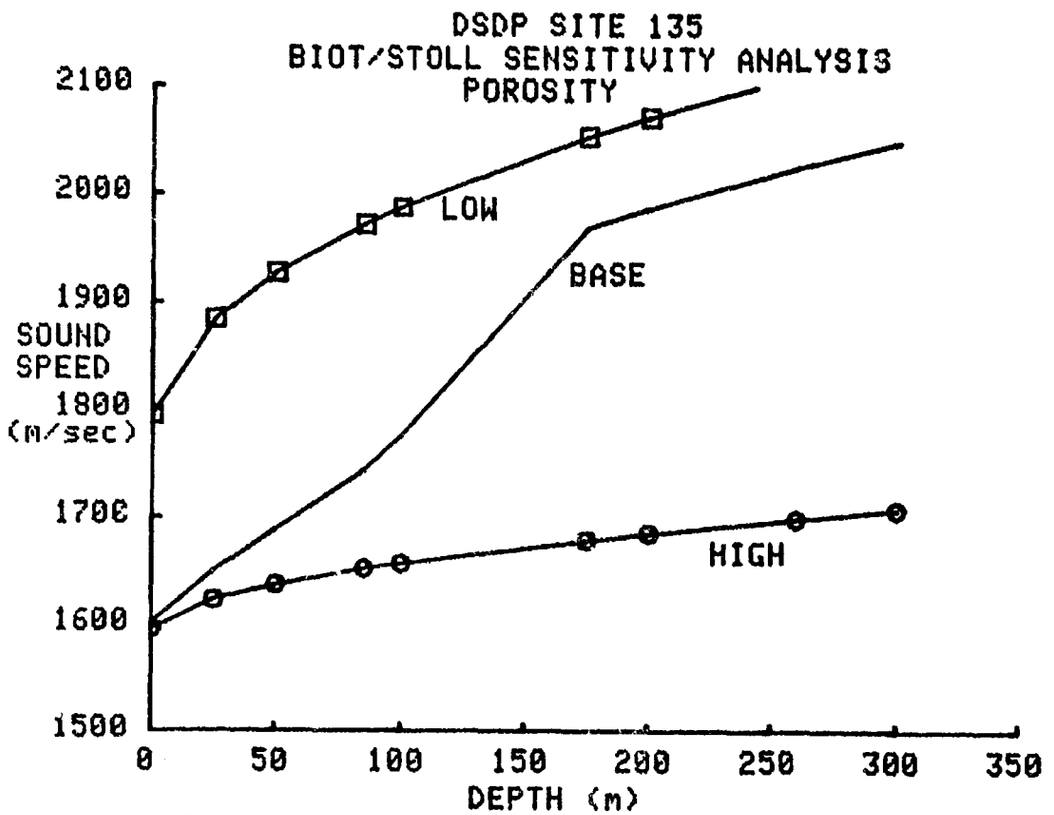

Figure 15. Sound Speed (at 200 Hz) versus Depth at DSDP Site 135 Showing the Effect that Fixing the Porosity Value as a Constant has on the Output of the Biot/Stoll Model. The Base Porosity Varies With Depth as in Table 6, the High Porosity is Fixed at .60, and the Low Porosity is Fixed at .40.

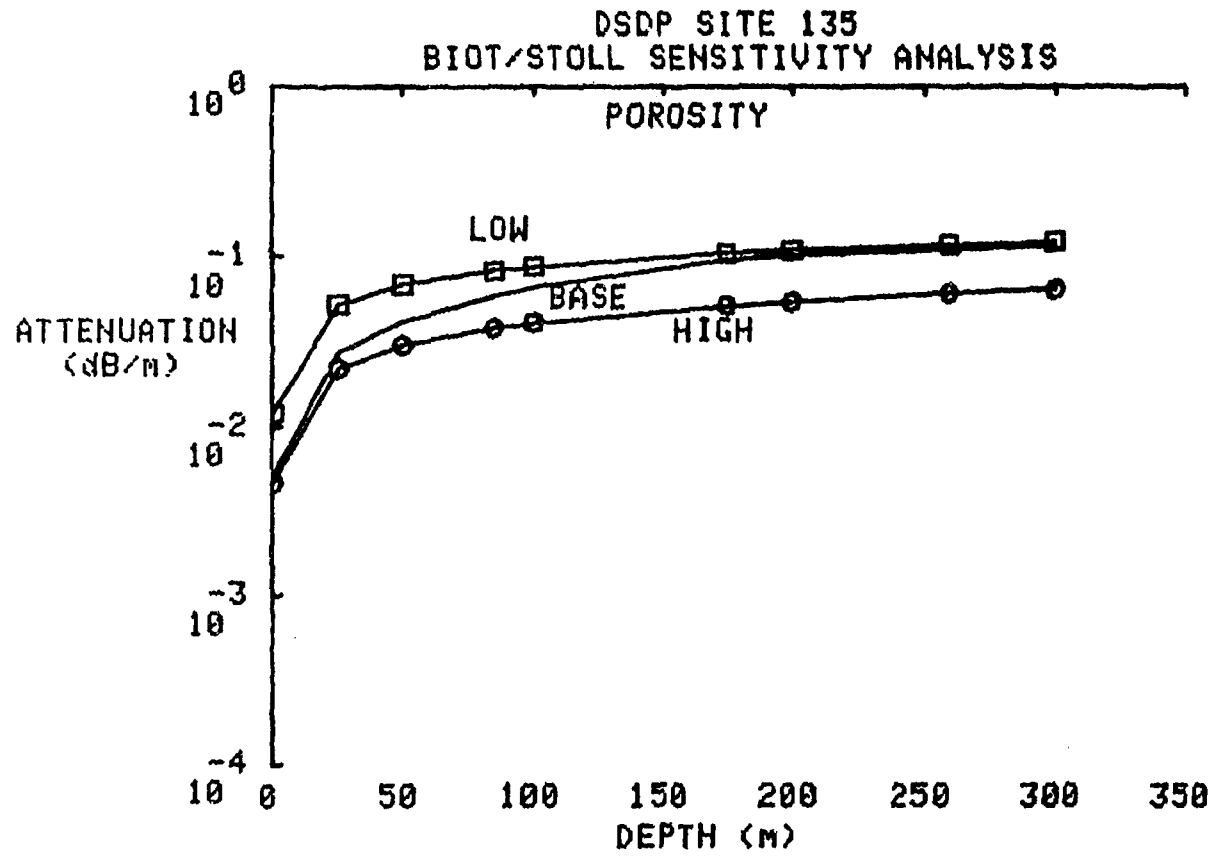

Figure 16. Same as Figure 15, but for Attenuation (at 200 Hz) versus Depth.

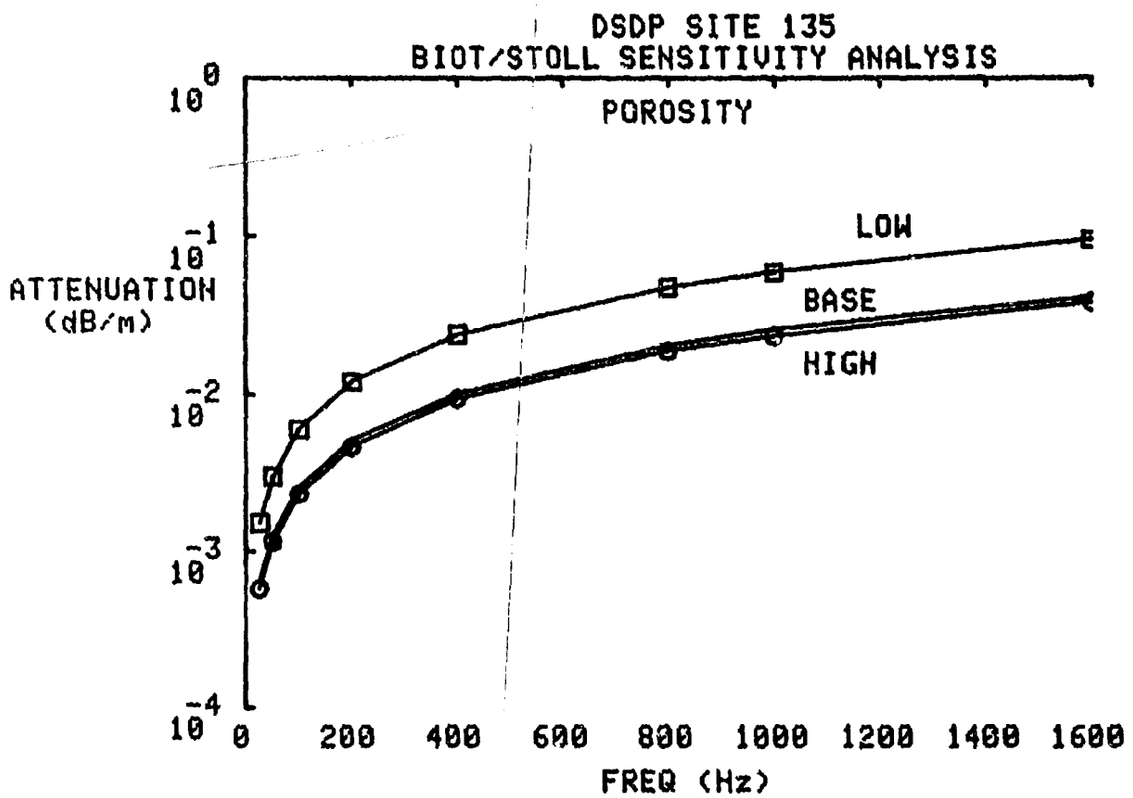

Figure 17. Same as Figure 15, but for Attenuation (at 0 m) versus Frequency.

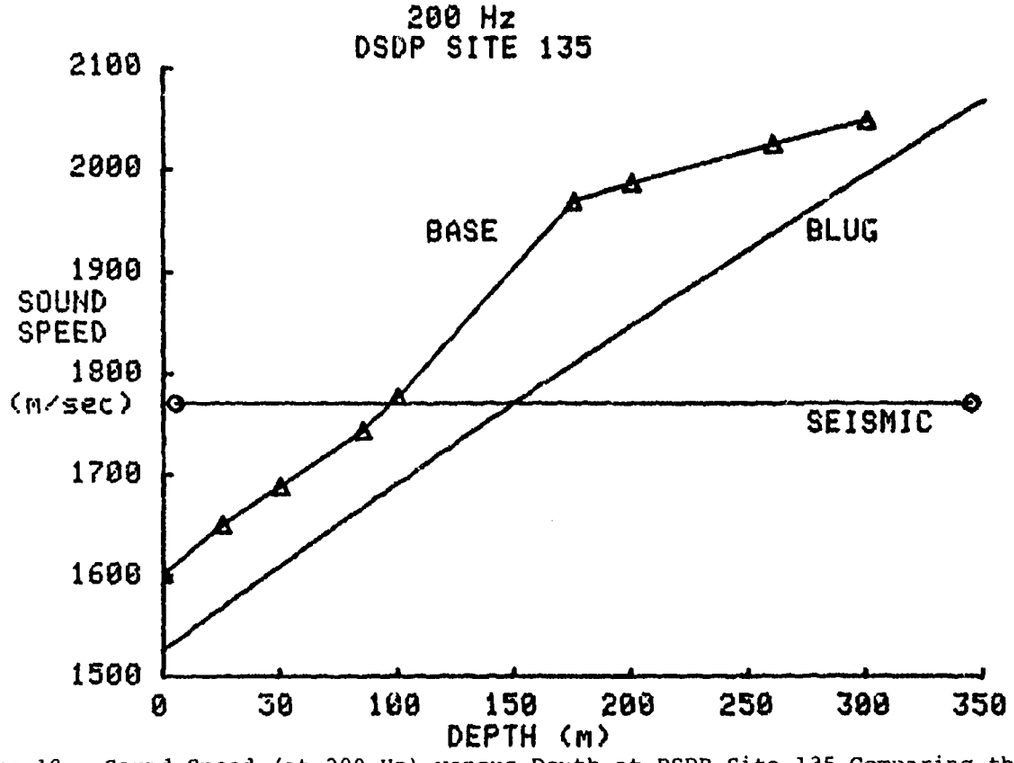

Figure 18. Sound Speed (at 200 Hz) versus Depth at DSDP Site 135 Comparing the Results of Biot/Stoll, BLUG, and an Average Computed by DSDP Scientists from Seismic Data. The Base Case of the Biot/Stoll Model is Defined in Table 8.

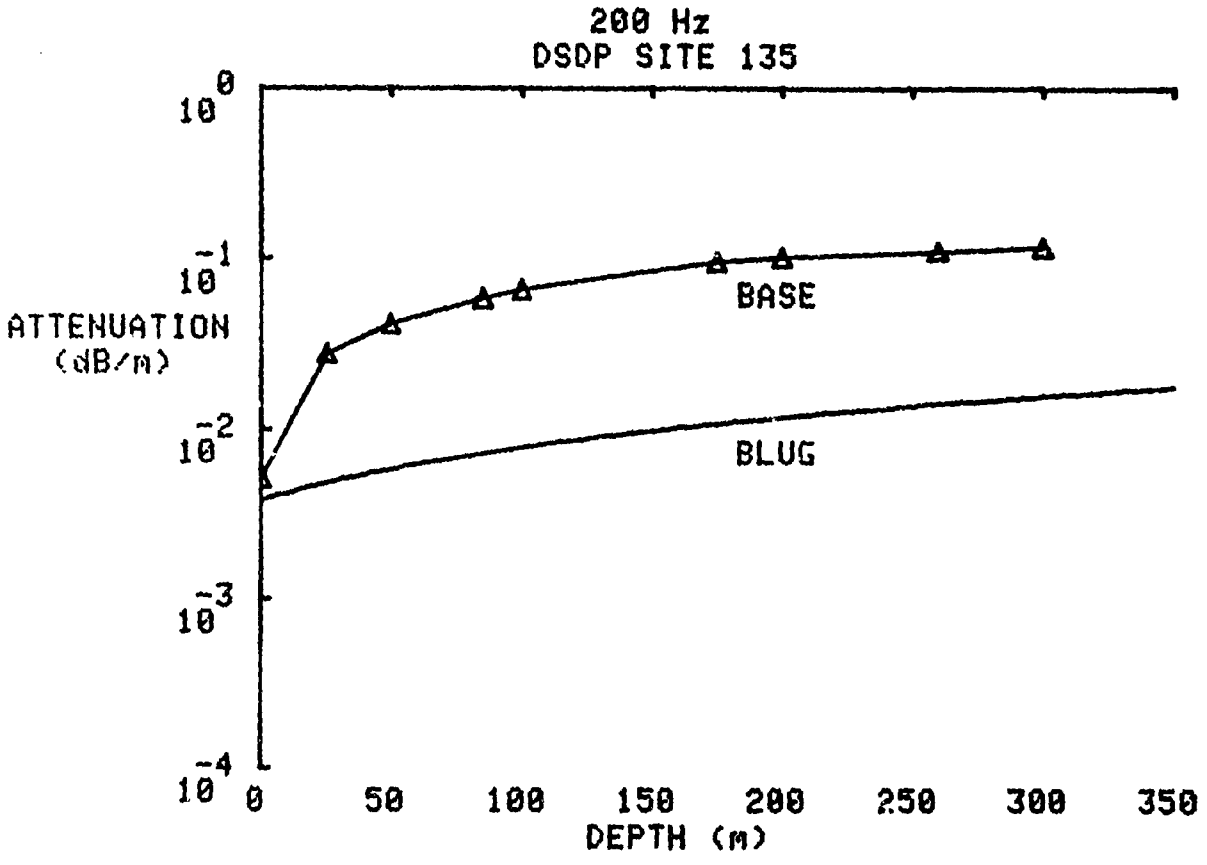

Figure 19. Same as Figure 18, but for Attenuation (at 200 Hz) versus Depth. There is no observation of Attenuation from the Seismic Data.

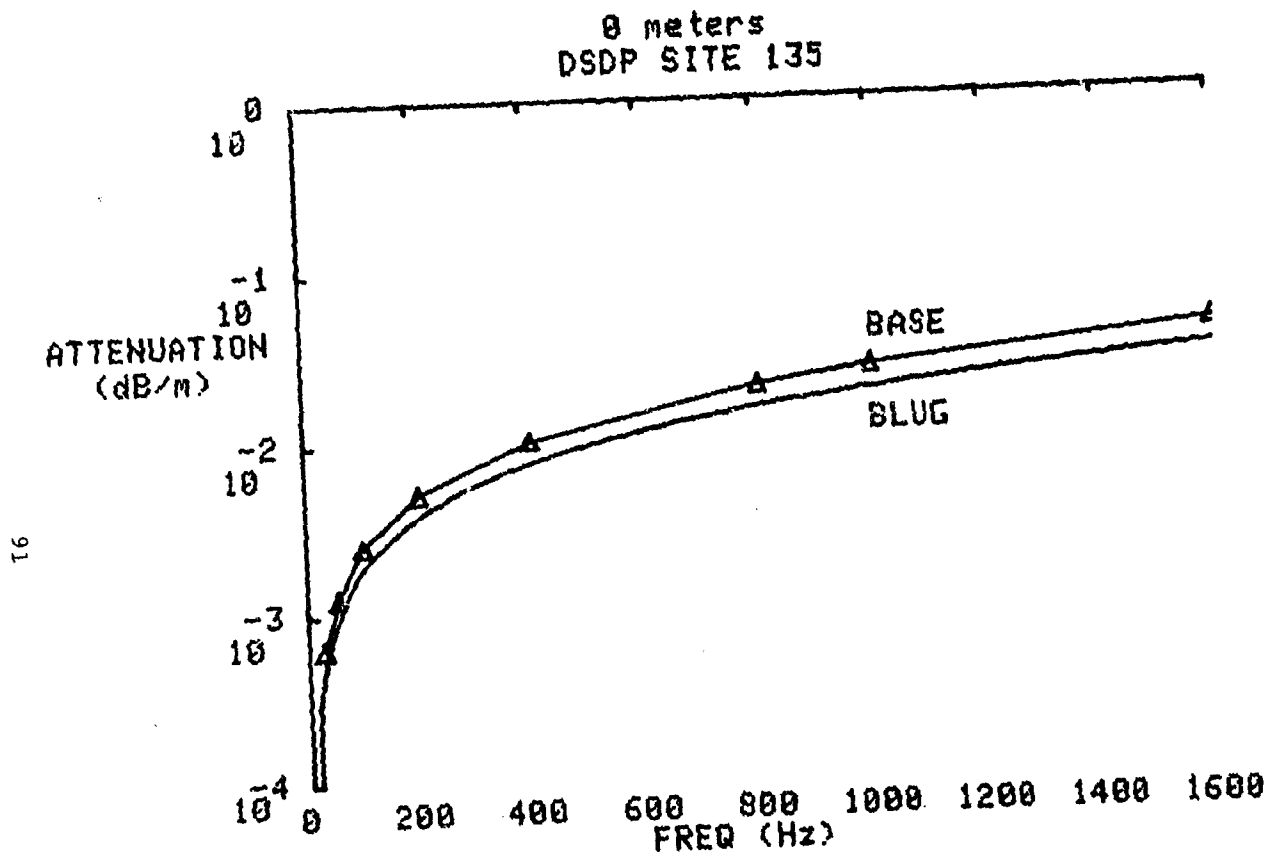

Figure 20. Same as Figure 19, but for Attenuation (at 0 m) versus Frequency.

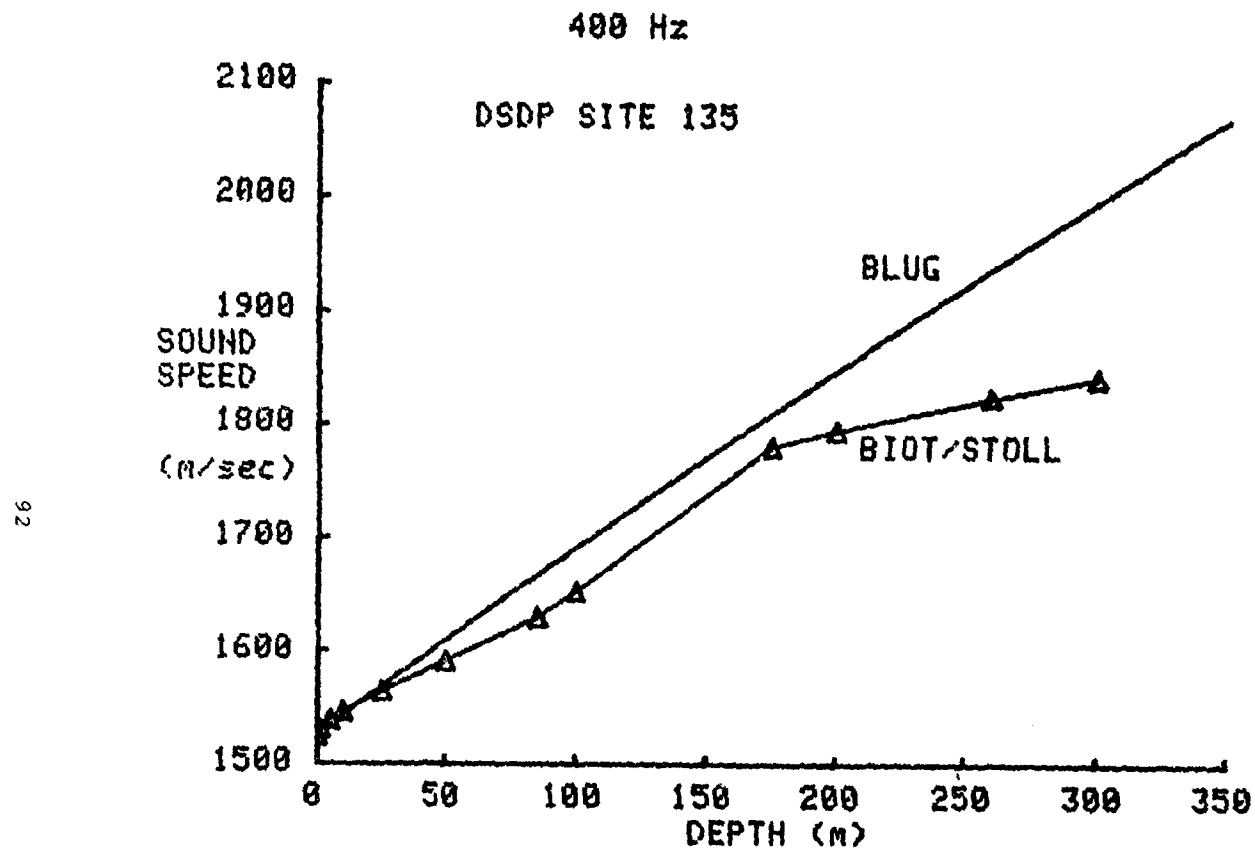

Figure 21. Sound Speed (at 400 Hz) versus Depth at DSDP Site 135 Comparing BLUG to the Results of the Biot/Stoll Model after Adjustments to the Input Values have been Applied, as Discussed in the Text.

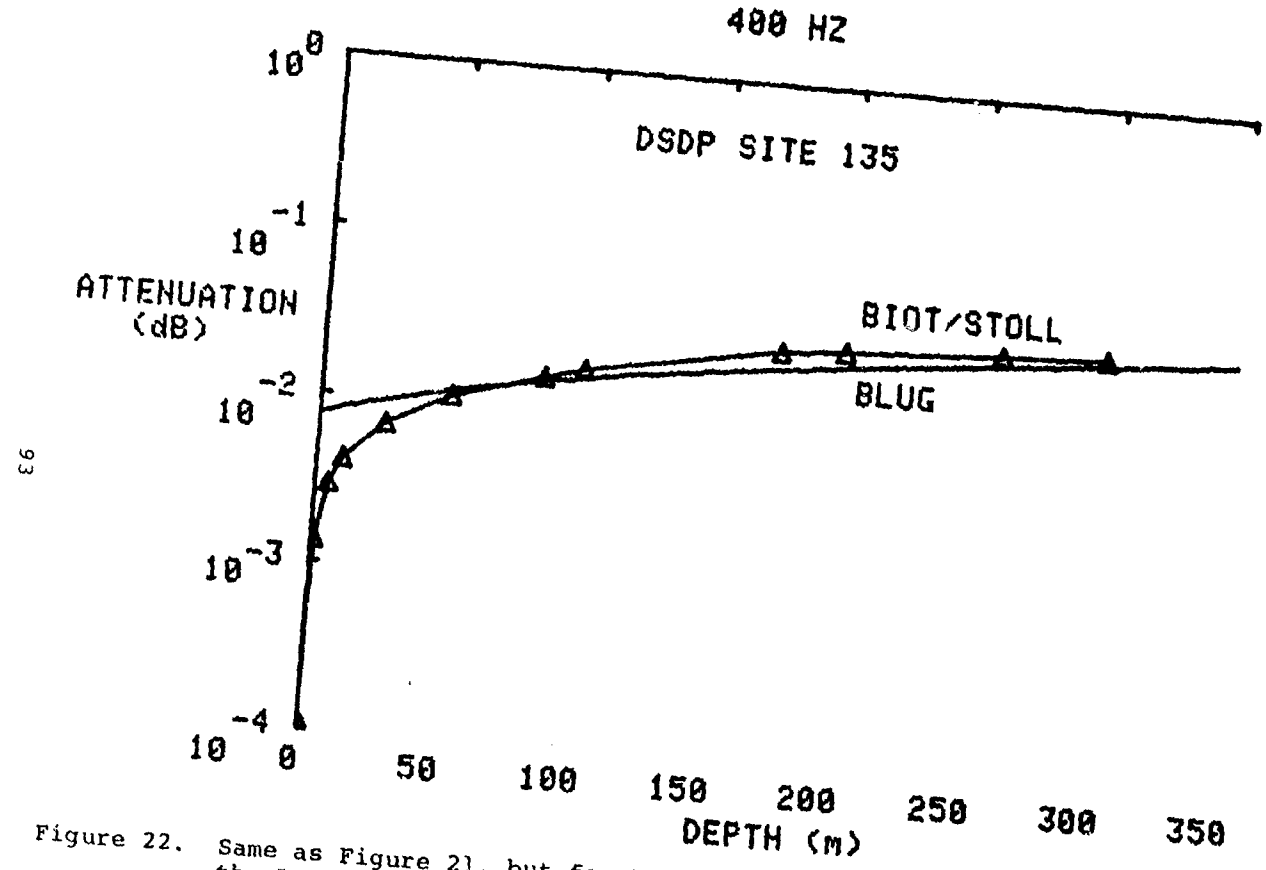

Figure 22. Same as Figure 21, but for Attenuation (at 400 Hz) versus Depth. Note the Large Discrepancy at 0 m.

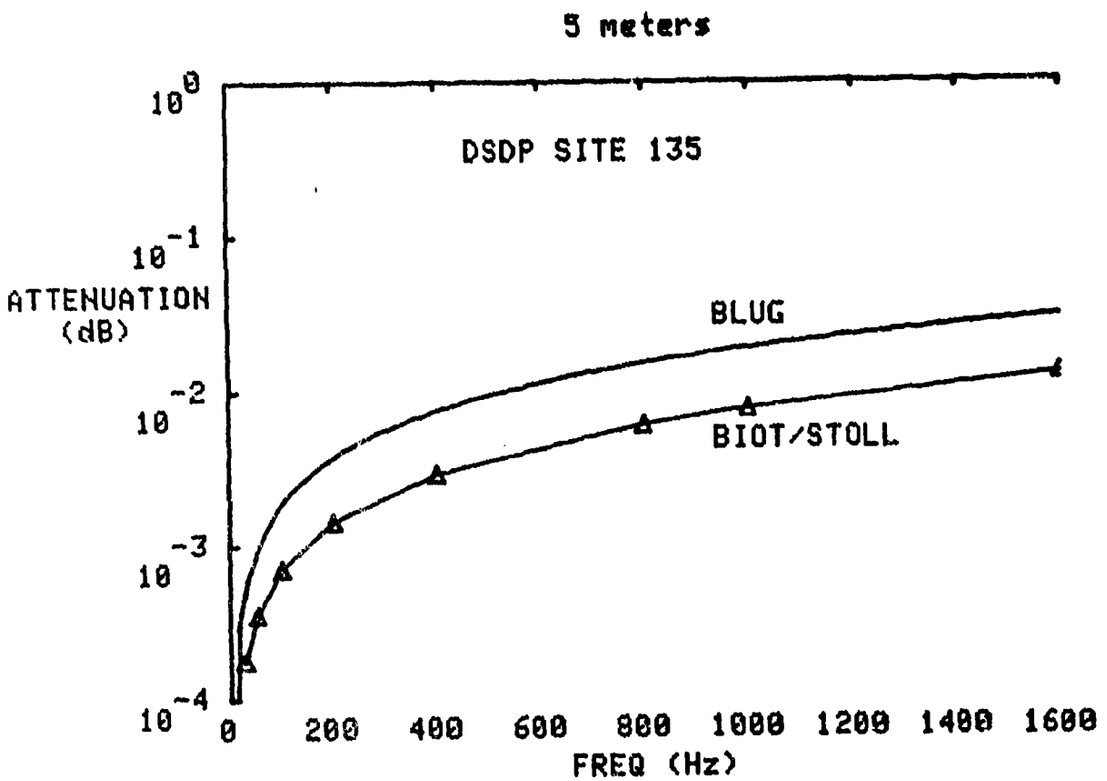

Figure 23. Same as Figure 21, but for Attenuation (at 5 m) versus Frequency.

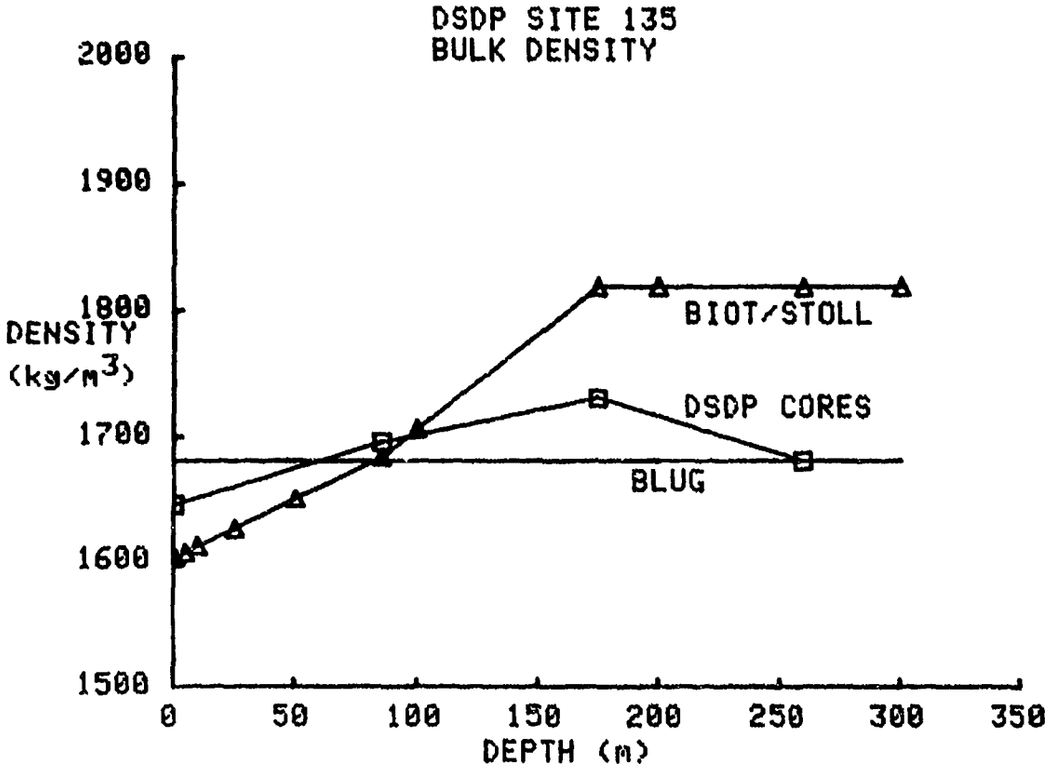

Figure 24. Saturated Bulk Density versus Depth at DSDP Site 135 Comparing the BLUG Value, the Measurements on the DSDP Cores, and the Values Derived from the Biot/Stoll Inputs of Porosity and Grain and Fluid Densities.

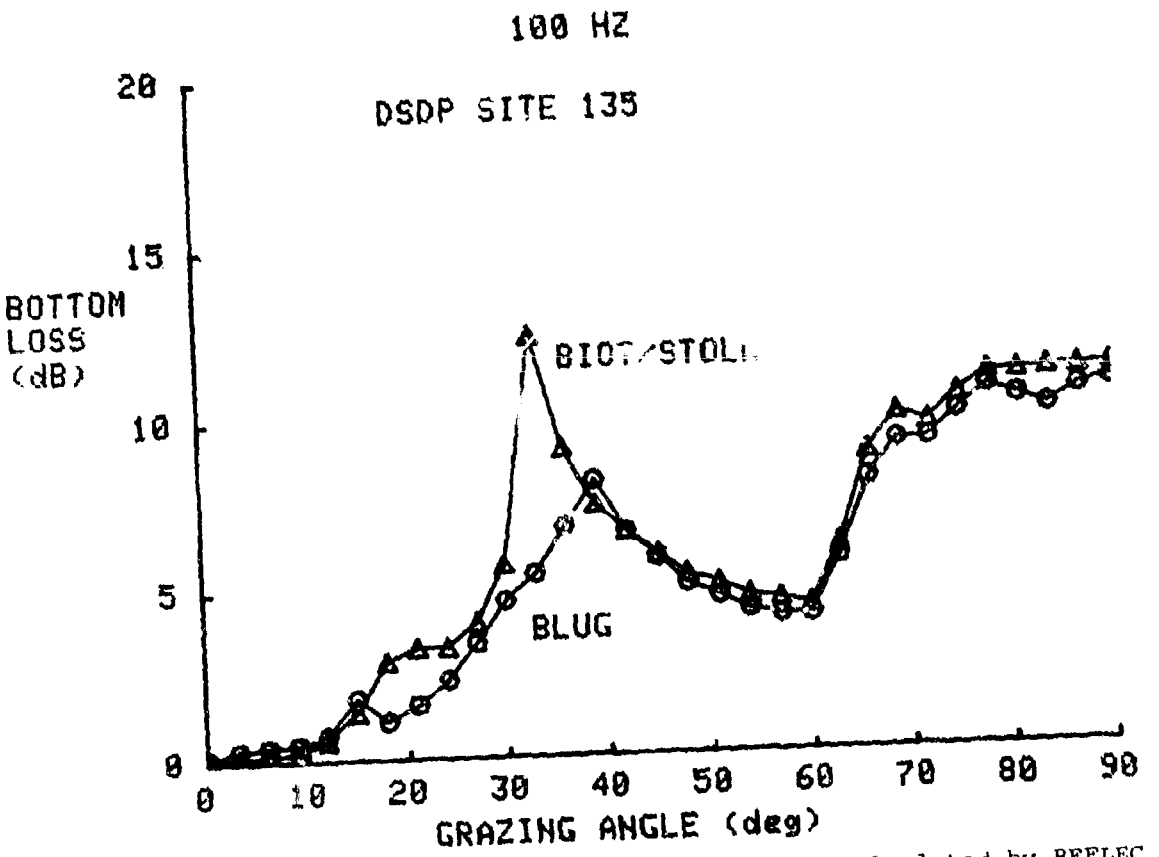

Figure 25. Plane Wave Bottom Loss versus Grazing Angle as Calculated by REFLEC at DSDP Site 135 Showing the Difference Between the Biot/Stoll Sediment and the BLUG Sediment, Calculated at 100 Hz.

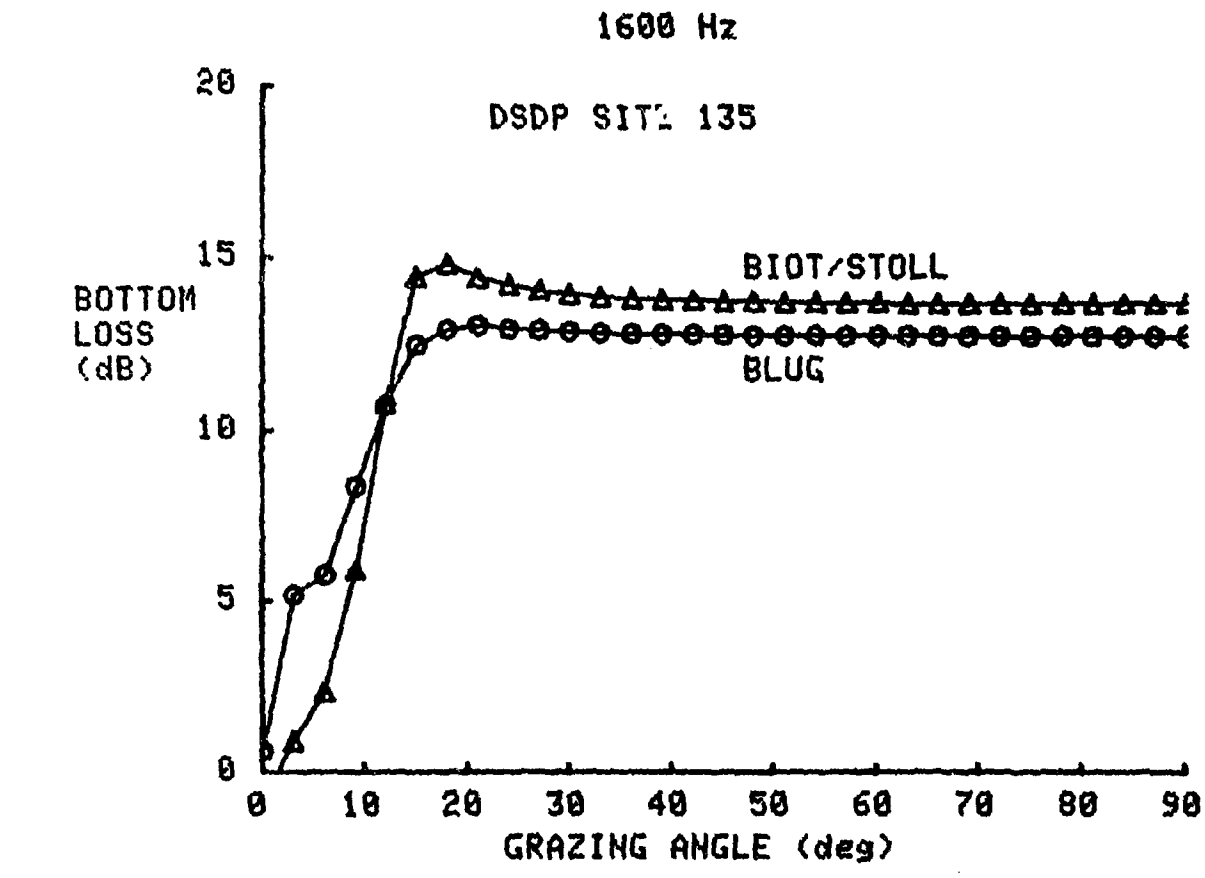

Figure 26. Same as Figure 25, but for 1600 Hz.

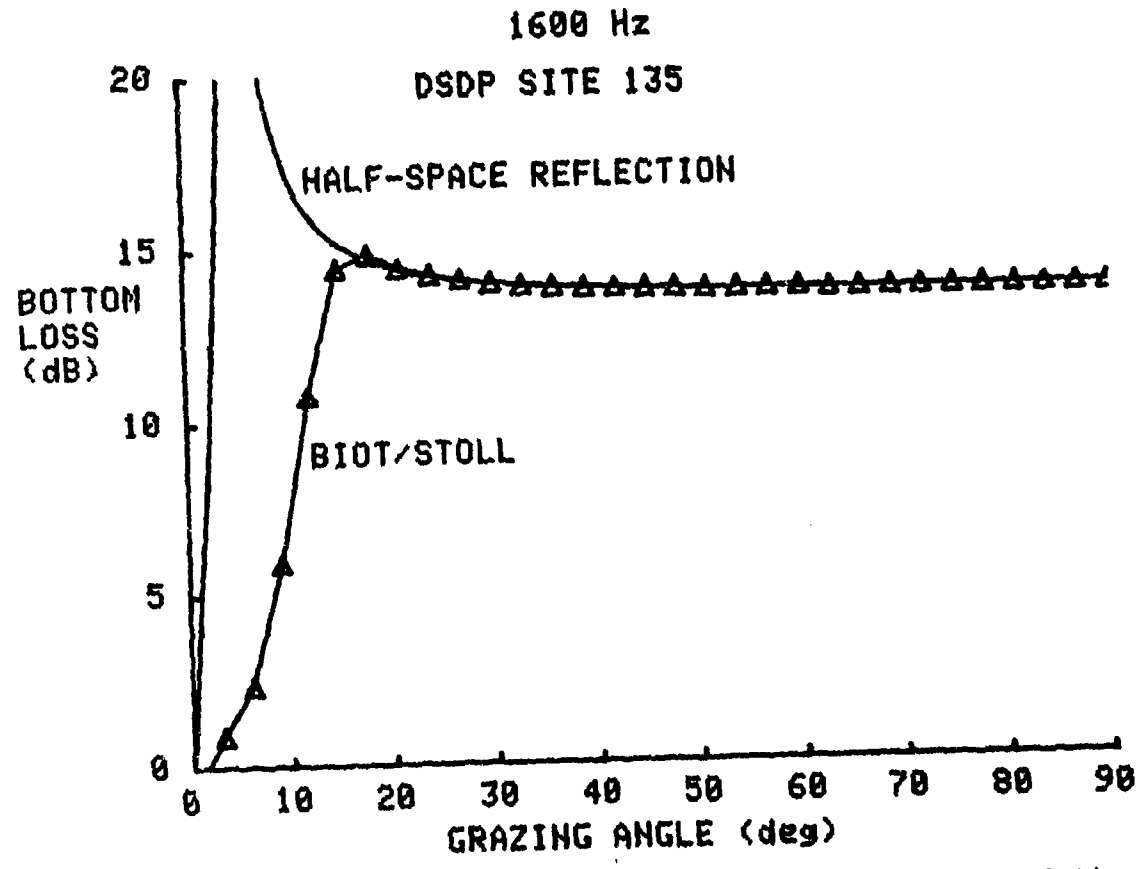

Figure 27a. Bottom Loss versus Grazing Angle Comparing the REFLEC Calculation for Biot/Stoll at 1600 Hz (from Figure 26) to Simple Rayleigh Reflection at the Surface of the Biot/Stoll Sediment. The Latter Curve Goes Off Scale Near 7°, the Angle of Total Transmission.

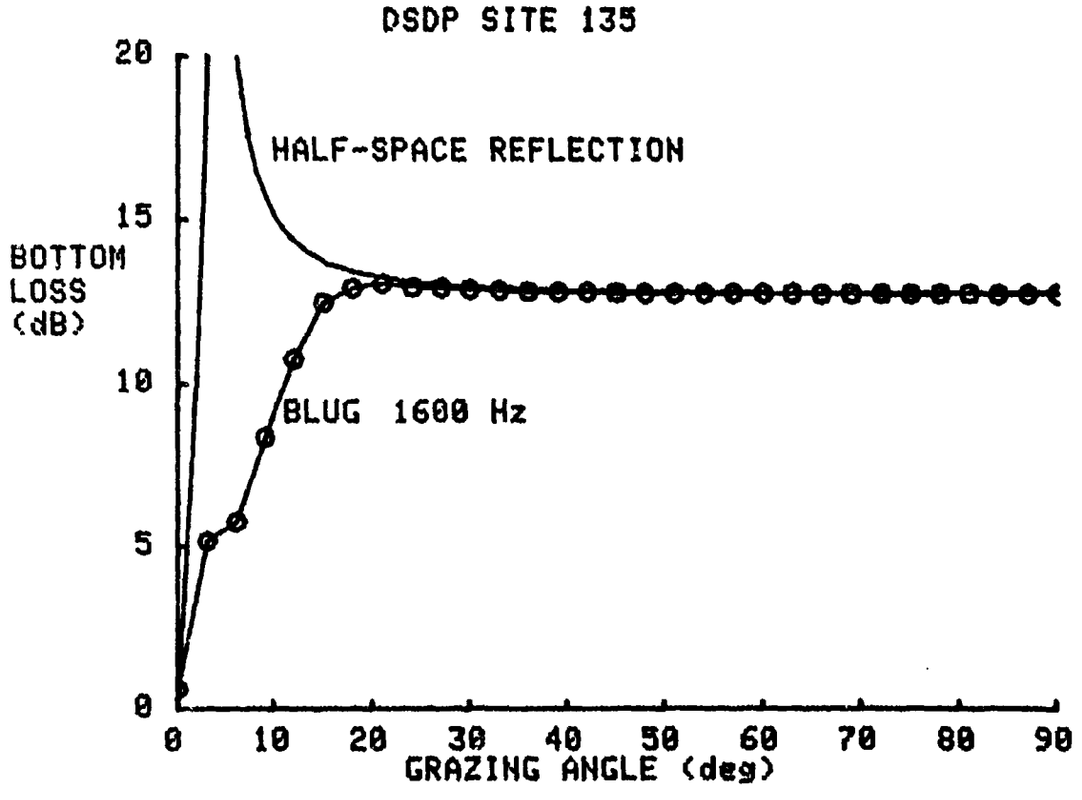

Figure 27b. Same as Figure 27a, but for the BLUG Sediment.

Panama City

This site, the second case studied, is a shallow water area with a thin layer of sand overlying a calcareous basement. It is a site that was described by Beebe[7] both in terms of its physical and its geoacoustic properties. BLUG also provided a generic "shallow water" set of geoacoustic parameters that were used for comparison.

According to Beebe,[7] the Panama City site is located about 15 km southwest of the Florida city in 18 m of water, well up on the continental shelf. This site has about 5 m of quartz-shell sands with a mean grain size given by the ϕ value 1.85, and a distribution given by the σ_ϕ value 0.53. The calcium carbonate content is about 18%. Sound speed in the water at the time of the geoacoustic measurements was 1525 m s^{-1}.

Properties--Fluid viscosity was interpolated from the seawater tables in Section III and is given in Table 9. The deep seawater tables return a density value of 1028 kg m^{-3} which is too high for such warm water, so we fixed this parameter at the more appropriate value of 1025 kg m^{-3}. We then calculated a fluid bulk modulus that would give the proper sound speed of 1525 m s^{-1}. This value, 2.38×10^9 N m^{-2}, is reported, as is the density, in Table 9.

Porosity measurements on cores in the area reported by Beebe for this site gave a value of 0.41. Porosity was not observed to vary with depth in the upper 4 meters, so we took it to be constant, as shown in Table 9. Beebe gives 2710 kg m^{-3} for the grain density and 4.2×10^{10} N m^{-2} for the grain bulk modulus, as reported in Table 9.

Beebe derived a permeability of 2.9×10^{-11} m^{-2} from the grain size distribution parameters ϕ and σ_ϕ using Equation (45). A ϕ of 1.85 corresponds to a grain size of $.277 \times 10^{-3}$ m which, in Equation (37), gave a permeability of 8.4×10^{-11} m^{-2}, a factor of three greater. Though a factor of three would not

TABLE 9. PANAMA CITY PHYSICAL PROPERTIES

	Depth in Sediment 0 m	Depth in Sediment 5 m	Units	Source
ρ_r	2710	2710	kg m^{-3}	Beebe[7]
κ_r	4.2×10^{10}	4.2×10^{10}	N m^{-2}	Beebe[7]
ρ_f	1025	1025	kg m^{-3}	shallow seawater value
κ_f	2.384×10^{9}	2.384×10^{9}	N m^{-2}	from water sound speed and ρ_f
η	19.4×10^{-4}	19.4×10^{-4}	kg m^{-1} s^{-1}	seawater tables
β	.41	.41	--	Beebe[7]
k	2.9×10^{-11} 8.4×10^{-11}	2.9×10^{-11} 8.4×10^{-11}	m^2	grain sizes from Beebe[7] and Eqs. (45) and (37)
a	2.1×10^{-5}	2.1×10^{-5}	m	Beebe[7]
α	1.25	1.25	--	Beebe[7]
μ_b	0	5.63×10^{7}	N m^{-2}	grain density porosity Eqs. (58) to (61)
μ_b^*	0	$.36 \times 10^{7}$	N m^{-2}	real frame shear modulus, shear log dec = .2 from Beebe[7], and Eq.(62)
K_b	0	7.5×10^{7}	N m^{-2}	real frame shear modulus, Poisson's ratio = .2, Eq. (55)
K_b^*	0	$.36 \times 10^{7}$	N m^{-2}	real frame bulk modulus, compressional log dec=.15

have been noticeable in the clays of DSDP site 135, in the Panama City sands it was expected to have more influence; we consequently report both values in Table 9.

The poresize parameter values of 2.1×10^{-5} m and the structure factor of 1.25 were provided by Beebe[7] and appear in Table 9.

Unlike the procedure followed by Beebe, we used Equations (58) through (61) to derive the real part of the frame shear modulus, because this gave the parameter's depth dependence and because this made our results analogous to those obtained for DSDP site 135. We obtained a value of 5.63×10^{7} N m^{-2} at 5 m (0.0 at the surface), while Beebe derived a depth independent value of 7.05×10^{7} N m^{-2} using Equation (56) and a value for V_s of 2.1×10^{2} m s^{-1} that Stoll describes as typical of sands. Beebe went on to derive μ_b^*, K_b, and K_b^* using his value of μ_b and Equations (62), (65), and (70). We did not follow up on Beebe's values and we do not report them in Table 9. Preliminary analysis showed that sensitivities to these parameters are roughly as described in the section on DSDP site 135. Suffice it to note, here, that taking a different derivation did not impair our ability to match his measurements of attenuation, as will be shown.

We derived $.36 \times 10^{7}$ N m^{-2} for the imaginary part of the frame shear modulus (Table 9) from Equation (62) and a value for the shear log decrement of 0.2. We derived 7.5×10^{7} N m^{-2} for the real part of the frame bulk modulus from Equation (55) using a Poisson's ratio of .2 which is appropriate for dry sands according to Hardin and Richart[45] and Domenico.[24] We derived $.36 \times 10^{7}$ N m^{-2} for the imaginary part of the frame bulk modulus from Equation (69) and a value for the compressional log decrement of 0.15.

Sensitivity Analysis--As stated, we did not repeat a set of sensitivity analyses on the frame moduli because preliminary work indicated no substantial differences from the sensitivities noted in a previous section of this report, and because there was less uncertainty in their values than in the previous case. The same was true of the grain bulk modulus. However, a different result was obtained for permeability at this shallow water site.

For a factor of three increase in permeability, there is a noticeable increase in attenuation by a factor of approximately two, as shown in Figures 28 through 30. Even the speed (Figure 28) is affected, though slightly (about 10 m s^{-1}, i.e., less than 1%). The shape of the curve of attenuation against depth (Figure 29) is slightly different with the higher permeability; the high permeability curve decreases a bit more steeply. The shape of the curve of attenuation against frequency (Figure 30) is also different in the case of higher permeability. The curve is steeper at low frequencies and flatter at high frequencies. Also shown in Figure 30 are data points from Beebe.[7] The high permeability ease demonstrates a better fit to the observed data. If the Beebe data and Biot/Stoll model are approximated by a power curve, the exponent of frequency varies between 1.69 for the low permeability case and 1.78 for the Beebe site D data. The high permeability case and Beebe site C data both show a frequency exponent of 1.73.

Geoacoustic Property Comparisons--The profiles of speed and attenuation output by the Biot/Stoll model were compared to values of attenuation vs. frequency derived from observations of mode attenuation by Beebe[7] and profiles independently derived from seismic inversion analyses and the BLUG bottom loss inversion technique. We arbitrarily chose the Biot/Stoll profiles derived from the low permeability case for this comparison.

Figure 31a shows the sound speed profiles in the upper 50 m from BLUG and Biot/Stoll. For both these cases, a calcareous basement, in which speed is 1850 m s^{-1}, was assumed to begin at 5 m depth. Figure 31b shows the sound-speed profiles determined from analyses of refraction and reflection data by Ingenito[44] and Caswell[45] for two sites and by Beebe.[7] One can conclude that there is a great deal of uncertainty in the observed speeds and that both Biot and BLUG lie well within the bounds of uncertainty.

Figure 32 shows that there is no difference between BLUG and Biot/Stoll in the depth dependence of attenuation. Both are constant in the upper 5 m at a value of .1 dB m^{-1} for 400 Hz. Both are below the Beebe observations of attenuation in the range of about .2 to .3 dB m^{-1}. Other plots not presented here indicated that BLUG did not deviate from Biot/Stoll in attenuation at 400 Hz until depths of 100 m or greater. Deeper than 5 m, the assumed basement has an attenuation of .06 dB m^{-1} at 400 Hz.

Figure 33 shows that Biot/Stoll and BLUG differ in attenuation at other frequencies. Below 400 Hz, the BLUG sediment suffers the greater attenuation; at higher frequencies, the Biot/Stoll sediment suffers more. Beebe's observations lie close in value to the BLUG curve at 200 Hz and less. In terms of shape, Beebe's data are definitely not linear in frequency as is the BLUG sediment. In fact, the data show much better agreement with Biot/Stoll. This frequency dependence is the effect of the viscous losses due to relative fluid flow. The agreement with Biot/Stoll is even more remarkable when we note that a reasonable but higher choice of permeability (Table 9)

[44]Ingenito, F., 1973, "Measurements of Mode Attenuation Coefficients in Shallow Water," J. Acoust. Soc. Amer., 53, pp. 858-863.

[45]Caswell, W.R., 1979, "The Frequency Dependence of Normal-Mode Attenuation in Shallow-Water Sound Propagation," Unpublished doctoral dissertaion, The Pennsylvania State University.

gives very good absolute values of attenuation as well as shape, a fact noted in our previous discussion of Figure 30 in the section on sensitivity analysis.

Acoustic Significance--The Biot/Stoll sediment and the BLUG sediments differ geoacoustically, as shown in Figures 31 to 33. They also differ in bulk density. The Biot/Stoll bulk density is 2.019, while the BLUG value is 1.800. Bottom loss as a function of grazing angle was calculated using REFLEC and the results are given in Figures 34 and 35 for two frequencies.

Again, at 100 Hz (Figure 34), the gross bottom loss structures of the two models are similar, with low loss up to a grazing angle of 33°, at which point effective transmission into basement abruptly increases the loss to a high level (~10 dB).

At high angles, the BLUG sediment is about 2 dB more lossy because its lower density (and hence lower impedance) allows more energy to penetrate to basement. At smaller angles, the losses are low and would allow multiple bounces with little accumulated loss. The BLUG sediment is more lossy due to its higher attenuation, but it is not much different from the Biot/Stoll sediment; therefore, the difference in mid-range propagation may not be too severe. For example, for a 20° grazing angle, the BLUG loss is about 0.5 dB per bounce, and the Biot/Stoll loss is about 0.3 dB per bounce. A 6 dB loss requires 12 bounces on the BLUG sediment and 20 on the Biot/Stoll sediment. In 20 m of water for a 20° ray, this bottom loss difference results in an increase in range from 1.3×10^3 m for the BLUG case to 2.1×10^3 m for the Biot/Stoll case, a difference of 800 m (an increase of 60%).

At 1600 Hz (Figure 35), the losses are lower at high angles (above 40°) and higher at low angles (below 35°) than they are at 100 Hz. Another difference at 1600 Hz is that,

for angles smaller than 25°, the Biot/Stoll sediment shows several times more bottom loss than the BLUG sediment. This greater loss is due to the Biot/Stoll sediment's greater attenuation which is considered more realistic as it agrees better with Beebe's data.

Figures 36 to 39 compare the bottom losses determined by REFLEC to those derived for simple Rayleigh reflection according to Brekhovskikh.[39] The latter values depend upon sediment acoustic impedance (ρc, where c = sound speed), so not only do Biot/Stoll reflections differ from BLUG, but for the Biot/Stoll sediment (whose speeds vary with frequency in sands) the 100 Hz reflections differ from the 1600 Hz reflections.

As can be seen, at 100 Hz (Figure 36), the Biot/Stoll sediment returns less acoustic energy at angles less than 20° than would be expected from simple reflection. This is due to absorption in the sediment accounted for in the REFLEC calculation, but not in the simple reflection calculation. From 20° to 34.5°, reflection from the basement returns more acoustic energy (i.e., suffers less loss) than predicted by simple reflection from the sediment surface.

At 1600 Hz (Figure 37), bottom loss is not reduced by basement-reflected waves at any angle. At these high frequencies, attenuation in the sediment is great enough to prevent the return of waves reflecting off the basement. At angles above 25°, the bottom loss curve is identical to that predicted by simple reflection from the surface sediment.

Figures 38 and 39 show similar relationships for the BLUG sediments. This thin sediment layer is relatively invisible at 100 Hz, except for some absorption, and reflection occurs off the basement. At the high frequencies and high angles, the bottom loss is equivalent to that for reflection from the surface of the sediment only.

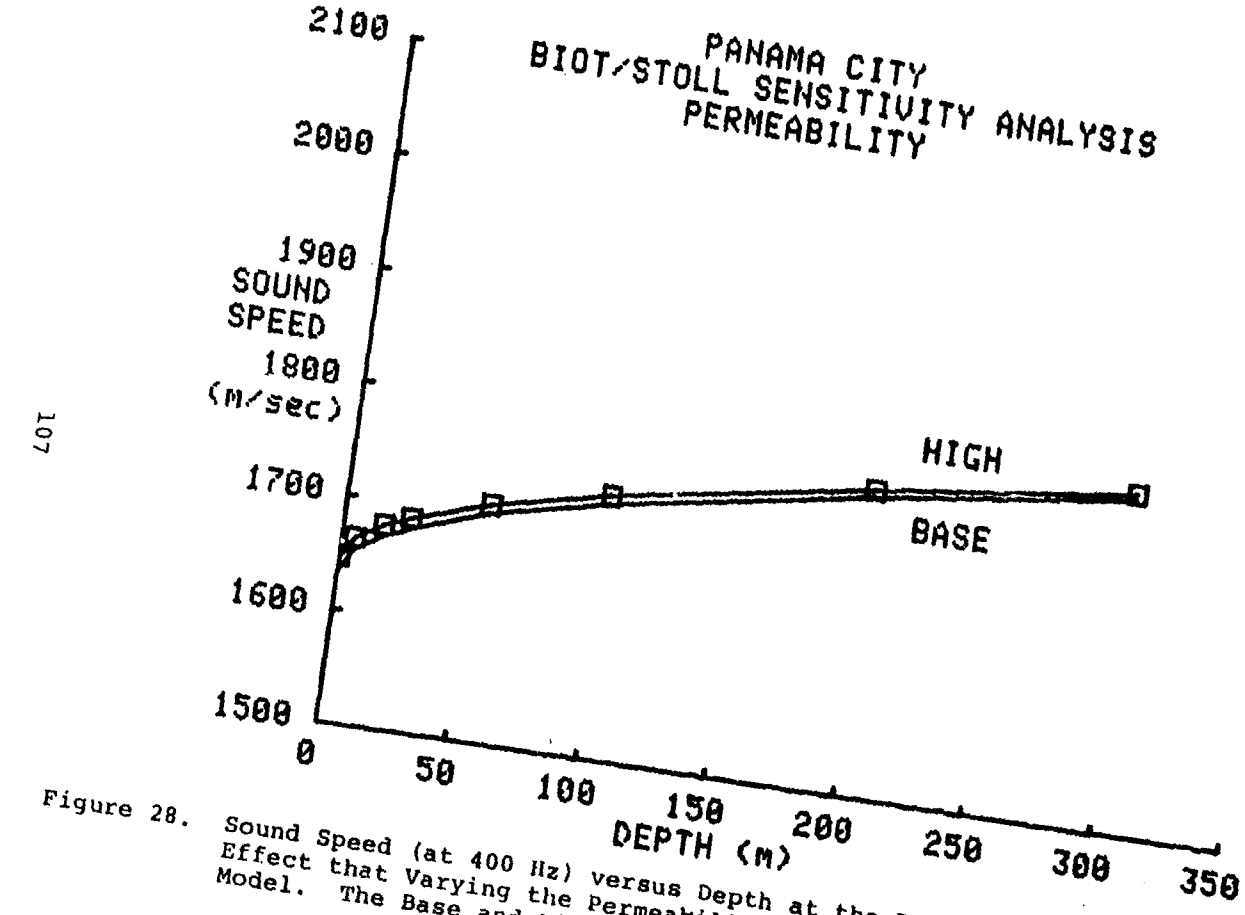

Figure 28. Sound Speed (at 400 Hz) versus Depth at the Panama City Site Showing the Effect that Varying the Permeability has on the Output of the Biot/Stoll Model. The Base and High Permeability are Defined in Text and in Table 9.

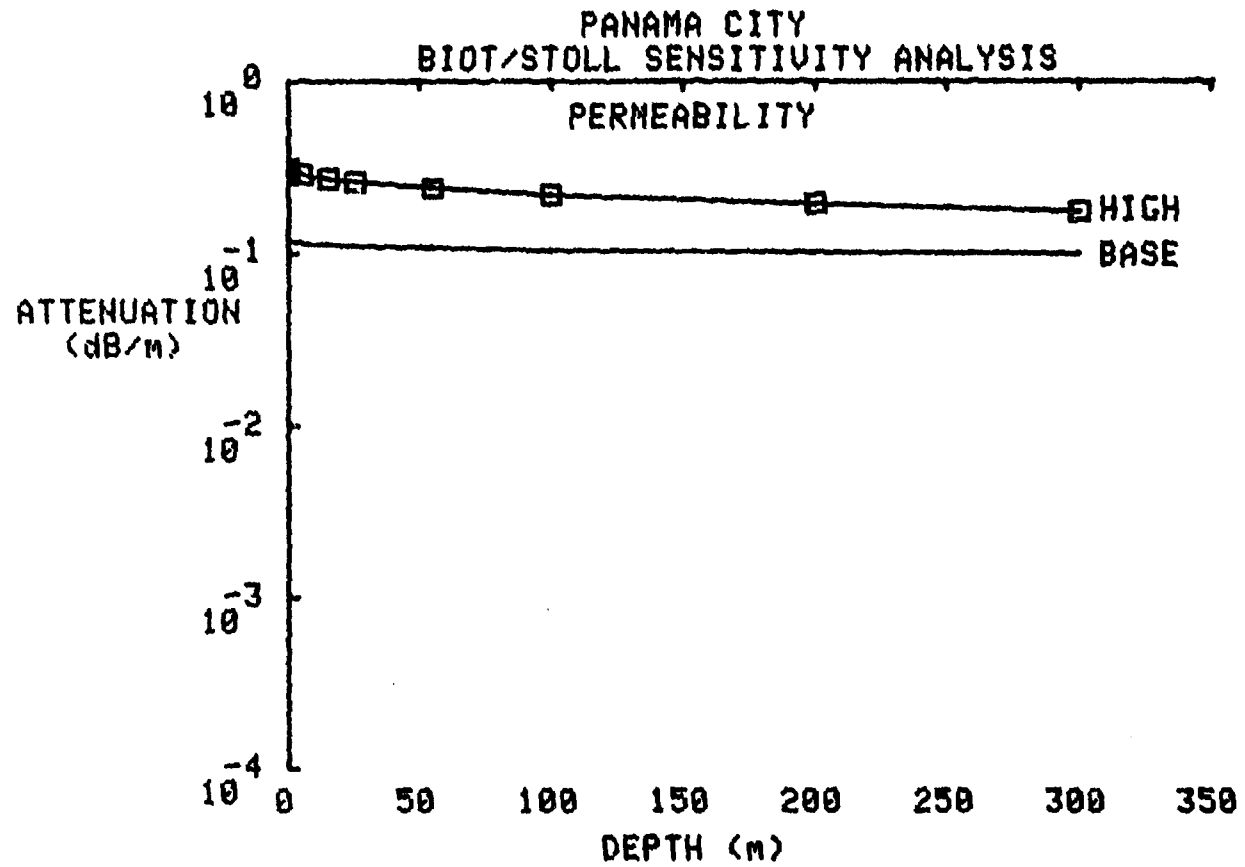

Figure 29. Same as Figure 28, but for Attenuation (400 Hz) versus Depth.

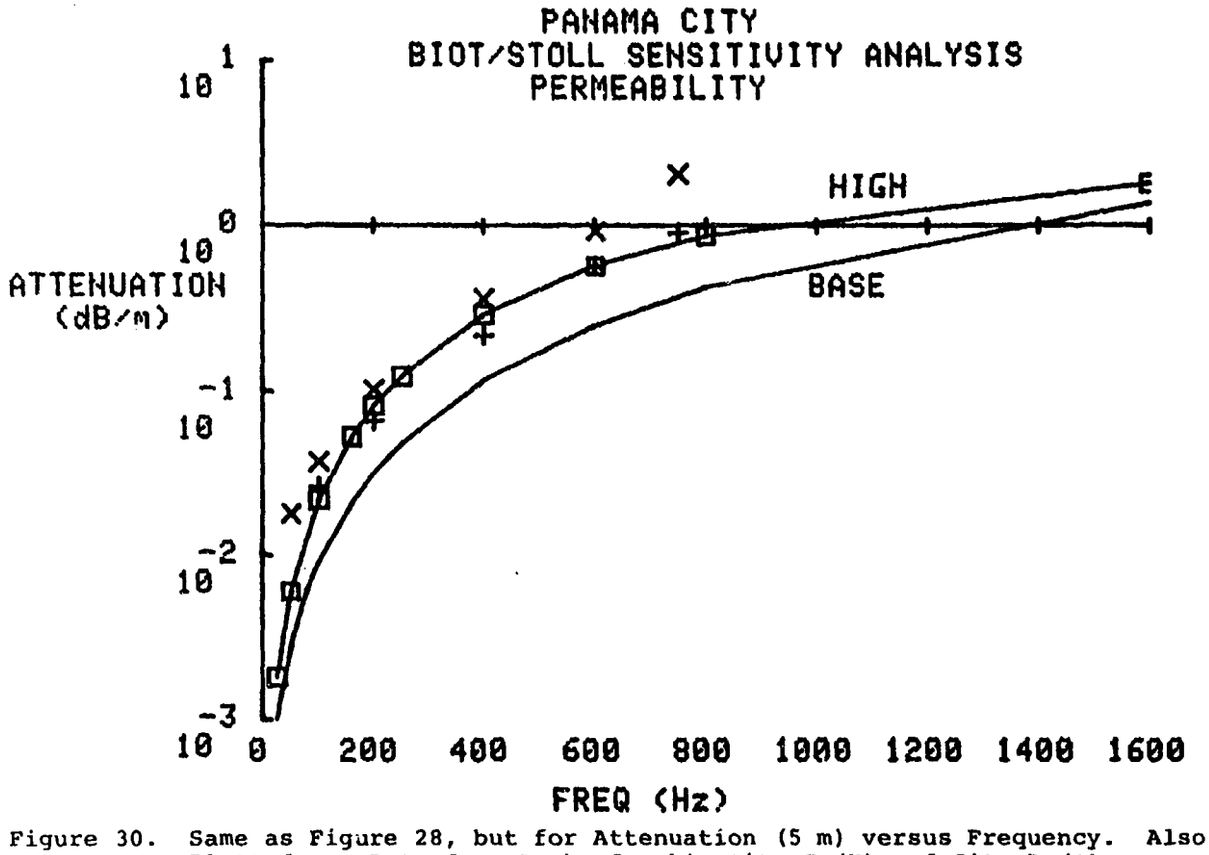

Figure 30. Same as Figure 28, but for Attenuation (5 m) versus Frequency. Also Plotted are Data from Beebe for his Site C (X) and Site D (+).

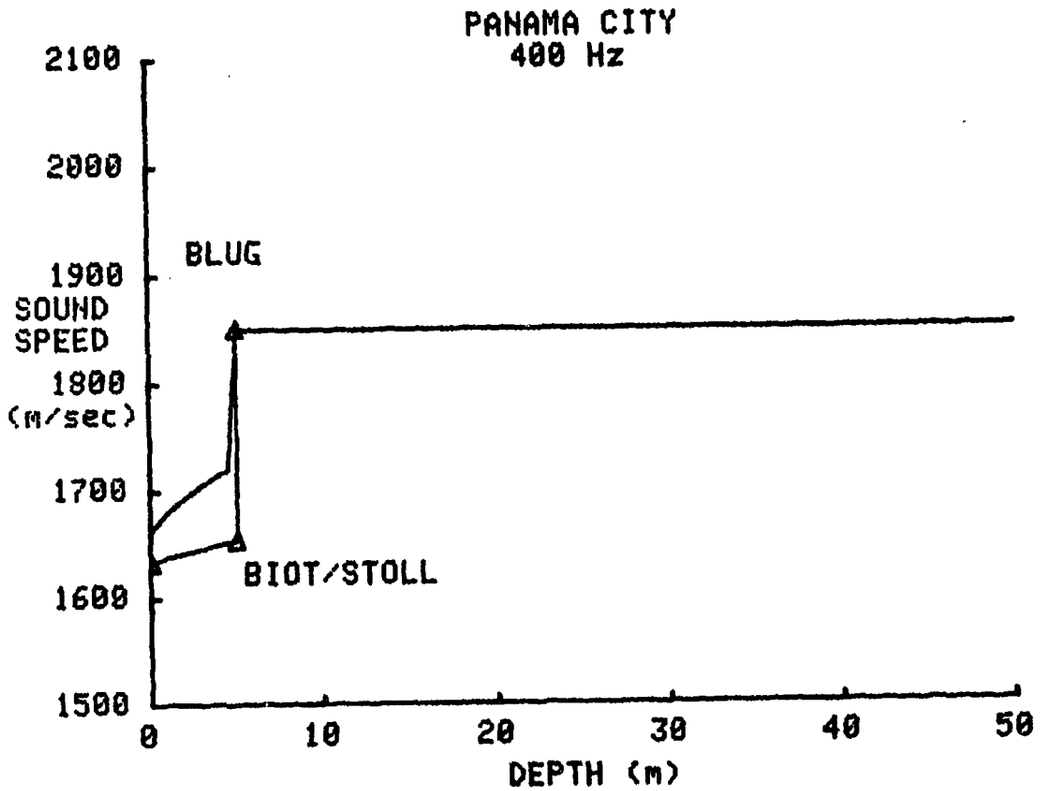

Figure 31a. Sound Speed (at 400 Hz) versus Depth at the Panama City Site Comparing BLUG to the Base Case of the Biot/Stoll Model in the Upper Five Meters and Showing the Properties of the Basement Below Five Meters. The Base Case is the Low Permeability Case as Defined in the Text.

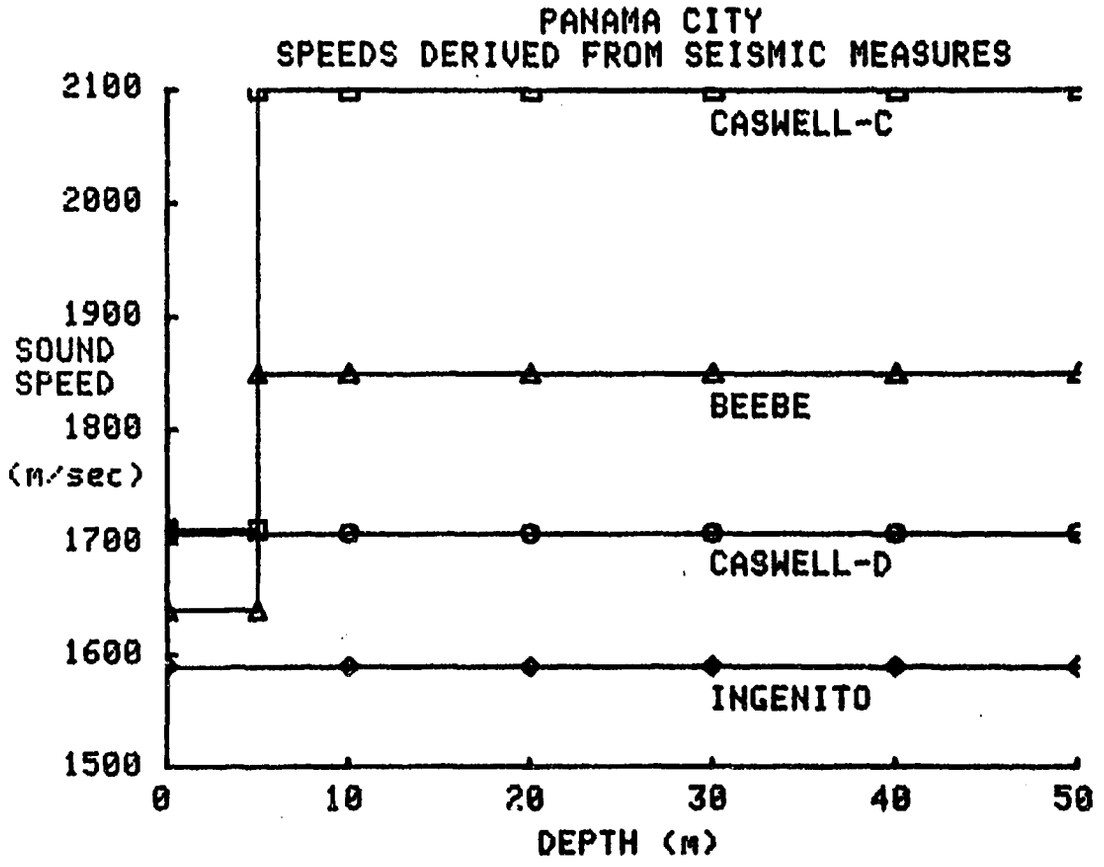

Figure 31b. Sound Speed versus Depth at the Panama City Site Showing the Various Solutions Derived from Seismic Measurements. References are Cited in the Text. Note that Both Biot/Stoll and BLUG in Figure 31a lie near Beebe, between Caswell-C and Caswell-D.

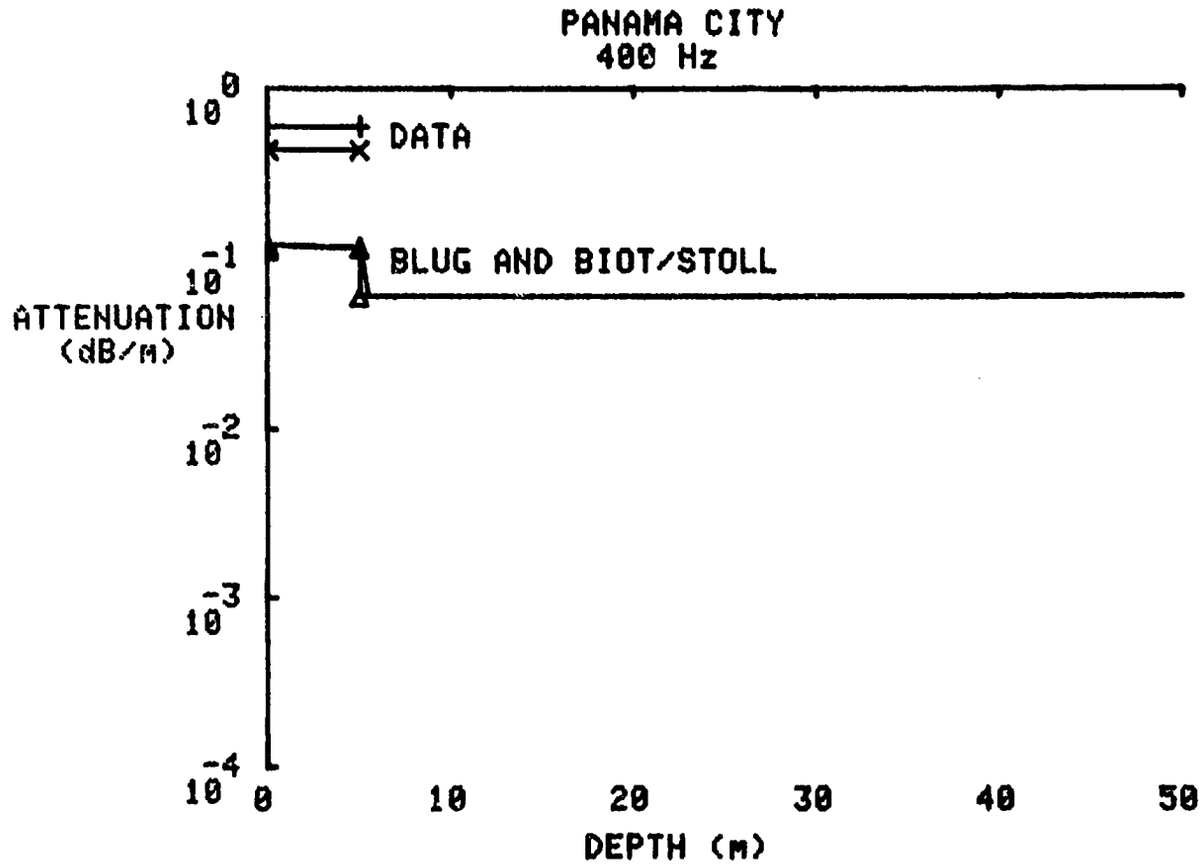

Figure 32. Same as Figure 31a, but for Attenuation (at 400 Hz) versus Depth. Also Shown are the Data from Beebe from His Sites C (X) and D (+) which apply as Constants in the Upper Five Meters.

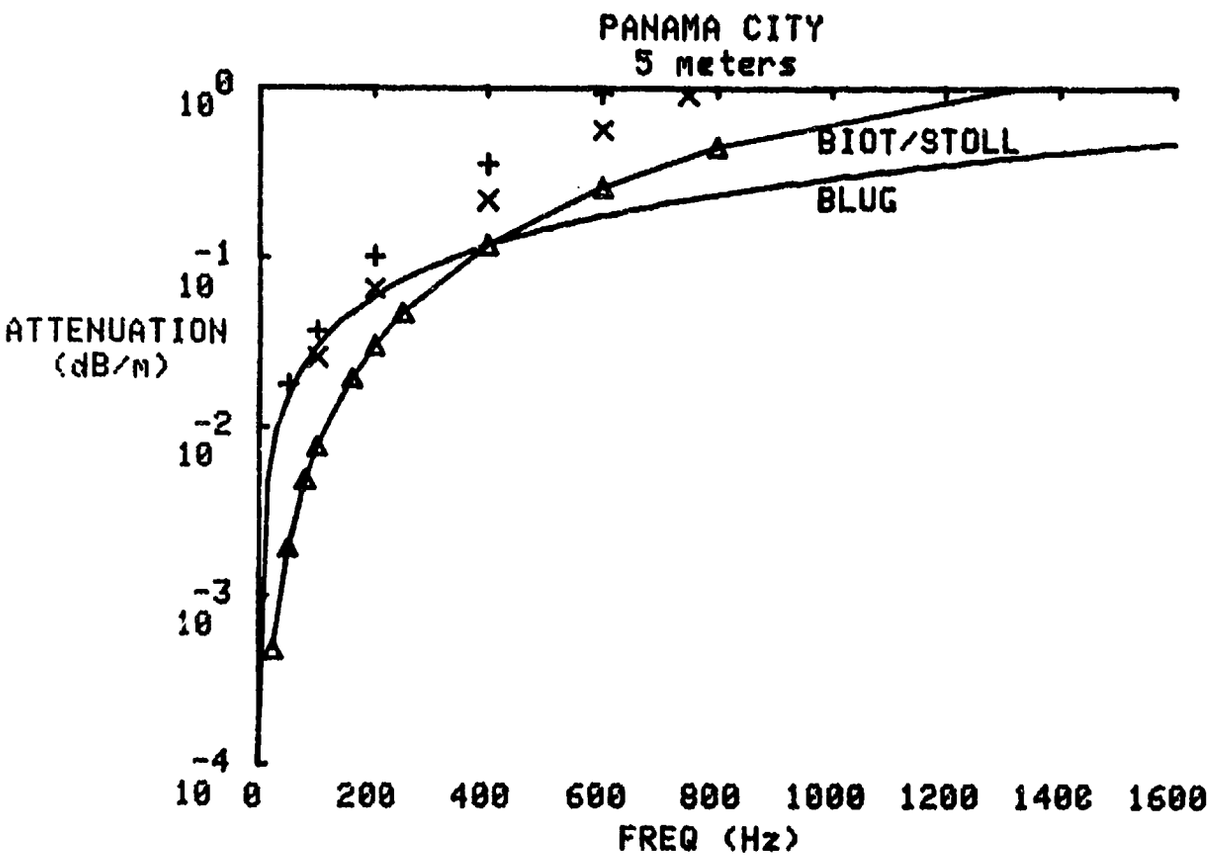

Figure 33. Same as Figure 32, but for Attenuation (at 5 meters) versus Frequency.

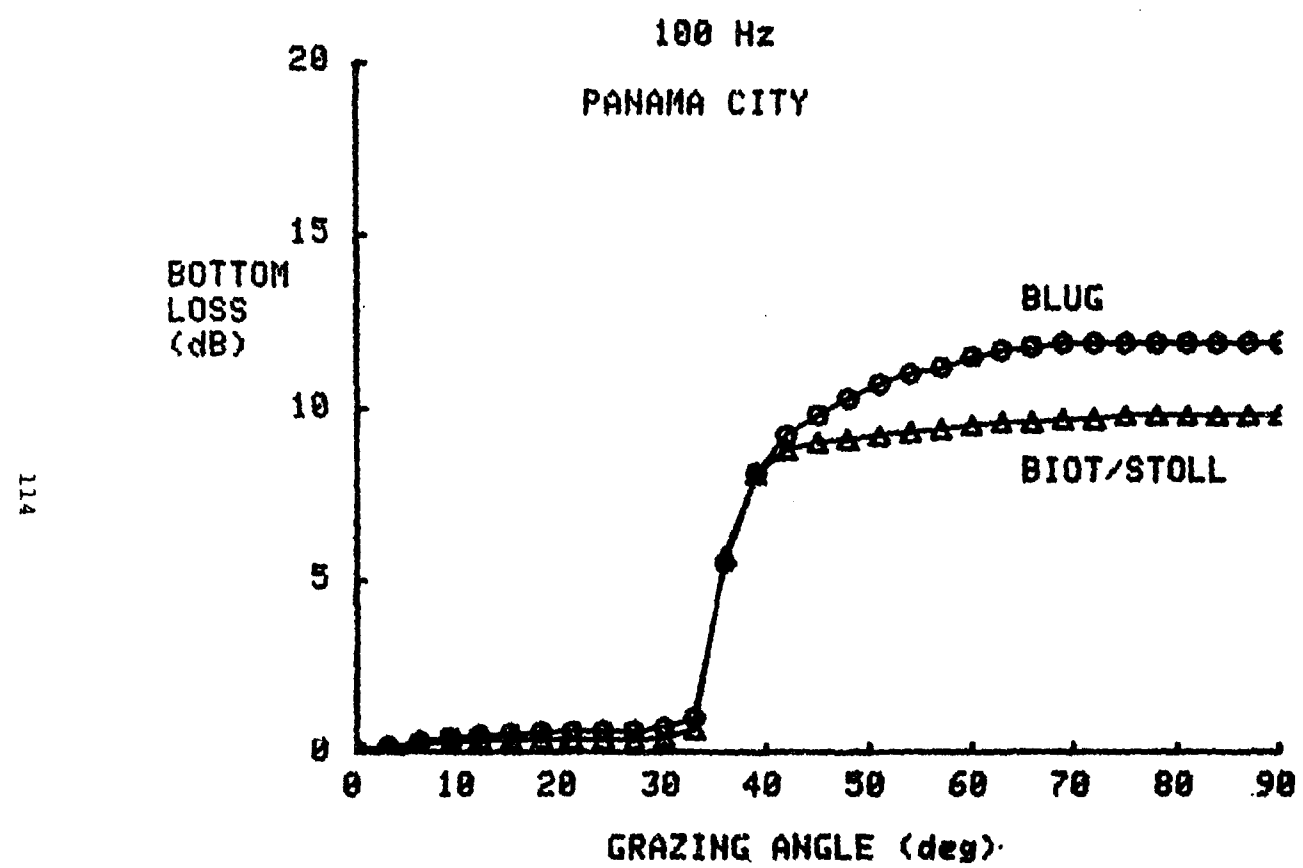

Figure 34. Plane Wave Bottom Loss versus Grazing Angle as Calculated by REFLEC at the Panama City Site Showing the Difference Between the Biot/Stoll Sediment and the BLUG Sediment, Calculated at 100 Hz.

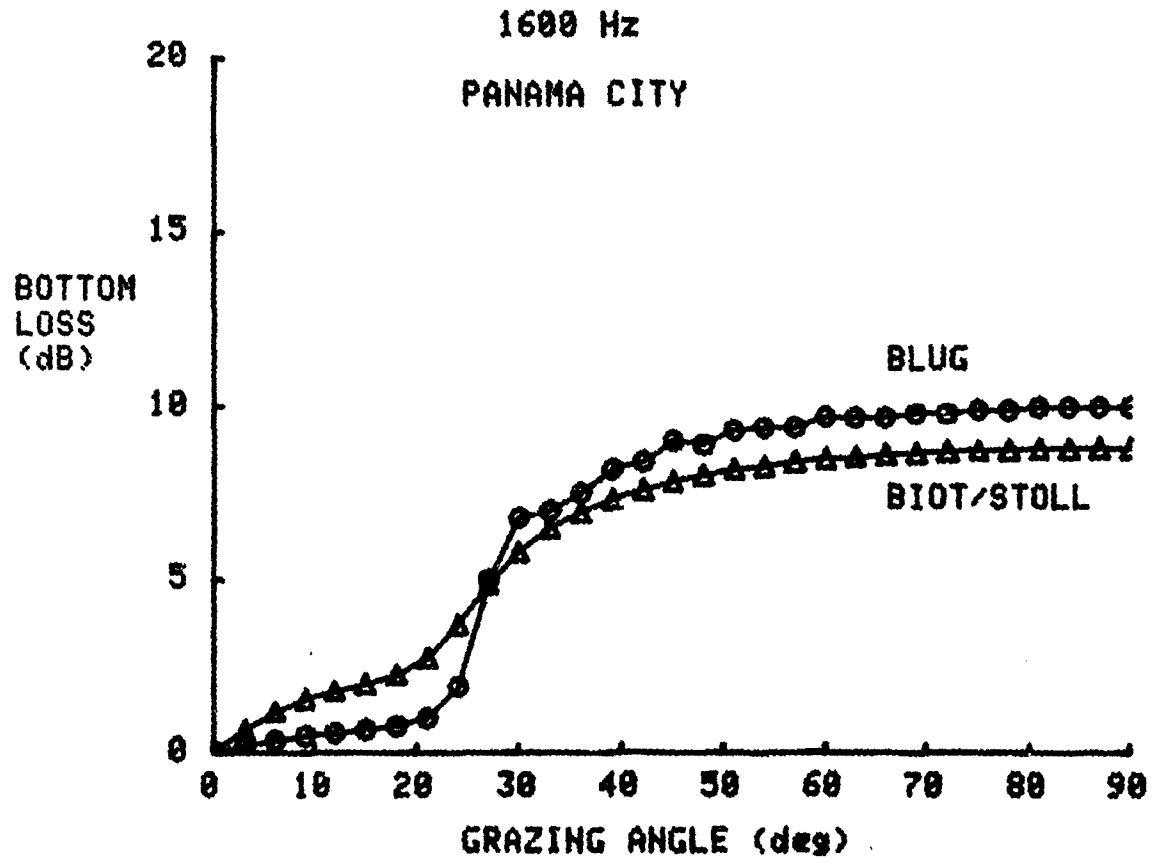

Figure 35. Same as Figure 34, but for 1600 Hz.

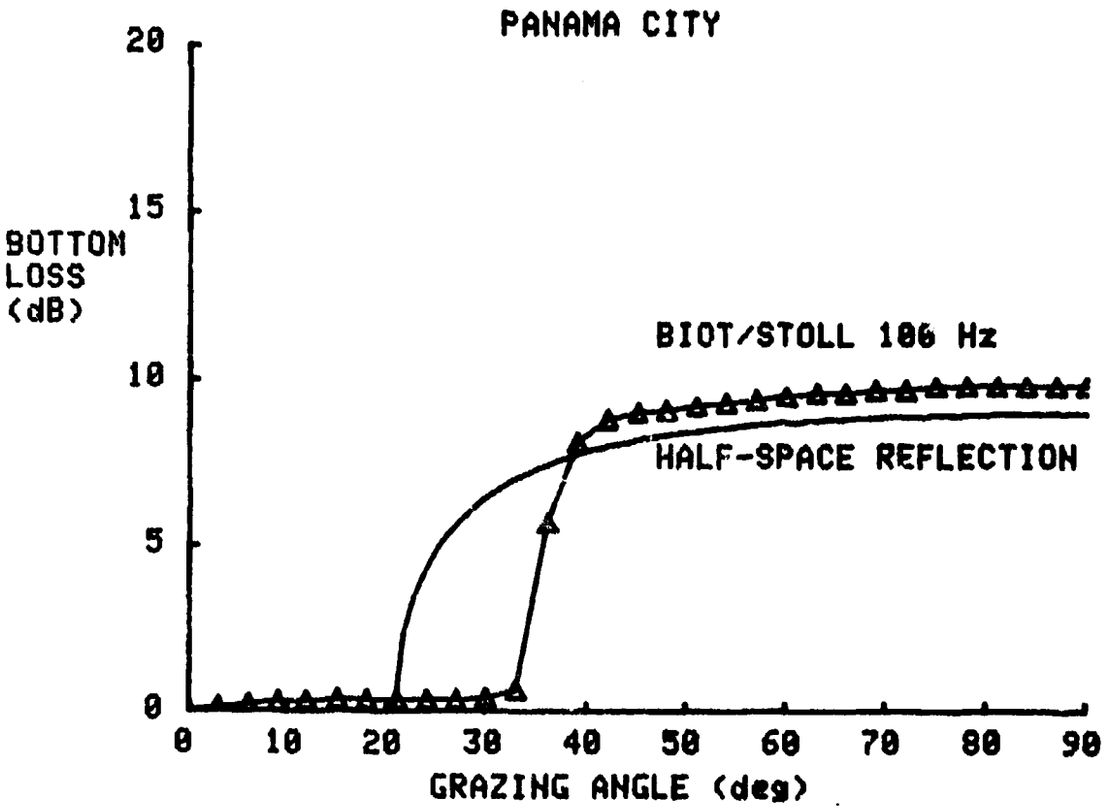

Figure 36. Bottom Loss versus Grazing Angle Comparing the REFLEC Calculation for Biot/Stoll at 100 Hz (from Figure 34) to Simple Rayleigh Reflection at the Surface of the Biot/Stoll Sediment. The latter Curve Shows Complete Internal Reflection up to 20°.

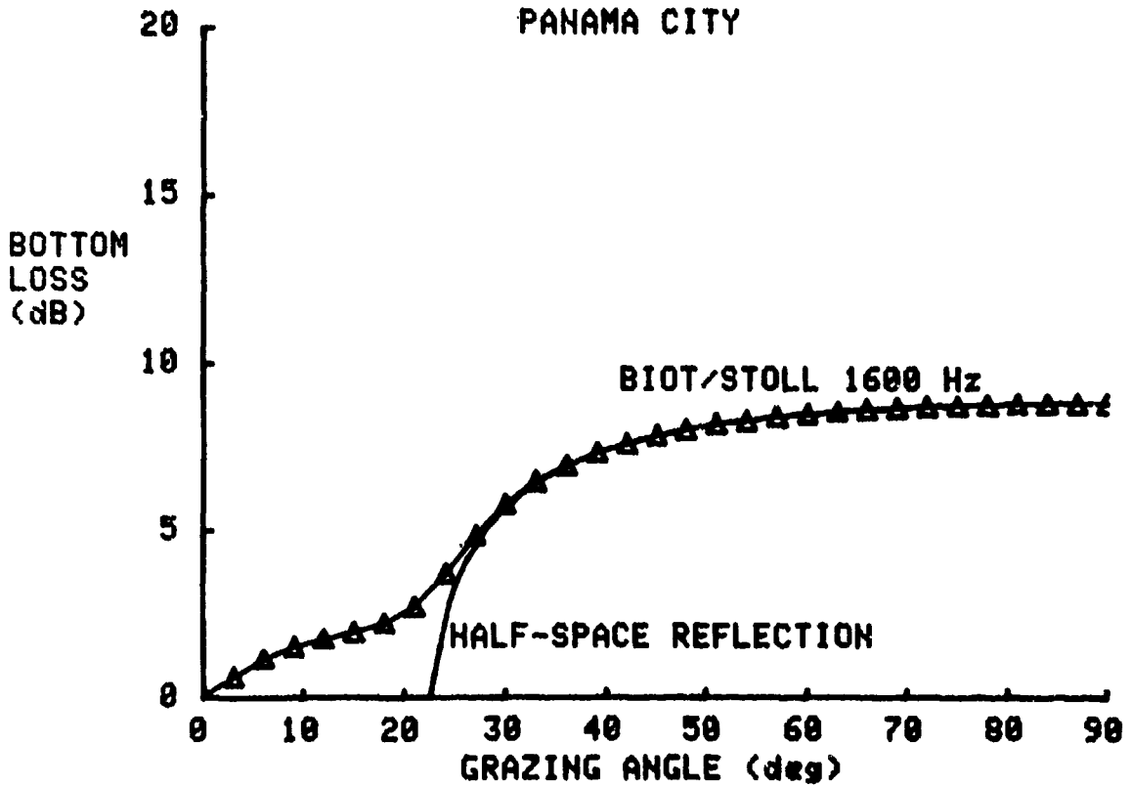

Figure 37. Same as Figure 36, but for 1600 Hz.

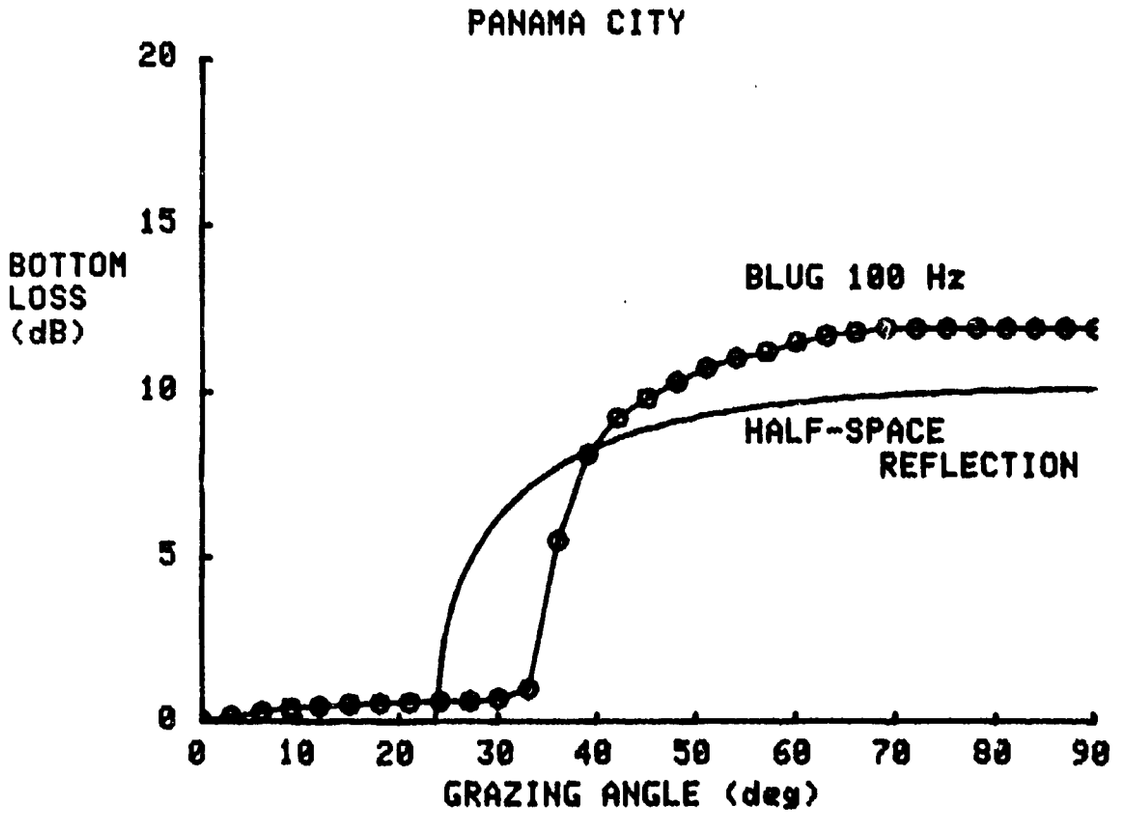

Figure 38. Same as Figure 36, but for the BLUG Sediment at 100 Hz.

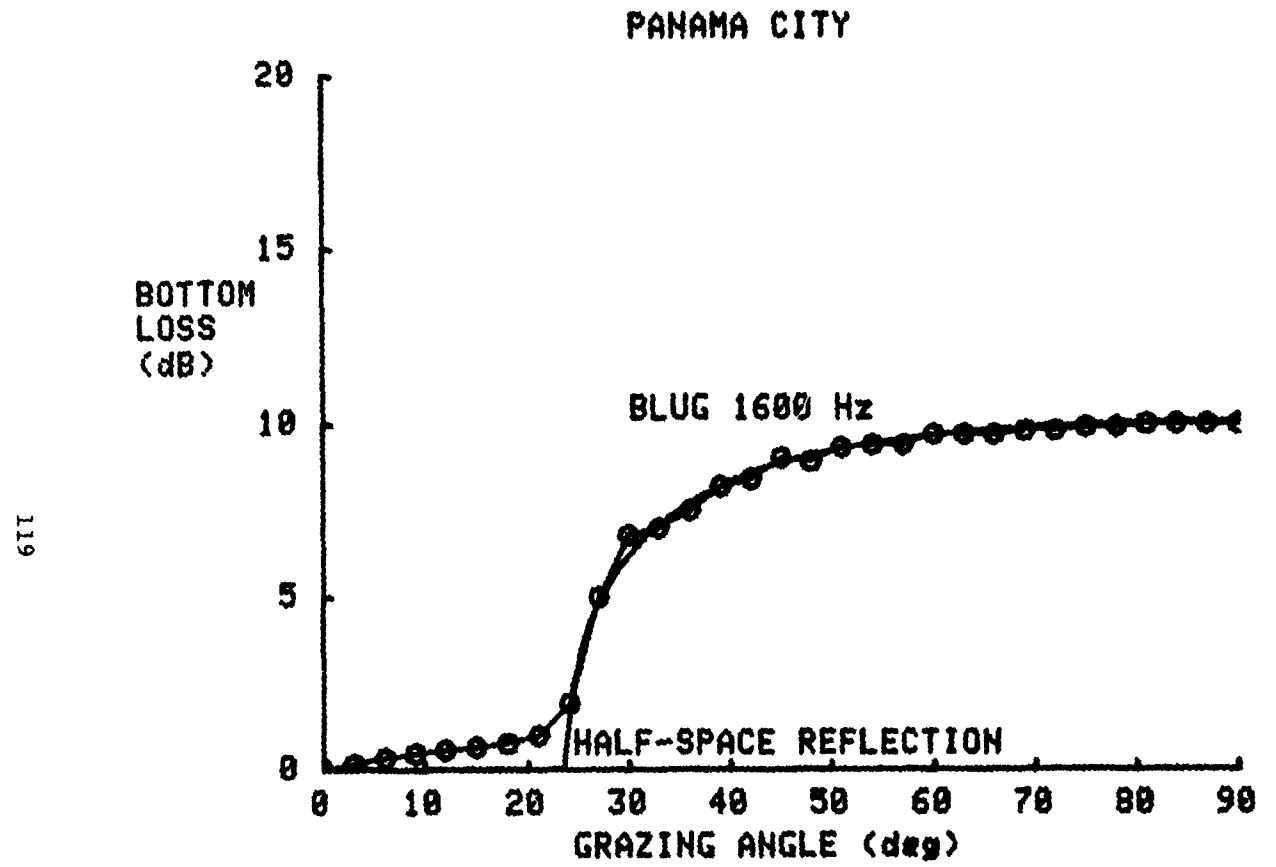

Figure 39. Same as Figure 36, but for the BLUG Sediment at 1600 Hz.

V. CONCLUSIONS

Summary

We have implemented and tested a version of the Biot/Stoll physical sediment model in a form which allows the prediction of those geoacoustic properties needed by current Navy acoustic or bottom loss calculation models. The model is able to predict the depth and frequency dependence of compressional and shear wave attenuation and speed. Efforts have concentrated on refining the compressional wave predictions since these are most important to acoustic modeling at the present time.

Model inputs consisting of sediment physical properties have been obtained from published measurements or generally accepted empirical or physical relationships between sediment physical properties. The sensitivity of the model outputs to variations in model inputs was assessed. As a result several "critical factors" have been identified. The accurate specification of these "critical factors" is considered essential to the prediction of geoacoustic properties of the sea floor.

Two test sites were selected to assess the performance of the Biot/Stoll model. A deep ocean location near DSDP Site 135 was selected to demonstrate the model's capability to predict sediment geoacoustic properties for small-grain, high porosity, low permeability sediments. A second site near Panama City was selected for demonstration of the model's ability to predict geoacoustic properties of low porosity, high permeability shallow-water sediments. The model predictions for these two sites were compared with measurements reported by the Deep Sea Drilling Project[41] for Site 135 and by Beebe[7] for the Panama City case. In addition, geoacoustic predictions from the Biot/Stoll model were compared with geoacoustic properties inferred from acoustic measurements of bottom loss using techniques described by Spofford[38] and applied in the Navy's Bottom Loss Upgrade (BLUG) project.

An attempt was made to show the acoustical significance of differences observed between the Biot/Stoll derived geoacoustic properties and those derived using the BLUG technique. The lack of a suitable primary standard in the form of directly measured bottom loss or acoustic propagation loss led to the use of a secondary standard. The measure of acoustical significance was a comparison of the bottom loss versus grazing angle as a function of frequency derived from a complex reflection coefficient model. This model provided bottom loss values using Biot/Stoll and BLUG sediment geoacoustic properties as inputs. The impact of differences in the depth and frequency dependences of compressional wave speed and attenuation were manifest as differences in calculated bottom loss versus grazing angle.

Discussion of Results

In this section we will discuss those aspects of this study which have added significantly to our understanding of the Biot/Stoll physical model and its applicability to Navy acoustic prediction problems.

We have demonstrated distinct and potentially important differences between the physical sediment model approach and the bottom loss inversion techniques currently being employed in the BLUG project. Biot/Stoll has the capability to provide more details of the vertical structure of the sediment column. This results from the model's ability to utilize all that is known about the sediment column whether the knowledge has been gained from direct measurement as in the case of DSDP cores, or through remote sampling such as seismic reflection or refraction profiles. Since the properties of a particular sediment constituent are constant, knowledge gained in situ or in the laboratory may be applied to the prediction process wherever that particular sediment occurs. This gives promise for using the physical model to provide valuable insight for a priori estimates of bottom interaction effects in geographic areas or frequency regimes which have not been acoustically surveyed, a capability inconsistent with the BLUG reliance on acoustic data to infer sediment geoacoustic properties.

Another potentially important property of the physical sediment model is its ability to predict the frequency dependence of attenuation and speed. In the Panama City test case described in Section IV, we demonstrated this by using the model to predict the compressional wave attenuation as a function of frequency. The agreement with attenuation data reported by Beebe[7] was good. For the cases reported, the data and model predictions exhibited nearly the same frequency exponent. This was shown to have some important acoustic effects which were manifested in the bottom loss simulation results. The geoacoustic and bottom loss differences between the Biot/Stoll

and BLUG approaches were primarily due to attenuation differences. The attenuation differences were, in turn, primarily due to the different frequency dependences in the two approaches. We feel that the frequency dependence exhibited by the Biot/stoll model is more realistic than the linear frequency dependence characteristic of BLUG or Hamilton's empirical approach as discussed in Section II. Beebe[7] showed comparisons between the Biot/Stoll and Hamilton models, while we have shown comparisons between Biot/Stoll and BLUG. These comparisons were made in shallow water for high-permeability sediments, and in all such cases the Biot/Stoll model was better able to estimate the frequency dependence of attenuation. Consequently, for those areas where this type of frequency dependence may be important, we feel that the Biot/Stoll approach should yield a more realistic description of the geoacoustic properties of the seafloor. An additional unique capability which the Biot/Stoll model offers is that it can predict speed attenuation for frequencies spanning the complete Navy applications band. Geoacoustic properties may be predicted for low-frequencies normally associated with surveillance applications as well as high frequencies characteristic of tactical applications. These predictions can be performed using the same set of input parameters, thus insuring a consistent set of frequency dependent bottom properties without the need for changing the data collection or processing techniques.

As stated previously, the ability of the Biot/Stoll model to yield reasonable estimates of the geoacoustic properties of the sea floor is dependent upon accurate descriptions of the physical properties of the sediment. A primary objective of this study was to identify these "critical factors" to which the model outputs are most sensitive. Through a series of sensitivity studies we have isolated several. The studies and their results are discussed in detail in Section IV, but we will reiterate the most important findings here.

Sensitivity studies performed for the deep water site showed the bulk modulus of the sediment grains (K_r) to be a "critical factor" for compressional wave speed predictions but not for attenuation. Varying K_r by a factor of ~6 caused a 10% change in the compressional wave speed.

The frame bulk modulus (K_b) was also deemed to be a "critical factor". Since K_b was determined using the Poisson's ratio (R_p) of the sediment frame, this parameter was varied in the sensitivity study. A change of R_p from 0.25 to 0.45 resulted in a 25% change in the compressional speed. For a more reasonable range of R_p values between 0.25 and 0.35 we would expect speed changes of approximately 5%. This points out the increased sensitivity of speed to R_p as R_p approaches its theoretical upper bound of 0.5. The compressional wave attenuation showed a four fold change as the R_p ranged from 0.25 to 0.45. This is primarily due to the interdependence of the imaginary part of the frame bulk modulus (K_b^*) on K_b. As with velocity, the increase of attenuation with increasing R_p is much smaller for ranges of R_p between 0.25 and 0.35. Since they are so interrelated in the present formulation of the model, one may consider either K_b or R_p to be the "critical factor."

In the model, we have used the dry frame log decrements (Δ_s and Δ_p) to determine the imaginary parts of the shear (μ_s^*) and bulk (K_b^*) frame moduli. Variation of these inputs has little or no effect on the wave speed, but a profound effect on the attenuation. The compressional wave attenuation was shown to change by an order of magnitude as the Δ_p and Δ_s values were varied across a reasonable range of values. Since attenuation has significant impact on the nature of acoustic bottom interaction, both of these log decrements have been identified as "critical factors".

A key parameter in determining the frequency dependence of attenuation as well as its magnitude is the permeability (k). This parameter is a measure of how easily the fluid moves relative to the sediment frame. This fluid mobility has a large impact on the amount of energy dissipated because of viscous drag as the fluid and frame move relative to one another. Once permeability decreases to a threshold, further restriction of fluid flow by reducing the permeability has little or no effect on the magnitude or frequency dependence of either attenuation or speed. This was demonstrated in the deep sea test case where a four orders of magnitude (10^{-4}) reduction in permeability showed no discernible impact on the model outputs. In the highly permeable sediments characteristic of the Panama City test case, this insensitivity did not hold. In that case an increase in permeability by a factor of three (3x) resulted in a doubling of the attenuation and a nonlinear frequency dependence consistent with the presence of significant viscous losses due to fluid motion relative to the sediment frame. Therefore, for highly permeable sediments like sands, the permeability is considered to be a "critical factor" in the model.

As we reviewed the literature of geology and geophysics, the importance of porosity (β) and grain size in relating the various physical properties of sediments became evident. Many empirical and physical relationships have been published relating porosity or grain size to other sediment properties. In Section IV we discussed the role of porosity in determining the depth dependence predicted by the Biot/Stoll model for DSDP Site 135. Much of the vertical structure displayed at that site could be related to the porosity values given as a function of depth. Because of its profound impact on so many physical and geoacoustic properties of the sediments, porosity is considered a "critical factor," as is grain size.

The determination of depth dependence of the geoacoustic properties of the sediments modeled in this study is an important subject in its own right. We have used the Stoll approach as described in Section III to relate the frame shear modulus (μ_b) to overburden stress and porosity. The shear modulus was in turn used to calculate the frame bulk modulus K_b using Equation (55). This obviously makes the frame shear modulus an important input parameter for depth dependent calculations. We feel that further study is needed to determine how well the Stoll method reflects the actual depth dependence of sediment frame moduli.

The results of the Biot/Stoll to BLUG comparisons lead to some general conclusions. As previously stated, the vertical structure of the Biot/Stoll sediment at DSDP Site 135 is quite different from the BLUG sediment. Biot/Stoll reflects the effects of sediment property changes such as porosity. It could, in principle, handle sediment type changes if the properties of the sediment were available or could be inferred through empirical or physical relationships. BLUG sediment profiles are described by a sound speed gradient and curvature; an attenuation gradient; and a sediment density. No structure can be determined using the current acoustic inversion technique. For the base case in the sensitivity studies of Section IV, DSDP Site 135, the two showed similar gradients to ~175m but Biot/stoll values were about 5% higher. An adjustment was made in the sediment grain bulk modulus (K_r) and the surface values became nearly coincident. The attenuation values showed the same frequency dependence, with Biot/Stoll values being slightly higher. The Biot/Stoll attenuation gradient was much steeper in the upper 25m and the values were generally higher at all depths. Adjustment of the frame log decrements (Δ_p and Δ_s) led to better agreement in magnitude at depth, but the higher attenuation gradient remained near the sediment surface.

The comparisons of Biot/Stoll and BLUG at the Panama City site are less conclusive in one sense due to the absence of local acoustic data upon which to base the BLUG geoacoustic parameters. However, there are a set of attenuation data with which to compare the two approaches. On this basis, the Biot/Stoll approach appears to be the more nearly correct, especially at the higher frequencies.

A common thread in the deep and shallow water modeling using the Biot/Stoll approach is the use of the same methods and relationships to obtain the needed model inputs. The specific relationships used have been discussed in Sections III and IV, but their common application resulting in reasonable approximations to the sea floor geoacoustic properties in both deep and shallow water is encouraging.

Conclusions

We feel that the results of this study have yielded positive evidence that the physical sediment model approach to geoacoustic modeling is useful. By using inputs of sediment physical properties obtained from published measurements or derived from generally accepted empirical and physical relationships between such sediment properties, we have been able to predict reasonable values for profiles of density and compressional wave speed and attenuation. These profiles have been shown to agree, to first order, with profiles inferred from seismic and bottom loss measurements.

The ability of the Biot/Stoll model to produce potentially significant details of the vertical sediment structure has been demonstrated. In addition, the model has been shown to yield depth and frequency dependence of attenuation and speed which are different from other geoacoustic modeling approaches but consistent with observations. The importance of the model's ability to properly account for viscous losses which lead to nonlinear frequency dependence of attenuation has been demonstrated for a shallow water test case.

The model sensitivity has been tested, certain "critical factors" have been identified and an approach has been devised to supply needed inputs to the model. The same approach has been applied in both shallow water and deep water test cases.

Given the model's independence from directly measured acoustic data, its ability to predict geoacoustic properties from a few key physical properties, and the realistic nature of its inputs including the ability to take into account vertical structure, we feel that the Biot/Stoll model is a potentially powerful tool for estimating or extrapolating geoacoustic parameters which are in turn controlling factors for many deep-water tactical applications and nearly all shallow-water applications. The approach may prove to be particularly valuable for a priori estimates of bottom interaction effects

in geographic areas or frequency regimes which have not been acoustically surveyed. The model may also prove valuable in isolating the controlling physical factors in acoustic propagation studies in sediments. Such insight has already proved valuable in designing and interpreting laboratory and field studies undertaken by one of the authors.

VI. RECOMMENDATIONS

For the reasons outlined in the introduction, it is an appropriate task to ascertain the usefulness of the Biot/stoll sediment model. This task must have three parts:

1. Identify the best way to implement the model, i.e., the best sources for the thirteen input parameters;
2. Determine how well the model works in terms of both the precision (or repeatability) and the accuracy (closeness to independent observations) of its results; and,
3. Describe the applications for the model and compare its performance to the performance of other methods.

For the first part, it is recommended that support and encouragement be generated for laboratory and field measurements which provide: values for grain bulk modulus as a function of mineral and plankton assemblage; grain size distribution and porosity as functions of geographic position and depth; values of grain specific surface area as a function of sediment type and size class; and values for dry frame bulk and shear moduli (or Poisson's ratio), and compressional and shear log decrements as a function of sediment type, size class and overburden stress (low ranges of stress appropriate to depths of burial from 0 to 1000m).

For the second part, further testing is recommended. The accuracies of the Biot/stoll velocity and attenuation predictions were found to be reasonably good considering both the uncertainties of the observations and the low precision of the predictions. The predictions were imprecise in that large uncertainties in specific inputs produced relatively large changes in the results. This precision will be improved when

the inputs become more certain as a result of recommendations made in the previous paragraph. Precision and accuracy were both improved in the deep water case by adjusting grain bulk modulus and dry frame log decrement values. Further testing should be aimed at validating these choices. We strongly recommend that another location of chalk ooze sediments be identified where measurements of porosity, grain size, density and sound speed, at least, are available to validate the choice of grain bulk modulus. Attenuation values as inferred from bottom loss or other acoustic measurements are also necessary if the log decrement choices are to be validated.

For the third part, more work is also required. For bottom loss problems, we have argued that the Biot/Stoll model represents a potential improvement over BLUG especially where a priori estimates of bottom loss are needed at locations and frequencies with no acoustic observations. For frequency the advantage of Biot/Stoll is clear. For location our argument needs to be further substantiated by a complete description of the geographic availability of data that can be used as sources for Biot/Stoll inputs and a comparison to the geographic distribution of bottom loss measurements (the only legitimate input for the BLUG model).

Applications beyond bottom loss also need to be addressed for the third part. BLUG, with its idealized frequency dependence and smoothed vertical structure makes no claims that its speed and attenuation profiles apply to problems where sediment propagation paths and arrival time structure are important - but the Biot/Stoll model could in principle support this claim. The applicability of Biot/Stoll in such problems should be addressed by performing propagation studies including acoustic model runs and comparisons to data--both transmission loss and time series. These would be particularly valuable in shallow water scenarios where the frequency dependence of attenuation may become important. An additional potentially

useful capability of the Biot/Stoll model in a shallow water area is its ability to predict sediment shear wave speeds and attenuations. Whether or not shear wave conversion is a significant factor in bottom interacting propagation has not been conclusively demonstrated, but the Biot/Stoll model offers the opportunity to test the hypothesis that it is important by providing the necessary geoacoustic descriptions for conversion calculations.

REFERENCES

1. Stoll, R.D., 1979, "Experimental Studies of Attenuation in Sediments," J. Acoust. Soc. Amer., 66, pp. 1152-1160.

2. Brunson, B.A. and R.K. Johnson, 1980, "Laboratory Measurements of Shear Wave Attenuation in Saturated Sand," J. Acoust. Soc. Amer., 68.

3. Stoll, R.D. and G.M. Bryan, 1970, "Wave Attenuation in Saturated Sediments," J. Acost. Soc. Amer., 47, pp. 1440-1447.

4. Stoll, R.D., 1974, "Acoustic Waves in Saturated Sediments," In L. Hampton (ed.), Physics of Sound in Marine Sediments, New York, Plenum Press, pp. 19-39.

5. Stoll, R.D., 1977, "Acoustic Waves in Ocean Sediments," Geophysics, 42, pp. 715-725.

6. Plona, T.J., 1980, "Observations of a Second Bulk Compressional Wave in a Porous Medium at Ultrasonic Frequencies," Appl. Phys. Lett., 36, pp. 259-261.

7. Beebe, J.H., 1980, "An Experimental Investigation of Ocean Sediment Effects Upon Long-Range Transmission Loss in Shallow Water," Technical Memorandum TM 80-247, Pennsylvania State University.

8. Brunson, B.A. and J.E. Matthews, 1981, "Grain Shape and Sorting Effects on the Frequency Dependence of Shear Wave Attenuation in Water Saturated Sediments," unpublished paper presented at 101st meeting, Session QQ, Acoustical Society of America.

9. Hamilton, E.L., 1971, "Prediction of in-situ Acoustic and Elastic Properties of Marine Sediments," Geophysics, 36, pp. 266-284.

10. Hamilton, E.L., 1974, "Prediction of Deep-Sea Sediment Properties: State-of-the-Art," In A.L. Inderbitzen (ed.) Deep-Sea Sediments, Physical and Mechanical Properties, New York, Plenum Press, pp. 1-43.

11. Hamilton, E.L., 1974, "Geoacoustic Models of the Sea Floor," In L. Hampton (ed.), Physics of Sound in Marine Sediment, New York, Plenum Press, pp. 181-221.

12. Hamilton, E.L., 1980, "Geoacoustic Modeling of the Sea Floor," J. Acoust. Soc. Amer., 68, pp. 1313-1340.

13. Ferry, J.D., 1961, "Viscoelastic Properties in Polymers," New York, John Wiley and Sons.

14. Scoll, R.D., 1980, "Theoretical Aspects of Sound Transmission in Sediments," J. Acoust. Soc. Amer., 68, pp. 1341-1350.

15. Biot, M.A., 1956, "Theory of Elastic Wave Propagation in a Fluid-Saturated Porous Solid," I. Low Frequency Range, J. Acoust. Soc. Amer., 28, pp. 168-178.

16. Biot, M.A., 1956, "Theory of Elastic Wave Propagation in a Fluid-Saturated Porous Solid," II. Higher Frequency Range, J. Acoust. Soc. Amer., 28, pp. 179-191.

17. Biot, M.A., 1962, "Generalized Theory of Acoustic Propagation in Porous Dissipative Media," J. Acoust. Soc. Amer., 34, pp. 1254-1264.

18. Ogushwitz, P.R., 1982, "Applicability of the Biot Theory," I. Low Porosity Materials, (manuscript to be submitted to Journal of the Acoustical Society of America).

19. Keller, G.H., 1974, "Marine Geotechnical Properties: Interrelationships and Relationships to Depth of Burial," Deep Sea Sediments, ed. by A.L. Inderbitzen, Plenum Pub. Corp., New York.

20. Hamilton, E.L., 1969, "Sound Velocity, Elasticity, and Related Properties of Marine Sediments, North Pacific," II. Elasticity and Elastic Constants, NUC TP 144, Naval Undersea Research and Development Center, San Diego, California.

21 Chen, C.T. and F.J. Millers, 1977, "Precise Equation of State of Seawater for Oceanic Ranges of Salinity, Temperature, and Pressure," Deep Sea Research, 24, pp. 365-369.

22. Hamilton, E.L., 1970, "Sound Velocity and Related Properties of Marine Sediments, North Pacific," J. Geophys. Res., 75, pp. 4423-4446.

23. Hamilton, E.L., 1975, "Acoustic and Related Properties of the Sea Floor: Density and Porosity Profiles and Gradients," NUC Tech Paper #459, p. 47.

24. Domenico, S.N., 1977, "Elastic Properties of Unconsolidated Porous Sand Reservoirs," Geophysics, 42, pp. 1339-1368.

25. Van der Knapp, W., 1960, "Non-linear Behavior of Elastic Porous Media," Journ. Soc. Petroleum Engineers AIME TP 8072.

26. Toksoz, M.N., C.H. Cheng, and A. Timur, "Velocities of Seismic Waves in Porous Rocks," Geophysics, 41, pp. 621-645.

27. Carman, P.C., 1956, Flow of Gases Through Porous Media, Academic Press, New York.

28. Brunson, B. 1982, Laboratory Measurements of Shear Wave Attenuation in Natural and Synthetic Sediments: The Importance of Grain Shape and Sorting, oral presentation given at the SEG/ USN Shear Waves and Pattern Recognition Symposium, NSTL Station, Mississippi, March 1982.

29. Bryant, W.R., W. Hottman, and P. Trabant, 1975, "Permeability of Unconsolidated and Consolidated Marine Sediments," Gulf of Mexico, Mar. Geotech., 1, pp. 1-14.

30. Krumbein, W.C. and G.D. Monk, 1942, "Permeability as a Function of the Size Parameters of Unconsolidated Sand," Petroleum Technology, Am. Inst. Mining and Metallurgical Engineers, Tech. Pub. No. 1942, pp. 1-9.

31. Hovem, J.M. and G.D. Ingram, 1979, "Viscous Attenuation of Sound in Saturated Sand," J. Acoust. Soc. Amer., 66, pp. 1807-1812.

32. Berryman, J.G., 1980, "Confirmation of Biot's Theory," Appl. Phys. Lett., 37, pp. 382-384.

33. Richart, Hall, and Woods, 1970, Vibrations in Solids.

34. Berryman, J.G., 1980, "Long Wavelength Propagation in Composite Elastic Media," I. Spherical Inclusions, J. Acoust. Soc. Amer., 68, pp. 1809-1819.

35. Berryman, J.G., 1980, "Long Wavelength Propagation in Composite Elastic Media," II. Ellipsoidal Inclusions, J. Acoust. Soc. Amer., 68, pp. 1820-1831.

36. Hamilton, E.L., 1971, "Elastic Properties of Marine Sediments," J. Geophys. Res., 76, pp. 579-604.

37. Ogushwitz, P.R., Bell Laboratories, Whippany, New Jersey. Personal communication.

38. Spofford, C.W., 1980, "Inference of Geo-Acoustic Parameters from Bottom Loss Data," in Bottom-Interacting Ocean Acoustics, edited by W.A. Kuperman and F.B. Jenson, Plenum Press, New York, pp. 154-173.

39. Brekhovskikh, L.M., 1960, Waves in Layered Media, Academic Press, New York.

40. Gilbert, K.E., 1980, "Reflection of Sound from a Randomly Layered Ocean Bottom," J. Acoust. Soc. Am., 68, pp. 1454-1458.

41. Pimm, A.C., editor, 1971, Initial Reports of the Deep Sea Drilling Project, Vol. XIV: Covering Leg 14 of the Cruises of the Drilling Vessel GLOMAR CHALLENGER, Lisbon, Portugal to San Juan, Puerto Rico, October-December 1970, Prepared for the National Science Foundation, Washington, D.C.

42. Kinsler, L.E. and A.R. Frey, 1962, Fundamentals of Acoustics, John Wiley and Sons, New York.

43. Hamilton, E.L., 1976, "Attenuation of Shear Waves in Marine Sediments," J. Acoust. Soc. Am., 60, pp. 334-338.

44. Ingenito, F., 1973, "Measurements of Mode Attenuation Coefficients in Shallow Water," JASA, 53, pp. 858-863.

45. Caswell, W.R., 1979, "The Frequency Dependence of Normal-Mode Attenuation in Shallow-Water Sound Propagation." Unpublished doctoral dissertation, The Pennsylvania State University.

LIST OF ABBREVIATIONS, ACRONYMS, AND SYMBOLS

a	poresize parameter
a_1	coefficient of the quardic term in the compressional wavenumber equation
a_2	coefficient of the quadratic term in the compressional wavenumber equation
a_3	coefficient of the constant term in the compressional wavenumber equation
A_1	coefficient of the frame dilatational wave
A_2	coefficient of the fluid dilatational wave
A_3	coefficient of the frame shear wave
A_4	coefficient of the fluid flow wave set up by shear motions in frame
bei	Kelvin function, imaginary part
ber	Kelvin function, real part
BLUG	the Bottom Loss Upgrade technique
b_1	coefficient of the quadratic term in the shear wavenumber equation
b_2	coefficient of the constant term in the shear wavenumber equation
bei	Kelvin function, imaginary part
ber	Kelvin function, real part
BLUG	the Bottom Loss Upgrade technique
cm	a centimeter, equal to 10^{-2} m
d	diameter of sphere or sediment grain
d_m	diameter of sphere with the same mean specific surface area as the sediment grains
d_{m_g}	mean diameter of sediment grains
D	a complex function of porosity and bulk moduli of grains and fluid
dB	decibels, a measure of relative intensities
DSDP	Deep Sea Drilling Project
DTNSRDC	David W. Taylor Naval Ship Research and Development Center
e	dilatation (volume strain of an element attached to the frame)
ε	void ratio
E	Young's modulus, real part
E*	Young's modulus, imaginary part
e_{ij}	strain tensor element
f	frequency (in cycles per second)
F	a frequency-dependent complex correction factor to the viscous resistance to fluid flow
FNOC	Fleet Numerical Oceanographic Center
g	gravitational acceleration, approximately equal to 9.8 m s^{-2}
gm	a gram, equal to 10^{-3} kg
GRAPE	Gamma Ray Attenuation Porosity Evaluator
H	a complex elastic constant of a sediment's frame
Hz	hertz, a frequency unit equal to one cycle per second

LIST OF ABBREVIATIONS, ACRONYMS, AND SYMBOLS

i	$(-1)^{1/2}$; as a subscript it is a counting index
j	a counting index
k	permeability (in m^2)
K	constant in the Kozeny-Carman equation
K_b	bulk modulus of sediment frame (real part)
K_b*	bulk modulus of sediment frame, imaginary part
K_c	bulk modulus of sediment frame
K_f	bulk modulus of pore fluid
K_r	bulk modulus of sediment grains
k_0	known or reference permeability
k_1	permeability in cm s^{-1}
K_1	bulk modulus of the 1st mineral in a sediment grain
K_2	bulk modulus of the 2nd mineral in a sediment grain
kg	a kilogram--unit of mass
kHz	kilohertz, equal to one thousand hertz
ℓ	complex wavenumber
log	logarithmic function to the base 10
log dec	logarithmic decrement
m	a meter--unit of length
m	apparent inertia of fluid
M	a complex elastic constant of a sediment's frame
MHz	Megahertz, equal to one million hertz
N	a newton, equal to 1 kg m s^{-2}
NADC	Naval Air Development Center
P	pore fluid pressure
r	a measure of induced mass of a fluid due to oscillation of particles in it, = 1/2 for spheres
r_h	hydraulic radius, equal to the ratio of the volume filled with fluid to the wetted surface
R_p	Poisson's Ratio
R&D	Research and Development
REFLEC	a computer code that models plane wave reflection from multiple layers
s	a second--unit of time
S_0	specific surface (i.e., surface area per unit volume)
SCM	self consistent method
t	time
T	a function of Kelvin functions and their derivatives used to calculate F
$\tilde{u}$	frame displacement vector
$\tilde{v}$	fluid displacement vector
V_E	sound speed of longitudinal waves in frame
V_S	sound speed of shear waves in frame
V_1	volume fraction of the 1st mineral in a sediment grain
V_2	volume fraction of the 2nd mineral in a sediment grain
$\tilde{w}$	curl vector of the frame displacement
x	variable, Cartesian coordinate in horizontal direction

LIST OF ABBREVIATIONS, ACRONYMS, AND SYMBOLS

x_i	general Cartesian coordinate
y	Cartesian coordinate in horizontal direction perpendicular to x
z	Cartesian coordinate in vertical direction
α	structure factor
β	porosity
β_0	known or reference porosity
δ_{ij}	Kronecker delta, = 0 when $i \neq j$
Δ_E	logarithmic decrement of longitudinal waves
Δ_p	logarithmic decrement of compressional waves
Δ_s	logarithmic decrement of shear waves
ζ	volume of fluid that flows out of an element attached to frame
η	fluid viscosity
$\tilde{\theta}$	a vector function of porosity, frame displacement and fluid displacement
κ	a function of fluid density and viscosity and frequency used as the variable of a Kelvin function
μ	shear modulus of sediment frame
μ_b	shear modulus of sediment frame, real part
μ_b^*	shear modulus of sediment frame, imaginary part
μ_r	shear modulus of grains
π	ratio of a circle's circumference to the diameter
ρ	density, saturated bulk density of sediment
ρ_f	density of pore fluid
ρ_r	density of sediment grains
σ_ϕ	standard deviation of grain size parameter
τ_{ij}	stress tensor element
τ_0	average stress
τ_1	vertical component of stress
τ_2	horizontal component of stress
τ_3	horizontal component of stress, perpendicular to τ_2
ϕ	grain size parameter, equal to negative log of the grain diameter in 10^{-3} m in the base 2
ϕ_m	mean value of grain size parameter
ω	angular frequency (radians per second)
$\frac{\partial}{\partial x}$	derivative operator with respect to the variable x
$\frac{\partial^2}{\partial x^2}$	second derivative operator with respect to the variable x
∇^2	Laplacian operator = $\frac{\partial^2}{\partial x^2} + \frac{\partial^2}{\partial y^2} + \frac{\partial^2}{\partial z^2}$
%	percent
°C	degrees in Celsius scale